UNIVERSIDADE FEDERAL DO RIO GRANDE DO NORTE
CENTRO DE CIÊNCIAS EXATAS E DA TERRA
PROGRAMA DE PÓS-GRADUAÇÃO EM GEODINÂMICA E GEOFÍSICA

DISSERTAÇÃO DE MESTRADO

TEXTURAS E QUÍMICA MINERAL DE ZIRCONOSILICATOS EM GRANITOS PERALCALINOS DO PLUTON PAPANDUVA, PR-SC

Autora:

LARISSA PRAXEDES GRANGEIRO

Orientador:

PROF. DR. FREDERICO CASTRO JOBIM VILALVA

Dissertação nº 295/PPGG

Agosto de 2024
Natal/RN, Brasil

LARISSA PRAXEDES GRANGEIRO

TEXTURAS E QUÍMICA MINERAL DE ZIRCONOSILICATOS EM GRANITOS PERALCALINOS DO PLUTON PAPANDUVA, PR-SC

Dissertação apresentada em 23 de agosto de 2024 ao Programa de Pós-Graduação em Geodinâmica e Geofísica (PPGG) da Universidade Federal do Rio Grande do Norte (UFRN) como requisito à obtenção do Título de Mestre em Geodinâmica e Geofísica, Área de Concentração Geodinâmica.

BANCA EXAMINADORA:

_____

PROF. DR. FREDERICO CASTRO JOBIM VILALVA

Presidente e orientador (PPGG-UFRN)

_____

PROF. DR. GASTON EDUARDO ENRICH ROJAS

Membro externo (IGc-USP)

_____

PROF. DR. PEDRO AUGUSTO DA SILVA ROSA

Membro externo (IGC-UFMG)

Universidade Federal do Rio Grande do Norte - UFRN
Sistema de Bibliotecas - SISBI
Catalogação de Publicação na Fonte. UFRN - Biblioteca Setorial Prof. Ronaldo Xavier de Arruda - CCET

Grangeiro, Larissa Praxedes.
Texturas e química mineral de zirconosilicatos em granitos peralcalinos do Pluton Papanduva, PR-SC / Larissa Praxedes Grangeiro. - 2024.
93 f.: il.

Dissertação (mestrado) - Universidade Federal do Rio Grande do Norte, Centro de Ciências Exatas e da Terra, Programa de Pós-Graduação em Geodinâmica e Geofísica. Natal, RN, 2024.
Orientação: Prof. Dr. Frederico Castro Jobim Vilalva.

1. Geodinâmica - Dissertação. 2. Elpidita - Dissertação. 3. Elementos traços - Dissertação. 4. Interação hidrotermal - Dissertação. 5. Estágios tardi- a pós-magmáticos - Dissertação. I. Vilalva, Frederico Castro Jobim. II. Título.

RN/UF/CCET CDU 551.2/.3(043.3)

Elaborado por Joseneide Ferreira Dantas - CRB-15/324

“Palavras são, na minha nada humilde opinião, nossa inesgotável fonte de magia. Capazes de formar grandes sofrimentos, mas, também, de remediá-los”.

Alvo Dumbledore

AGRADECIMENTOS

Chega o fim de mais um ciclo na minha vida de estudante e o início de uma vida cada vez mais adulta. Nesses anos de dedicação e esforço (de algumas escorregadas e desânimo também) algumas pessoas foram essenciais para que o tão esperando momento da defesa chegasse. Por isso, expresso através de palavras, um pouquinho da importância que cada uma dessa pessoas tiveram, e ainda têm, na conquista desse título. Reconheço também a todos aqueles que estiveram sempre comigo, nomidados ou não nestes agradecimentos.

Primeiro, gostaria de agradecer e reconhecer a dedicação e ajuda do meu orientador Fred. Você foi acima de tudo amigo, humano e o maior responsável por eu ter topado esse desafio, sempre deixei claro para todos que “eu só resolvi fazer mestrado porque era com Fred”. Você é exemplo de ser humano, de professor e, agora, de pai. Eu poderia passar uma vida descrevendo todas as coisas boas que você apresenta, poderia descrever a sua compreensão nos momentos que eu não estava com ânimo, seu respeito em entender todas as minhas ausências e seu ensinar tranquilo e calmo. Obrigada por me trazer até aqui, ainda bem que você escolheu ser professor e ainda bem que você me aceitou como sua orientanda (agradeça a Dudu também, que nos primeiros dias de vida, precisou dividir o pai dele comigo e que pacientemente, ou não, participou das nossas reuniões).

À minha família, meus pais, meus irmãos e meu noivo, que sempre estiveram comigo nos momentos mais difíceis, que seguraram a barra, que entenderam quando eu precisava me ausentar de aniversários, jantares ou reuniões de família. Sem vocês eu nada seria. Obrigada por tornarem a carga mais leve.

Aos meus amigos de graduação e aos fora do muro da UFRN, gratidão por todos os momentos compartilhados. À Dhulya, minha parceira de sala desde os primeiros semestres, passamos por várias fases juntas e a conclusão do meu mestrado tem um pouco de você em cada linha. Agradeço aos demais (Rafael, Hemerson, Marília, Richely, Adriano e Flora – uma das maiores responsáveis por eu estar aqui hoje) pela companhia, foram épocas de encontros mais escassos, mas com vínculo cada vez mais aproximado.

Aos meus “filhos” do judô, que me salvaram diariamente de todos os medos, que me trouxeram uma esperança na humanidade e que me mostraram que eu só

precisava ser EU para ser amada, vocês me motivam diariamente a ser melhor, a ser compreensiva, a torcer para que o mundo permita que vocês tenham tantas oportunidades na vida como eu tive até aqui. Minha eterna gratidão e orgulho do que vocês têm conquistado e obrigada por me permitir participar tão de pertinho da vida de vocês. Contêm sempre comigo para tentar quebrar as barreiras desse mundo.

Ao Conselho Nacional de Desenvolvimento Científico e Tecnológico (CNPq), agradeço a bolsa de Mestrado (proc. 130482/2023-4) que permitiu o desenvolvimento desta pesquisa. À Universidade Federal do Rio Grande do Norte (UFRN), ao Programa de Pós-Graduação em Geodinâmica e Geofísica e ao Departamento de Geologia da UFRN, à Fundação de Amparo à Pesquisa do Estado de São Paulo (FAPESP) pelo apoio financeiro através do projeto de pesquisa “19/17343-4 *Propriedades geoquímicas e texturais de minerais acessórios como indicadoras petrológicas e geocronológicas em rochas graníticas e greisens associados*”. Ao Professor Silvio Vlach e a Professora Raquel pelas importantes considerações nas análises do meu trabalho.

Por fim, manifesto gratidão a cada um dos amigos/professores/colegas de faculdade que aqui não foram citados, mas que levarei para sempre na minha vida.

RESUMO

A elpidita ($Na_2ZrSi_6O_{15}\cdot 3H_2O$) e (Na,K)-zirconossilicatos são minerais portadores de zircônio identificados em granitos peralcalinos do Plúton Papanduva da Província Graciosa, no Sul-Sudeste do Brasil. Estes minerais cristalizam durante as fases tardias a pós-magmáticas, proporcionando insights sobre os processos de formação e evolução em ambientes magmáticos complexos. A elpidita ocorre em três tipos texturais distintos: (1) cristais isolados de formato subédrico a euédrico, (2) agregados granulares, e (3) agregados em veios, cada qual apresentando variações composicionais específicas. Adicionalmente, foram identificadas duas fases de (Na,K)-zirconossilicatos, denominadas (Na,K)ZrS-I e (Na,K)ZrS-II, que exibem propriedades texturais e composicionais distintas. A análise química revela que a elpidita possui uma composição majoritariamente uniforme, com variações nos teores de Zr, Al, Ca e K, alinhando-se ao membro final ideal da elpidita. Em contraste, os (Na,K)-zirconossilicatos são enriquecidos em K em relação a Na, demonstrando tendências composicionais diversas. A fase (Na,K)ZrS-II tem maior afinidade composicional com a melansonita, enquanto (Na,K)ZrS-I representa uma fase de transição entre membros finais com baixo e alto teor de K. Contudo, as substituições elementares ocorrem em faixas limitadas, sugerindo a ausência de uma solução sólida completa entre esses elementos. A análise de elementos traços da elpidita revela concentrações menores para a maioria dos elementos em comparação ao zircão, incluindo os elementos terras-raras (ETR), mas com enriquecimentos significativos em Ba, Pb e Sr. As relações texturais e os dados composicionais dos zirconossilicatos do Plúton Papanduva sugerem uma evolução complexa desses minerais, refletindo uma transição de rochas menos evoluídas, onde o zircão predomina como portador de zircônio, para rochas mais evoluídas. A elpidita provavelmente se formou durante estágios magmáticos tardios, seguida pelo desenvolvimento de variedades granulares e em veios. A interação com fluidos hidrotermais ricos em K, possivelmente facilitada por deformação submagmática, resultou em significativa alteração hidrotermal, remobilização química (incluindo HFSE e ETR) e incorporação de elementos, originando as fases (Na,K)ZrS-I e (Na,K)ZrS-II a partir de um zirconossilicato precursor, idealmente a elpidita, ou diretamente dos fluidos. Essa transição está associada ao aumento da peralcalinidade (atividade de álcalis), fugacidade de O_2 e variação na quantidade de água, favorecendo a estabilização dos zirconossilicatos como fases portadoras de Zr.

PALAVRAS-CHAVE: Elpidita; Elementos traços; Interação hidrotermal; Estágios tardi- a pós-magmáticos.

ABSTRACT

Elpidite ($Na_2ZrSi_6O_{15}\cdot 3H_2O$) and (Na,K)-zirconosilicates are zirconium-bearing minerals identified in the peralkaline granites of the Papanduva Pluton, located in the Graciosa Province in southern Brazil. These minerals crystallized during the late- to post-magmatic stages, providing insights into the formation and evolution processes in complex magmatic environments. Elpidite occurs in three distinct textural types: (1) isolated crystals with subhedral to euhedral forms, (2) granular aggregates, and (3) vein-like aggregates, each exhibiting specific compositional variations. Additionally, two phases of (Na,K)-zirconosilicates, designated as (Na,K)ZrS-I and (Na,K)ZrS-II, were identified, each displaying distinct textural and compositional properties. Chemical analysis reveals that elpidite has a predominantly uniform composition, with variations in Zr, Al, Ca, and K, aligning with the ideal end-member of elpidite. In contrast, (Na,K)-zirconosilicates are enriched in K relative to Na and exhibit diverse compositional trends. The (Na,K)ZrS-II phase shows greater compositional affinity with melansonite, whereas (Na,K)ZrS-I represents a transitional phase between lower and higher K end-members. However, elemental substitutions occurred within a limited range, suggesting the absence of a complete solid solution between these elements. Trace element analysis of elpidite revealed lower concentrations of most elements compared to zircon, including rare earth elements (REE), but with significant enrichments in Ba, Pb, and Sr. The textural relationships and compositional data of zirconosilicates from the Papanduva Pluton suggest a complex evolution of these minerals, reflecting a transition from less evolved rocks, where zircon predominates as the zirconium carrier, to more evolved rocks. Elpidite likely formed during the late magmatic stages, followed by the development of granular and vein-like varieties. Interaction with K-rich hydrothermal fluids, possibly facilitated by sub-magmatic deformation, resulted in significant hydrothermal alteration, chemical remobilization (including HFSE and REE), and element incorporation, forming (Na,K)ZrS-I and (Na,K)ZrS-II phases from a precursor zirconosilicate, ideally elpidite, or directly from the fluids. This transition is associated with increased peralkalinity (alkali activity), oxygen fugacity, and variation in water content, favoring the stabilization of zirconosilicates as zirconium-bearing phases.

KEYWORDS: Elpidite; Trace Elements; Hydrothermal Interaction; Late- to Post-Magmatic Stages.

LISTA DE FIGURAS

LISTA DE TABELAS

SUMÁRIO

1. INTRODUÇÃO

O elemento químico zircônio (Zr) está presente em uma ampla gama de rochas ígneas, frequentemente em concentrações de elemento-traço (ppm). Nestas rochas, a cristalização, geralmente precoce, do mineral zircão ($ZrSiO_4$) costuma incorporar o Zr devido à sua alta compatibilidade. No entanto, em condições de excesso de halogênios e álcalis, a solubilidade do Zr pode aumentar, resultando na acumulação deste elemento no líquido residual até as fases finais do processo de cristalização (Linthout, 1984; Keppler, 1993). Nessas circunstâncias, o Zr pode ser incorporado (i) na estrutura de clinopiroxênios e/ou anfibólios sódicos (Andersen et al., 2012); (ii) em silicatos complexos contendo álcalis e Zr, conhecidos como álcali-zirconossilicatos (Borst et al., 2016; Estrade *et al.*, 2018).

Entre os álcali-zirconossilicatos, as variedades mais comuns pertencem ao grupo da eudialita (EGM; “eudialyite-group minerals”), um complexo ciclossilicato de Na, Ca e Zr com a fórmula geral: $Na_{15}(Ca,REE)_6(Fe,Mn)_3Zr_3Si(Si_{25}O_{72})(O,OH,H2O)_3(Cl,OH)_2$ (Johnsen et al., 2003). Entretanto, em granitos e pegmatitos peralcalinos, também foram identificados outros zirconossilicatos (Estrade *et al.*, 2018), tais como: dalyita ($K_2ZrSi_6O_{15}$), wadeita ($K_2ZrSi_3O_9$), elpidita ($Na_2ZrSi_6O_{15}\cdot 3H_2O$), catapleiita ($Na_2ZrSi_3O_9\cdot 2H_2O$) e, mais raramente, gittinsita ($CaZrSi_2O_7$) e armstrongita ($CaZrSi_6O_{15}\cdot 2H_2O$).

Álcalis-zirconossilicatos foram descritos em granitos peralcalinos do Plúton Papanduva por Vilalva (2007). Este plúton faz parte do Complexo Morro Redondo e aflora em uma área de ~100 km^2 nas proximidades de Tijucas do Sul (PR), no contexto geológico da Província Graciosa de granitos e sienitos de tipo-A, de idade neoproterozoica (Gualda & Vlach, 2007). Neste plúton, o principal mineral portador de Zr é, ora o zircão em granitos peralcalinos menos evoluídos e de estrutura maciça, ora zirconossilicatos de Na e K, principalmente a elpidita, além de clinopiroxênio enriquecido em Zr, em granitos peralcalinos mais evoluídos e de estrutura foliada. Estes últimos apresentam ainda uma mineralogia acessória que inclui minerais típicos de rochas agpaíticas, tais como narsarsukita, astrofilita, enigmatita, neptunita, nacareniobsita, britholita, turkestanita, entre outros (Vilalva, 2007; Vilalva & Vlach, 2010; 2014; Vilalva et al., 2013; Siachoque et al., 2022; Vlach & Vilalva, 2023).

A elpidita ($Na_2ZrSi_6O_{15}\cdot 3H_2O$) é o zirconossilicato prevalente no Plúton Papanduva. Este mineral se cristaliza no sistema ortorrômbico, com estrutura inicialmente atribuída ao grupo espacial *Pbm* e posteriormente refinada para *Pbcm* (Zubkova et al., 2019). Embora estudos anteriores tenham abordado a ocorrência e aspectos gerais desse mineral (Vilalva, 2007; Oliveira, 2019), há uma demanda evidente por uma investigação textural e química detalhada a fim de se compreender mais profundamente esse zirconossilicato, assim como outras variedades mais ricas em potássio encontradas no plúton (e.g., Vilalva, 2007). Isso inclui a investigação das condições de sua cristalização, suas relações com outros minerais e os padrões de substituição e alteração pós-magmática.

1.1 Objetivos

Este estudo tem como foco a caracterização textural e química, englobando a composição de elementos maiores e traços, da elpidita e outros álcali-zirconossilicatos identificados no Plúton Papanduva. Com o intuito de alcançar o objetivo geral deste trabalho, foram estabelecidos objetivos específicos, a saber:

1. Identificar as distintas variações e gerações texturais da elpidita e de outros álcali-zirconossilicatos.
2. Analisar comparativamente, sob o prisma químico, as diferentes gerações desses zirconossilicatos, considerando tanto elementos maiores quanto traços.
3. Identificar padrões e produtos de alteração dos zirconossilicatos.
4. Efetuar análises quimiográficas para correlacionar as assembleias mineralógicas observadas e as teoricamente esperadas, enfocando zirconossilicatos nas rochas em estudo.
5. Deduzir as condições que propiciaram a formação da elpidita e demais álcali-zirconossilicatos nos granitos peralcalinos do Plúton Papanduva.

1.2 Área de estudo

A área de estudo está situada na divisa entre os estados de Paraná e Santa Catarina, abrangendo os municípios de Tijucas do Sul e Guaratuba (PR). A mesma

está enquadrada nas seguintes folhas topográficas: SG.22-X-D-V-3 (Pedra Branca do Araraquara, IBGE) e SG.22-X-D-IV-4 (Tijucas do Sul, Serviço Geográfico do Exército. O acesso à área se dá, partindo de Curitiba (PR), pela rodovia federal BR-376 e estradas vicinais (Figura 1.1).

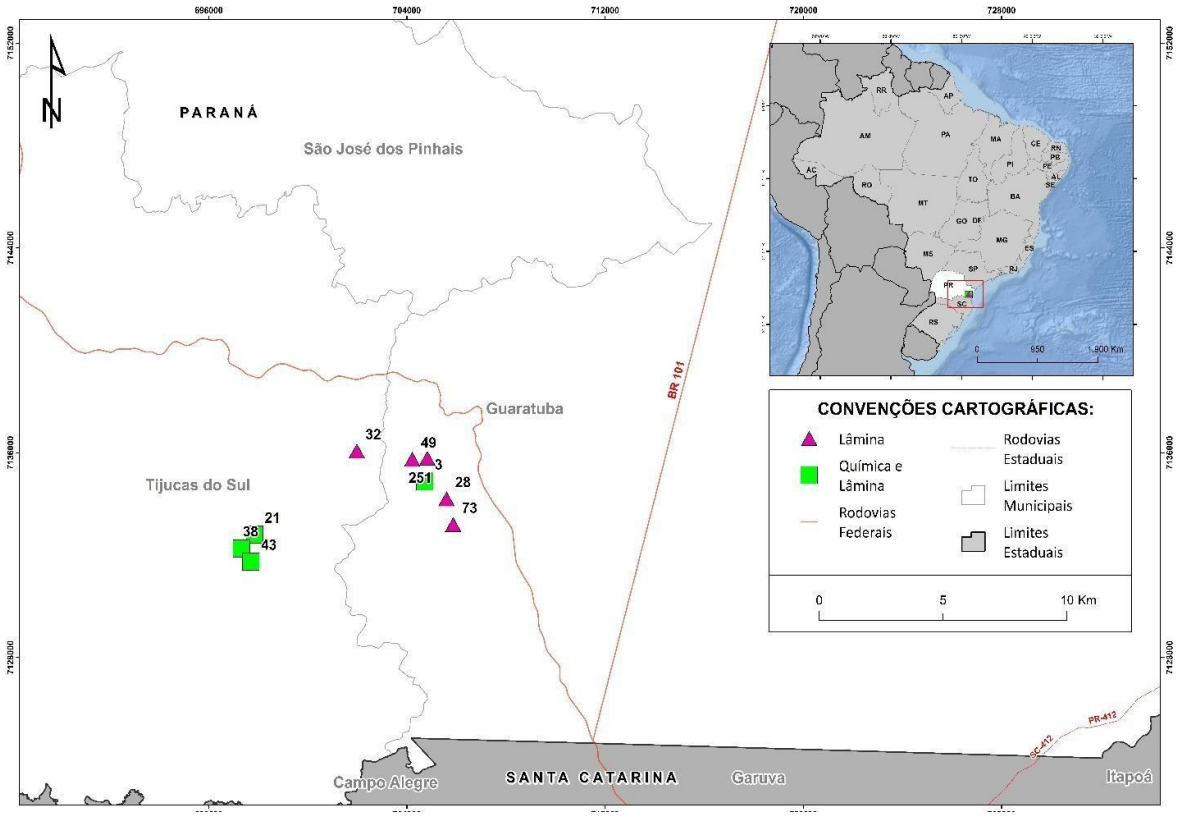

Figura 1.1- Mapa de Localização da área de estudo.

1.3 Estrutura da Dissertação

Esta dissertação está estruturada em quatro capítulos, a saber: (1) introdução e objetivos; (2) revisão bibliográfica sobre a ocorrência de zirconossilicatos em rochas peralcalinas silícicas; Os materiais e métodos serão apresentados no capítulo (3) na forma de um artigo científico, que será submetido a periódico indexado com os resultados texturais e químicos para a elpidita e outros zirconossilicatos do plúton Papanduva, bem como discussões e conclusões; e, por fim, (4) considerações finais.

2. REVISÃO BIBLIOGRÁFICA: ZIRCONOSSILICATOS EM ROCHAS PERALCALINAS SILÍCICAS

Este capítulo se destina a fornecer uma visão abrangente dos sistemas magmáticos peralcalinos, definir os termos *agpaíticos* e *miasquítico*, e apresentar um panorama geral da mineralogia do zircônio, particularmente os principais álcalis-zirconossilicatos, nessas rochas.

2.1 Mineralogia do zircônio em rochas peralcalinas

De forma geral, o mineral zircão é o principal hospedeiro de Zr na maioria das rochas ígneas. A cristalização deste mineral em magmas silícicos é controlada por vários fatores, incluindo a concentração de Zr, a composição dos elementos maiores, conteúdo de voláteis no magma e a temperatura (Watson & Harrison, 1983; Andersen et al., 2010). Entretanto, em algumas rochas félsicas muito evoluídas, tipicamente peralcalinas, o zircão é, notavelmente, ausente, apesar da alta concentração de Zr. Nestes casos, o Zr encontra acomodação em (Na,K,Ca)-silicatos complexos de Zr, vários dos quais estão listados na Tabela 1 (Sörensen, 2006; Khomyakov, 1995; Salvi & Williams-Jones, 1995; Schilling et al., 2009; Andreeva, 2016; Estrade *et al*., 2018; Andersen et al., 2010; Marks et al., 2011).

Tabela 2. 1 Alguns silicatos portadores de Zr em rochas de afinidade alcalina

Minerais de Zircônio		Fórmula	Rochas em que ocorrem	Exemplos de Ocorrência
zircão		$ZrSiO_4$	Diversos tipos de rochas	diversos sienitos e granitos alcalinos
fases de Na	catapleiita 1	$Na_2\ Zr(Si_3O_9)\cdot 2H_2O$	rochas graníticas e sieníticas	Monte Saint Hilaire (Canadá)/Strange Lake (Canadá), Complexo Ilímaussaq (Groenlândia), Complexo Evisa (Córsega), Maciço Passa Quatro (Brasil)
	elpidita	$Na_2ZrSi_6O_{15}\cdot 3H_2O$	rochas graníticas e sieníticas	Plúton Papanduva (Brasil), Monte Saint-Hilaire (Canadá), Monte Malosa (Malawi), Co
	parakeldyshita	$Na_2ZrSi_2O_7$	Rochas Sieníticas	Maciço Khibiny (Rússia), Monte Saint-Hilaire (Canadá)
	vlasovita	$Na_2ZrSi_4O_{11}$	Rochas Sieníticas	Complexo Alcalino Kipawa, (Canadá)
	gaidonnayita	$Na_2Zr(Si_3O_9)\cdot 2H_2O$	Rochas Sieníticas	Monte Saint-Hilaire (Canadá), Maciço Alcalino de Poços de Caldas (Brasil)
	Hilairita	$Na_2Zr[SiO_3]_3\cdot 3H_2O$	Rochas Sieníticas	Monte Saint-Hilaire (Canadá)
	Eudialita	$Na_{15}Ca_6Fe_3Zr_3Si(Si_{25}O_{73})(O,OH,H_2O)_3(Cl,OH)_2$	Rochas Graníticas e Sieníticas	Straumsvola (Antartica), Khibiny e Lovozero (Russia), Complexo Poços de Caldas (Brasil), Complexo Alcalino Ambohimirahavavy (Madagascar)
	Townendita	$Na_8ZrSi_6O_{18}$	Rochas Sieníticas	Ilímaussaq (Groenlândia)
fases de Ca	Gittinsita	$CaZrSi_2O_7$	Rochas Graníticas e Sieníticas	Complexo Alcalino Kipawa, (Canadá), Complexo Alcalino Shuangshan (China), Complexo Khan Bogd (Mongólia)
	Armstrongita	$CaZr[Si_6O_{15}]\cdot 3H_2O$	Rochas Graníticas e Sieníticas	Complexo Khan Bogd (Mongólia), Complexo Strange Lake (Canadá)
fases de K	Wadeita	$K_2Zr(Si_3O_9)$	Rochas Sieníticas	Complexo Poços de Caldas (Brasil), Maciço

				Khibiny (Rússia)
	Dalyita	$K_2ZrSi_6O_{15}$	Rochas Sieníticas	Complexo Strange Lake (Canadá), Complexo Amis (Namíbia)
	Kostylevita	$K_2Zr(Si_3O_9) \cdot H_2O$	Rochas Sieníticas	Maciço Khibiny (Rússia)
fases de Na-Ca	Lovozerita	$Na_2Ca(Zr,Ti)(Si_6O_{12})[(OH_4O_2]\cdot H_2O$	Rochas Sieníticas	Monte Saint-Hilaire (Canadá), Complexo Ilímaussaq (Groenlândia)
	låvenita	$Na_2Ca_2Mn_2Zr_2(Si_2O_7)_2O_2F_2$	rochas sieníticas	Complexo Evisa (Córsega), Complexos Alcalinos de Poços de Caldas e Itatiaia (Brasil)
	rosenbuschita	$Na_6Ca_6Zr_3Ti(Si_2O_7)_4O_2F_6$	rochas sieníticas	Complexo Poços de Caldas (Brasil), Complexo Alcalino de Monchique (Portugal)
	hiortdahlita	$Na_2Ca_4(Ca_{0,5}Zr_{0,5})Zr(Si_2O_7)2OF_3$	rochas sieníticas	Complexo Alcalino Kipawa (Canadá), Complexo Alcalino de Itatiaia (Brasil), Complexo Strange Lake (Canadá)
	Wöhlerita	$Na_2Ca_4ZrNb(Si_2O_7)_2O_3F$	Rochas Sieníticas	Monte Saint-Hilaire (Canadá), Suíte Monte de Trigo (Brasil), Complexo Alcalino de Búzios (Brasil)
fases de K-Na	Georgechaoita	$NaKZr[Si_3O_9] \cdot 2H_2O$	Rochas Sieníticas	Maciço Khibiny (Rússia), Complexo de Poços de Caldas (Brasil)
	Melansonita	$Na\square KZrSi_8O_{19}\cdot 5H_2O$	Rochas Sieníticas	Monte Saint-Hilaire (Canadá)

Rochas peralcalinas são aquelas com razão molar (Na + K)/Al > 1 e incluem tanto vulcânicas quanto plutônicas, insaturadas, saturadas e supersaturadas em sílica (Le Maitre, 2003; Frost & Frost, 2008; Marks & Markl, 2017). Como importante característica química, essas rochas são, em geral, enriquecidas em elementos litófilos de raio iônico grande (LILE; e.g., Na, K, Li), halógenos (F, Cl), terras-raras (ETR) e elementos de alto potencial iônico (HFSE; e.g., Zr, Ti, Nb, Hf).

As rochas peralcalinas são divididas em *agpaíticas* e *miasquíticas* (Khomyakov, 1995; Sørensen, 1997; Le Maitre, 2003). No primeiro caso, em face do enriquecimento extremo em álcalis, LILE, HFSE, ETR e halógenos durante a diferenciação magmática, tem-se a formação de diversos álcali-minerais raros, estruturalmente complexos e portadores de HFSE e ETR, em especial aqueles do grupo da eudialita. Já no caso das rochas miasquíticas, zircão e titanita são os principais minerais que particionam HFSE (Sørensen, 1997; Le Maitre, 2003; Andersen et al., 2010; Marks et al., 2011; Marks & Markl, 2017).

Embora os termos *miasquítico* e *agpaítico* terem sido definidos e seu uso é recomendado especificamente para rochas sieníticas peralcalinas (Sørensen, 1997; Le Maitre, 2003), é fato que diversas outras rochas alcalinas descritas na literatura, incluindo granitos e pegmatitos peralcalinos, possuem assembleias agpaíticas e miasquíticas (Marks et al., 2011; Vilalva et al., 2013; Estrade et al., 2014; Vlach & Vilalva, 2023). Desta forma, este trabalho segue a proposta de Marks & Markl (2017; ver também Marks et al., 2011; Vlach & Vilalva, 2023, Vlach & Gualda, 2007) para se referir aos granitos peralcalinos do plúton Papanduva portadores de álcali-silicatos de Zr e Ti como “agpaíticos” e aqueles portadores de zircão, ilmenita± titanita como “miasquíticos”.

A diferenciação mineralógica entre rochas agpaíticas e miasquíticas está intrinsecamente ligada a parâmetros geoquímicos e intensivos, como f_{O2}, $a$$SiO_2$, peralcalinidade, atividade de voláteis e $a$$H_2O$ dos líquidos magmáticos (Andersen et al., 2010; Marks et al., 2011; Bernard, 2020), bem como, durante estágios pós-magmáticos, de parâmetros como salinidade e o pH dos fluidos hidrotermais (Gysi et al., 2016; Marks & Markl, 2017). Condições de formação de rochas agpaíticas envolvem ambientes inicialmente reduzidos (abaixo do tampão QFM: quartzo-faialita-magnetita), baixo $a$$H_2O$ e altas salinidades, inibindo a formação de minerais portadores de FeO, levando à cristalização de anfibólios alcalinos e piroxênios, o que resulta em aumento da peralcalinidade e diminuição do $a$$SiO_2$, gerando altos teores de halogênios e grandes quantidades de HFSE. Em contrapartida, as rochas miasquíticas requerem elevada f_{O2}, (entre os tampões QFM e HM: hematita-magnetita) promovendo alta $a$$H_2O$ resultando na exsolução precoce de fluidos, empobrecendo os líquidos peralcalinos em halogênios, HFSE e ETR, tornando as rochas miasquíticas menos concentradas em metais raros em comparação com suas equivalentes agpaíticas (Migdisov et al., 2016).

Linthout (1984) observou que a solubilidade do Zr é maior em ambientes com excesso de álcalis. Em magmas peralcalinos, o Zr permanece no líquido até o final da

cristalização, quando é incorporado nas estruturas dos zirconossilicatos ou de piroxênios e/ou anfibólios sódicos. Essa característica resulta em temperaturas de cristalização relativamente baixas para álcali-zirconossilicatos (Currie & Zaleski, 1985; Marr & Wood,1992). Contudo, há de ressaltar que, embora mais comuns, assembleias minerais agpaíticas não estão restritas a estágios tardi-magmáticos, uma vez que as condições necessárias para sua estabilização podem ser atingidas também em estágios magmáticos precoces e estágios hidrotermais (cf. Marks & Markl, 2017).

Adicionalmente, Linthout (1984) e Cegielka *et al* (2022) enfatizam que em sistemas peralcalinos, a percolação de fluidos estágios pós-magmáticos/hidrotermais pode desestabilizar os zirconossilicatos (AZrS), resultando na liberação de álcalis e precipitação de zircão, conforme a equação 2.1 a seguir:

$$(Na, K)_2ZrSiO_5 = ZrSiO_4 + (Na,K)_2O \qquad \text{(Eq. 2.1)},$$

(AZrS) Zircão álcalis

Onde a composição do AZrS se relaciona com a fórmula geral desses minerais $(Na,K)_2ZrSiO_5.nSiO_2$ (Linthout, 1984). A partir desta mesma reação, é possível observar que sob excesso de álcalis, o zircão se desestabiliza formando álcali-zirconossilicatos.

2.2 Principais Álcalis-Zirconossilicatos em Assembleias Agpaíticas

Os álcali-zirconossilicatos (AZrS) predominantes em rochas agpaíticas pertencem ao grupo da eudialita (EGM, *Eudialyte Group Minerals*). São ciclossilicatos ricos em Na, com a fórmula geral $(Na_{15}Ca_6Fe_3Zr_3Si(Si_{25}O_{73})(O,OH,H_2O)_3(Cl,OH)_2$. Atualmente, existem 27 espécies minerais válidas para este grupo. A notável diversidade de membros no EGM é uma consequência da complexidade composicional e estrutural inerente a este grupo (Rastsvetaeva & Chukanov, 2012; Chukanov et al., 2015).

Todos os EGM exibem simetria romboédrica, enquadrando-se no grupo espacial R3*m*. A feição característica distintiva deste grupo é a presença de ciclos de três e nove tetraedros $[SiO_4]$, cuja disposição ao longo do eixo C forma a base estrutural fundamental (Johnsen et al., 2003)

Uma associação mineral de importância significativa que envolve AZrS é exemplificada no Complexo de Strange Lake, Canadá (Salvi & Williams-Jones, 1995). Este complexo compreende plútons graníticos peralcalinos distribuídos em três áreas

concêntricas altamente diferenciadas, totalizando 36km². Dentre os zirconossilicatos enriquecidos em Na, Ca e K presentes nesse complexo, aqueles com cristaloquímica mais complexa cristalizam nas fases magmáticas tardias, sob temperaturas mais baixas, ou em estágios pós-magmáticos (Siégel et al., 2018; Vasyukova & Williams-Jones, 2019). Incluem-se aqui a elpidita, gittinsita ($CaZrSi_2O_7$), armstrongita ($CaZr[Si_6O_{15}]\cdot 3H_2O$), catapleita ($Na2ZrSi3O9.\ 2H_2O$), Ca-catapleita ($CaZrSi_3O_9.\ 2H_2O$), dalyita ($K_2ZrSi_6O_{15}$), hilairita ($Na_2ZrSi_3O_9.3H_2O$), vlasovita ($Na_2ZrSi_4O_{11}$), zircão, dentre outros Siégel et al. (2018 e referências citadas).

No complexo Strange Lake, a elpidita é ortomagmática e apresenta relações complexas com outros AZrS, aparecendo, por vezes, pseudomorfoseada para gittinsita e quartzo. A armstrongita é fase tipicamente secundária, como um produto da desestabilização da elpidita primária (Salvi & Williams-Jones, 1995). De fato, a maioria dos AZrS no Complexo Strange Lake, especialmente as ricas em Ca, como gittinsita, é de origem secundária, resultante de intenso metassomatismo envolvendo fluidos ortomagmáticos e hidrotermais ácidos, promovendo a troca Na-Ca e a mobilização de Zr, ETR e outros elementos (Roelofsen & Veblen, 1999; Salvi & Williams-Jones, 2006; Gysi et al., 2016). Similarmente, o Complexo de Khan Bogd (Mongólia) registra padrões análogos, com a elpidita desestabilizando-se inicialmente, seguida pela formação de armstrongita, gittinsita e zircão, de acordo com as reações a seguir (Kynicky *et al*, 2011):

$$\underset{\text{elpidita I}}{Na2ZrSi6O15\cdot 3H2O} + xCa2+ \Leftrightarrow \underset{\text{elpidita II (x = 0.2–0.6) ou armstrongita (x = 1,0)}}{(Na2-2xCax)ZrSi6O15\cdot 3H2O} + 2xNa+$$

$$\underset{\text{elpidita I}}{Na2ZrSi6O15\cdot 3H2O} + Ca2+ + 5H2O \Leftrightarrow \underset{\text{gittinsita}}{CaZrSi2O7} + 2Na+ + 4(H4SiO4)aq$$

$$\underset{\text{armstrongita}}{CaZrSi6O15\cdot 3H2O} + 5H2O \Leftrightarrow \underset{\text{gittinsita}}{CaZrSi2O7} + 4(H4SiO4)aq \quad (3)$$

$$\underset{\text{elpidita I}}{Na2ZrSi6O15\cdot 3H2O} + 6H2O + 2H+ \Leftrightarrow \underset{\text{zircão}}{ZrSiO4} + 5(H4SiO4)aq + 2Na+$$

A análise de de seis complexos alcalinos distintos: Amis (Namíbia), Evisa (Corsica), Khan Bogd (Mongolia), Strange Lake (Canadá) e Ambohimirahavavy e

Manongarivo (Madagascar), realizada por Bernard (2020), revelou que os EGM e a elpidita não coexistem no mesmo estágio em um dado complexo. Tal fato pode ser atribuído às condições específicas de cristalização, uma vez que os EGM requerem uma faixa restrita de concentração de Na e temperaturas superiores a 440ºC, enquanto a elpidita cristaliza a temperaturas inferiores a 380ºC. Ademais, Borst et al. (2016) ao comparar a formação de EGM e gittinsita, destacaram a relevância da aH_2O na precipitação dessas fases.

No Brasil, diversos zirconossilicatos são descritos em sienitos e fonolitos agpaíticos do Complexo Alcalino de Poços de Caldas, MG (Ulbrich et al., 2005), incluindo minerais do grupo da eudialita, wöhlerita, hiortdahlita, låvenita, rosenbuchita, catapleíta, gaidonnayita, georgechaoíta, hilairita, wadeíta, dentre outros (cf. revisões em Gomes et al., 2021). Outras importantes ocorrências de minerais do grupo da eudialita, wöhlerita, hiortdahlita, låvenita, dentre outros, incluem os sienitos da suíte alcalina Monte de Trigo (Enrich et al., 2016) e dos complexos alcalinos de Itatiaia (Melluso et al., 2017) e Passa Quatro (Guarino et al., 2019).

No Plúton Papanduva, a elpidita é o principal zirconossilicato identificado. Além disso, uma fase mais potássica foi também identificada por Vilalva (2007). Outras ocorrências de elpidita no Brasil incluem Poços de Caldas (e.g. Gomes et al., 2021) e em granitos peralcalinos da Suíte Intrusiva Ouro Fino, Rondônia (Buch, 2018).

2.3 Elpidita: Aspectos Gerais e Cristaloquímica

A elpidita é um zirconossilicato de fórmula química ideal $Na_2ZrSi_6O_{15}.\ 3H_2O$. Suas cores macroscópicas variam de incolor e branco até tonalidades bege-amareladas, e seu hábito prismático é comum. Apresenta dureza 5 e clivagem perfeita em {110}. Ao microscópio petrográfico, sob luz transmitida, a elpidita exibe caráter biaxial (+) e birrefringência (δ) máxima de 0.014.

A simetria ortorrômbica da elpidita a classifica no grupo espacial *Pbcm*, e seus parâmetros da cela unitária *a, b* e *c*, são, respectivamente, 7,11, 14,68 e 14,60 Å (Cametti et al., 2016). A estrutura cristalina, elucidada por Canillo et al. (1973), é constituída por duas cadeias duplas de tetraedros de Si (sítios T na Figura 2.1) interconectadas por octaedros de Zr (sítios B na Figura x.x). O sódio ocupa dois sítios de coordenação independentes: um sítio de coordenação [VI] (sítios A na Figura 2.1.),

integrante da cadeia, e interstícios na estrutura compartilhados com moléculas de H_2O (figura 2.1).

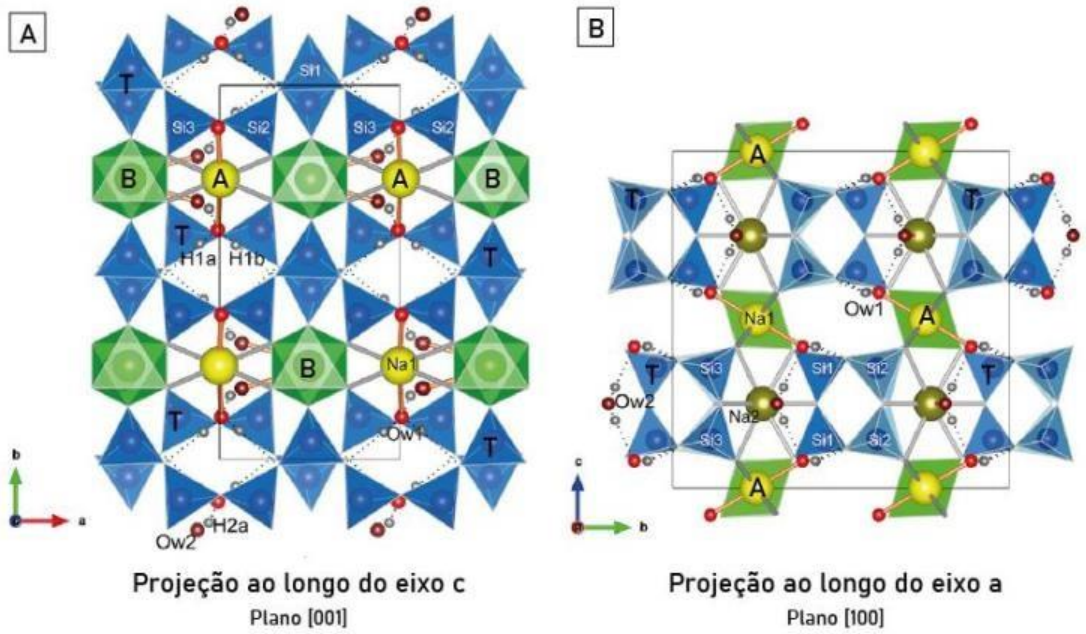

Figura 2.1 Estrutura cristalina da elpidita . A) Projeção ao longo do eixo cristalino c. B) Projeção ao longo do eixo a. Sítio T – tetraedros azuis. Sítio A – esferas amarelas. Sítio B – octaedros verdes. Interstícios na estrutura são preenchidos por Na (esferas amarelo-escuras) e H_2O (pequenas esferas em cinza e vermelho). Extraído de Cametti et al. (2016).

Seguindo a classificação hierárquica dos silicatos de Day e Hawthorne (2020), a elpidita é um silicato em fita ("*ribbon silicate*") com uma polimerização tetraédrica unidimensional. A fita $[Si_6O_{15}]^{6-}$ na elpidita se estende ao longo do eixo *a* , com fitas adjacentes interconectadas por poliedros de Zr e Na, formando uma estrutura aberta. O radical Si-O tem a designação $^3T_6$, onde T significa "tetraedro", 3 é a conectividade do tetraedro e 6 é o número destes tetraedros na unidade geométrica de repetição (cf. Bogdanov et al., 2021).

Em experimentos conduzidos por Currie e Zaleski (1985), foi observado que a elpidita é estável em temperaturas entre 595 ºC e 400 ºC considerando 1Kbar de pressão. Acima dessas temperaturas, seria esperada a paragênese vlasovita+quartzo, enquanto nas temperaturas mais baixas, ocorrem Ca-zirconossilicatos formados pela desestabilização da elpidita.

A elpidita demonstra uma notável capacidade de trocas catiônicas, onde íons de K e Rb são facilmente incorporados à estrutura do mineral, mesmo em baixas temperaturas (90-185ºC), devido à presença de “cavidades zeolíticas” na estrutura cristalina, refletindo em uma excelente microporosidade gerada durante a desidratação do mineral, que ocorre a uma temperatura mínima de 75 ºC (Cametti *et al.*, 2016; Grigor’eva et al., 2011). Além disso, durante o processo de perda da molécula de H_2O, uma transição significativa do grupo *Pbcm* para *Cmce* é observada a partir de ~100 ºC, com a estrutura tornando-se anidra em ~225 ºC (Cametti *et al.,* 2016*;* Kostov-Kytin *et al.,* 2020).

3. ARTIGO CIENTÍFICO SUBMETIDO À PERIÓDICO INDEXADO

EXPLORING THE LATE- TO POST-MAGMATIC CRYSTALLIZATION OF ELPIDITE AND (Na,K)-ZIRCONOSILICATES IN PERALKALINE GRANITES: INSIGHTS FROM THE PAPANDUVA PLUTON, SOUTH BRAZIL

Larissa Praxedes Grangeiro[1*]; Frederico Castro Jobim Vilalva[1,2]; Silvio Roberto Farias Vlach[3]; Armando Lucas Souza de Oliveira[4]

[1]Programa de Pós-Graduação em Geodinâmica e Geofísica, Universidade Federal do Rio Grande do Norte. 59078-970, Natal-RN, Brazil.

[2]Departamento de Geologia, Centro de Ciências Exatas e da Terra, Universidade Federal do Rio Grande do Norte. R. das Engenharias, s/n. 59078-970, Natal-RN, Brazil

[3]Instituto de Geociências, Universidade de São Paulo. Rua do Lago, 562. 05508-080, São Paulo-SP, Brazil

[4]Programa de Pós-Graduação em Geociências (Mineralogia e Petrologia), Instituto de Geociências, Universidade de São Paulo. 05508-080, São Paulo-SP, Brazil

*corresponding author: larissapraxedes28@gmail.com

Abstract

This study investigates the textural, compositional, and paragenetic characteristics of zirconosilicates in the peralkaline granites of the Papanduva Pluton, southern Brazil. Three distinct elpidite textural types—euhedral crystals, granular aggregates, and vein-like aggregates—were identified, each exhibiting specific compositional variations. Additionally, two (Na,K)-zirconosilicate phases, (Na,K)ZrS-I and (Na,K)ZrS-II, were characterized based on their textural and compositional properties. Elpidite, the primary zirconosilicate, shows

compositional uniformity with variations in Zr, Al, and K. The (Na,K)-zirconosilicates are enriched in K relative to Na and display distinct compositional trends. (Na,K)ZrS-II exhibits a closer compositional affinity to melansonite, while (Na,K)ZrS-I represents a transitional phase between lower and higher K endmembers. Elpidite trace element analyses reveal depletion in most elements compared to zircon, with notable enrichments in Ba, Pb, and Sr. Elpidite also displays LREE depletion and HREE enrichment, contrasting with the HREE-dominated zircon. Textural relationships and compositional data suggest a complex evolution for zirconosilicates. Elpidite likely formed during late-magmatic stages, followed by the development of granular and vein-like varieties. The interaction with hydrothermal K-rich fluids, likely facilitated by sub-magmatic deformation, caused significant hydrothermal alteration, chemical remobilization (including HFSE and REE) and element incorporation, forming (Na,K)ZrS-I and (Na,K)ZrS-II from a precursor zirconosilicate, ideally elpidite.

KEYWORDS: Hydrothermal fluids; Elemental remobilization; Trace elements; Mineral chemistry

1. Introduction

Zirconium is a common trace element in igneous rocks, typically concentrated in early crystallizing minerals like zircon ($ZrSiO_4$). However, halogen- and alkali-rich environments can significantly increase Zr solubility in the melt, leading to its enrichment during later stages of crystallization (Linthout, 1984; Keppler, 1993). Under these conditions, Zr can be incorporated into clinopyroxenes and sodium amphiboles (Andersen et al., 2012) or form complex alkali-zirconosilicates (Borst et al., 2016; Estrade et al., 2018), particularly those belonging to the eudialyte group (Johnsen et al., 2003). Peralkaline granites and pegmatites can host a variety of additional zirconosilicates, including dalyite, wadeite, elpidite, catapleiite, and less commonly, gittinsite and armstrongite (Marks et al., 2011; Estrade et al., 2018).

The Papanduva Pluton, located near Tijucas do Sul, Paraná, southern Brazil, comprises peralkaline granites with distinct lithofacies (Vilalva & Vlach, 2014). The Zr-bearing mineralogy in these granites varies with their degree of evolution. Less evolved varieties contain zircon as the primary Zr mineral, while more evolved ones are enriched in Na- and K-rich zirconosilicates. These evolved varieties also exhibit an accessory mineralogy typical of agpaitic rocks (cf. Marks et al. 2011; Marks & Markl, 2017), including narsarsukite, astrophyllite, neptunite, nacareniobsite, britholite, and turkestanite (Vilalva, 2007; Vilalva & Vlach, 2010, 2014; Vilalva et al., 2013; Siachoque et al., 2022; Vlach & Vilalva, 2023).

Elpidite ($Na_2ZrSi_6O_{15}{\cdot}3H_2O$) is the dominant alkali zirconosilicate in the Papanduva Pluton. This mineral crystallizes in the orthorhombic system, initially assigned to the space

group Pbm and later refined to Pbcm (Zubkova et al., 2019) with unit cell parameters a = 7.11 Å, b = 14.68 Å, and c = 14.60 Å (Cametti et al., 2016). Its crystal structure (Canillo et al., 1973), consists of double chains of Si tetrahedra interconnected by Zr octahedra. Sodium occupies two independent coordination sites: a [VI] coordination site within the chain and interstitial spaces shared with H_2O molecules. According to hierarchical classification of silicates by Day and Hawthorne (2020), elpidite is a ribbon silicate with one-dimensional tetrahedral polymerization. The $[Si_6O_{15}]^{6-}$ ribbon extends along the a-axis, with adjacent ribbons interconnected by Zr and Na polyhedra, forming an open structure. The Si-O radical is designated as 3T6, where T stands for "tetrahedron," 3 for the tetrahedral connectivity, and 6 for the number of tetrahedra in the repeating unit (cf. Bogdanov et al., 2021).

Previous studies (Vilalva, 2007; Oliveira, 2019) identified the occurrence of elpidite and other alkali-zirconosilicates in the Papanduva Pluton but have not fully explored their complex formation conditions. This gap underscores the need for an in-depth textural and chemical analysis to provide valuable insights not only for understand the specific occurrence of elpidite within the pluton, but also for elucidating the broader controls on elpidite formation in peralkaline oversaturated melts and related post-magmatic fluids, as well as to clarify the interplay between Zr behavior, melt evolution, and the formation of complex Zr-bearing minerals in such environments. Therefore, this work aims to provide a detailed textural and chemical characterization of elpidite and other alkali-zirconosilicates from the Papanduva Pluton. We focus on major and trace element compositions and investigate alteration patterns and byproducts. Our findings are expected to shed light on the conditions that promote the formation of these minerals in peralkaline granites.

2. Geological Context

The Papanduva Pluton, located in the northern segment of the Morro Redondo Complex (southern Brazil), belongs to the Graciosa Province (Gualda & Vlach, 2007), a major Neoproterozoic (~580 Ma; Vlach et al., 2011) post-collisional magmatic province of A-type affinity (Fig 3.1). This province, extending along the Atlantic coastline includes a range of A-type granitic and syenitic plutons, along with minor basic and hybrid rocks, extending along the Atlantic coastline from southern São Paulo to northeastern Santa Catarina states, comprises a range of A-type granitic and syenitic plutons with minor basic and hybrid rocks (Vlach et al., 2011). Spanning ~100 km², the Papanduva Pluton represents the most evolved lithotypes within the Graciosa Province (Vilalva & Vlach, 2014). U-Pb zircon dating indicates an age of 580 ± 5 Ma (Vilalva et al., 2019) for the pluton, which intrudes Archean to Paleoproterozoic granulites and migmatitic gneisses of the Luis Alves Terrain (Basei et al., 2010; Quiroz-Valle et al., 2023; Vilalva & Vlach, 2014; Vilalva et al., 2019).

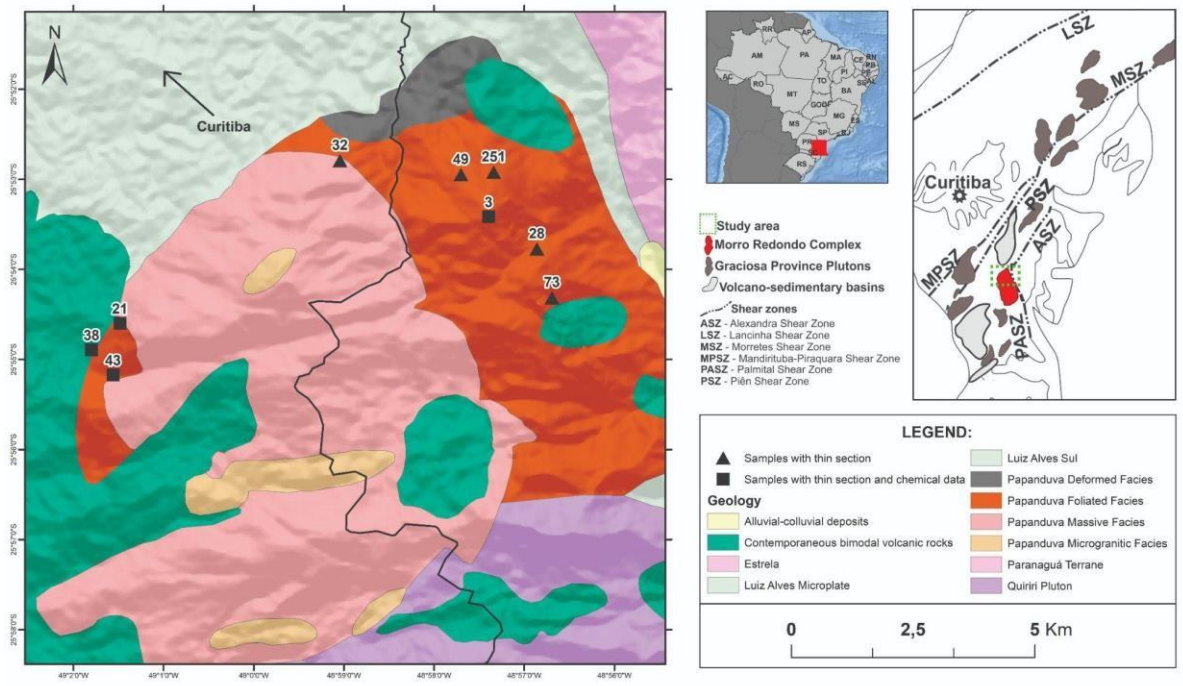

Fig 3.1 Geological setting of the studied granite. The study area is delimited by the green square and the samples with thin section represented by triangles while the samples with thin section and chemical datas represented by squares.

The pluton is predominantly composed of hypersolvus alkali-feldspar granites exhibiting diverse structures and textures. These granites are classified into four petrographic facies: massive (most common), cataclastic, foliated, and microgranular. These granites are characterized by an agpaitic-like crystallization sequence, in which the mafic minerals and most accessories precipitated after the felsic phases, filling the remaining interstices (Vilalva & Vlach, 2014; Vilalva et al., 2016). Key mafic minerals include Na-Ca and Na-amphiboles and clinopyroxenes, with zircon, chevkinite, astrophyllite, and aenigmatite as accessory minerals. Notably, in the foliated facies, zircon is replaced by elpidite, which is associated with other Zr-, Ti- and REE-bearing alkali-rich minerals (Vilalva & Vlach, 2014; Vilalva et al., 2013). Geochemically, these granites are classified as peralkaline and ferroan A-type granites (Table 3.1 summarizes some key chemical parameters).

Table 3.1 Relevant Chemical Parameters for the Peralkaline Granites of the Papanduva Pluton *(Data sourced from Vilalva & Vlach, 2014)*

Chemical Parameter	Range
SiO_2 (wt.%)	74 - 78%
Na_2O+K_2O (wt.%)	8.7 - 9.3%
FeOt/(FeOt+MgO) (wt.%)	0.96 - 1.0
agpaitic index [IA: $(Na_2O+K_2O)/Al_2O_3$ molar	1.04 - 1.28
Zr (ppm)	618 - 2697

The foliated facies, occurring along the pluton borders, display textures ranging from porphyroclastic to protomylonitic due to submagmatic deformation (Vilalva & Vlach, 2014; Vilalva et al., 2016). These textures are characterized by oriented megacrysts of mesoperthite, arfvedsonite, and quartz set within a fine-grained quartz-feldspathic matrix (Fig 3.2). Intense albitization, evident by ubiquitous post-magmatic albite laths, and widespread exsolution in alkali-feldspar have affected the foliated facies (as well as the other Papanduva facies). Notably, the foliated rocks exhibit the highest agpaitic indices and Zr contents (Table 3.1). This geochemical signature is reflected in their mafic mineral assemblage, which includes arfvedsonite and aegirine, and a unique Zr-, Ti-, and REE-bearing accessory mineralogy typical of agpaitic rocks (sensu Marks & Markl, 2017). Examples include elpidite, narsarsukite, nacareniobsite-(Ce), britholite-(Ce), neptunite, and turkestanite (Vilalva & Vlach, 2010; Vilalva et al., 2013; Vlach & Vilalva, 2023).

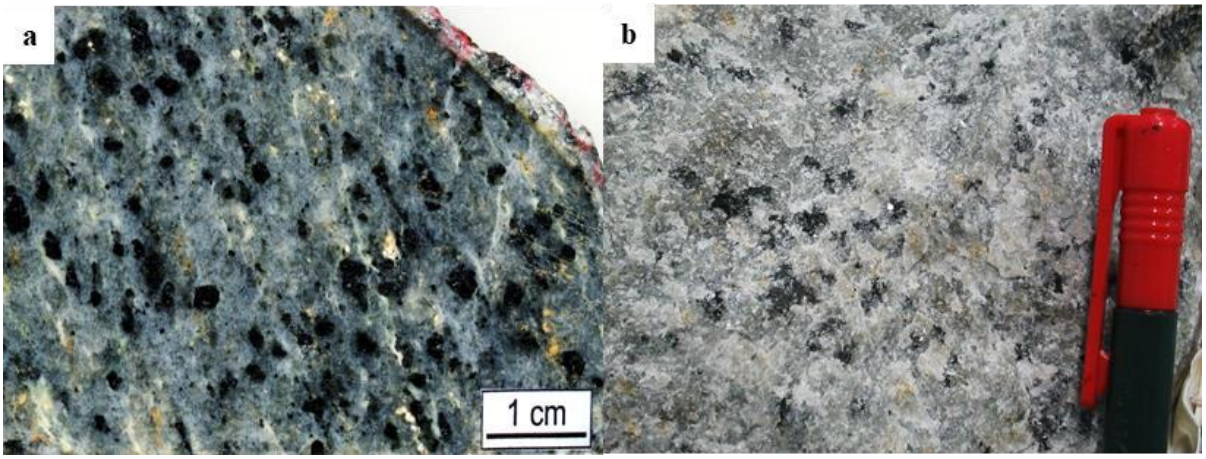

Fig 3.2 Macroscopic Textural Aspects of Zirconosilicate-bearing Granites from the Foliated Facies of the Papanduva Pluton (a) Protomylonitic Alkali-Feldspar Granite (Sample MR-03): This sample features megacrysts of arfvedsonite (black) along with oriented crystals and aggregates of narsarsukite and/or other zirconosilicates (white and yellow) set in a fine-grained quartz-feldspar matrix. (b) Porphyroclastic Alkali-Feldspar Granite (Sample MR-21): Characterized by arfvedsonite (black) and zirconosilicates and/or narsarsukite (yellow) embedded in a quartz-feldspar matrix exhibiting a saccharoidal texture. These descriptions highlight the distinctive textural features of the granites, which are key to understanding the petrographic characteristics of the foliated facies within the Papanduva Pluton

3. Materials and Methods

Ten thin sections of elpidite-bearing peralkaline granite (foliated facies) from key locations within the Papanduva Pluton were chosen for a detailed petrographic analysis, focusing specifically on their textural properties and crystallization sequence. Major element compositions of elpidite and other (Na,K)-zirconosilicates were determined using an Electron Probe Microanalyzer (EPMA) on 17 crystals selected from five of these samples at the GeoAnalítica Core Facility, Geosciences Institute, University of São Paulo, Brazil. Trace element analysis using Laser Ablation Inductively Coupled Plasma Mass Spectrometry (LA-ICP-MS) was conducted on 10 elpidite crystals from four additional samples at the same facility. Due to extensive alteration and the small grain size of the (Na,K)-zirconosilicates, obtaining reliable trace element compositions proved challenging. Nevertheless, the major element compositions of the (Na,K)-zirconosilicates offer valuable insights into their formation.

The EPMA analyses were performed using JEOL JXA-8600S and JXA-FE-8530 instruments under identical conditions: 15 kV, 10 nA and 30 µm for column accelerating voltage, beam current and diameter, respectively. Detailed information on the measured elements, analyzer crystals, spectral lines, count times, and calibration standards are presented in Table 3.2. Raw data correction for matrix effects and conversions to mass concentrations were performed using PROZA (Bastin and Heijligers, 1990) for the JXA-8600S, and the PRZ/Armstrong software for the JXA-FE-8530. All analyzed elements present detection limits below 0.01 wt%. Backscattered electron (BSE) images in compositional mode were acquired to assess intracrystalline chemical zoning. Structural formulae and cationic proportions for elpidite were calculated based on 15 oxygens and 6 Si (cf. Zubkova et al., 2020), following the ideal formula $Na_2ZrSi_6O_{15}\cdot 3H_2O$ (Cannillo et al., 1973). For the (Na,K)- zirconosilicates, calculations were performed assuming two structural models: 15 oxygens and 6 Si, or 19 oxygens and 8 Si per formula unit, According to the chemical formula of elpidite..

Table 3.2 Measured Elements, Analyzer Crystals, Spectral Lines, Counting Times, and Standards Used for WDS Analyses of Zirconosilicates from the Papanduva Pluton

Element	Cristal analisador	Spectral Line	Peak Count Time	Background Count Time	Analytical Standardss
Si	TAP	Kα	10s	5s	Zircon
Al	TAP	Kα	20s	10s	Anorthoclase

Fe	LIFL	Kα	10s	5s	Fayalite
Gd	LIFL	Lβ	20s	10s	Synthetic GdPO4)
Dy	LIFL	Lβ	20s	10s	Synthetic DyPO4)
Hf	LIFL	Lα	30s	15s	Zircon
Yb	LIFL	Lα	20s	10s	Synthetic YbPO4
K	PETJ	Kα	10s	5s	Orthoclase
Ca	PETJ	Kα	10s	5s	Wollastonite
P	PETJ	Kα	10s	5s	Fluoroapatite
Ti	PETJ	Kα	20s	10s	Rutile
Zr	PETJ	Lα	10s	5s	Zircon
Y	PETJ	Lα	20s	10s	Synthetic YPO4
Nb	PETJ	Lα	20s	10s	Ilmenite
Th	PETJ	Mα	30s	15s	Rhyolitic glass
Na	TAPH	Kα	5s	2,5s	Albite
F	TAPH	Kα	10s	5s	Fluoroapatite

LA-ICP-MS analyses (spot and raster mode) were conducted with a Thermo Scientific iCAP Q ICP-MS equipment coupled to a CETAC LSX-213 G2+ Laser Ablation system, following the procedures developed by Andrade (2016). Analytical conditions were 30 µm for beam diameter, energy fluence of 7.67 J/cm², and a repetition rate of 20 Hz. The total acquisition time was 80s (30s background, 50s signal). Calibration and quality control employed NIST SRM-610, GJ-Zircon and Zr-91500 standards, with elpidite SiO_2 contents (measured by EPMA) as the internal reference. Analytes included: ^{7}Li, ^{23}Na, ^{24}Mg, ^{27}Al, ^{31}P, ^{39}K, ^{42}Ca, ^{44}Ca, ^{45}Sc, ^{49}Ti, ^{51}V, ^{52}Cr, ^{55}Mn, ^{56}Fe, ^{59}Co, ^{66}Zn, ^{71}Ga, ^{85}Rb, ^{88}Sr, ^{89}Y, ^{91}Zr, ^{93}Nb, ^{95}Mo, ^{118}Sn, ^{121}Sb, ^{137}Ba, ^{139}La, ^{140}Ce, ^{141}Pr, ^{143}Nd, ^{147}Sm, ^{151}Eu, ^{157}Gd, ^{159}Tb, ^{161}Dy, ^{165}Ho, ^{166}Er, ^{169}Tm, ^{173}Yb, ^{175}Lu, ^{179}Hf, ^{181}Ta, ^{182}W, ^{206}Pb, ^{207}Pb, ^{208}Pb, ^{232}Th, and ^{238}U. Data reduction was performed using Glitter software (Griffin et al., 2008). Detection limits, accuracy, and precision are provided along with the analytical results in the Supplementary materials, to generate the graph correlating log(aNa2O) vs. log(aK2O), illustrating the stability regions for minerals such as zircon, aenigmatite, elpidite, and other relevant Na and K zirconosilicates, ChatGPT was used to analyze the thermodynamic data associated with the simplified chemical system Na2O-K2O-Al2O3-SiO2-H2O. This was achieved through the Schreinemaker analysis method for precise positioning and intersection of stability limits.

4. Results

4.1 Zirconosilicate microtextures and crystallization sequence

Detailed microscopic analysis of thin sections of the Papanduva Pluton foliated facies revealed three types of zirconosilicates: elpidite, and two (Na,K)-bearing varieties, (Na,K)ZrS-

I and (Na,K)ZrS-II. These zirconosilicates were absent in samples containing zircon. Elpidite

appears as isolated crystals or interstitial aggregates with colors ranging from light brown to pale yellow; darker hues suggest alteration into fine-grained secondary minerals. Elpidite exhibits a prismatic or tabular habits, low birefringence, and a biaxial (+) optical signal (Fig 3.3).

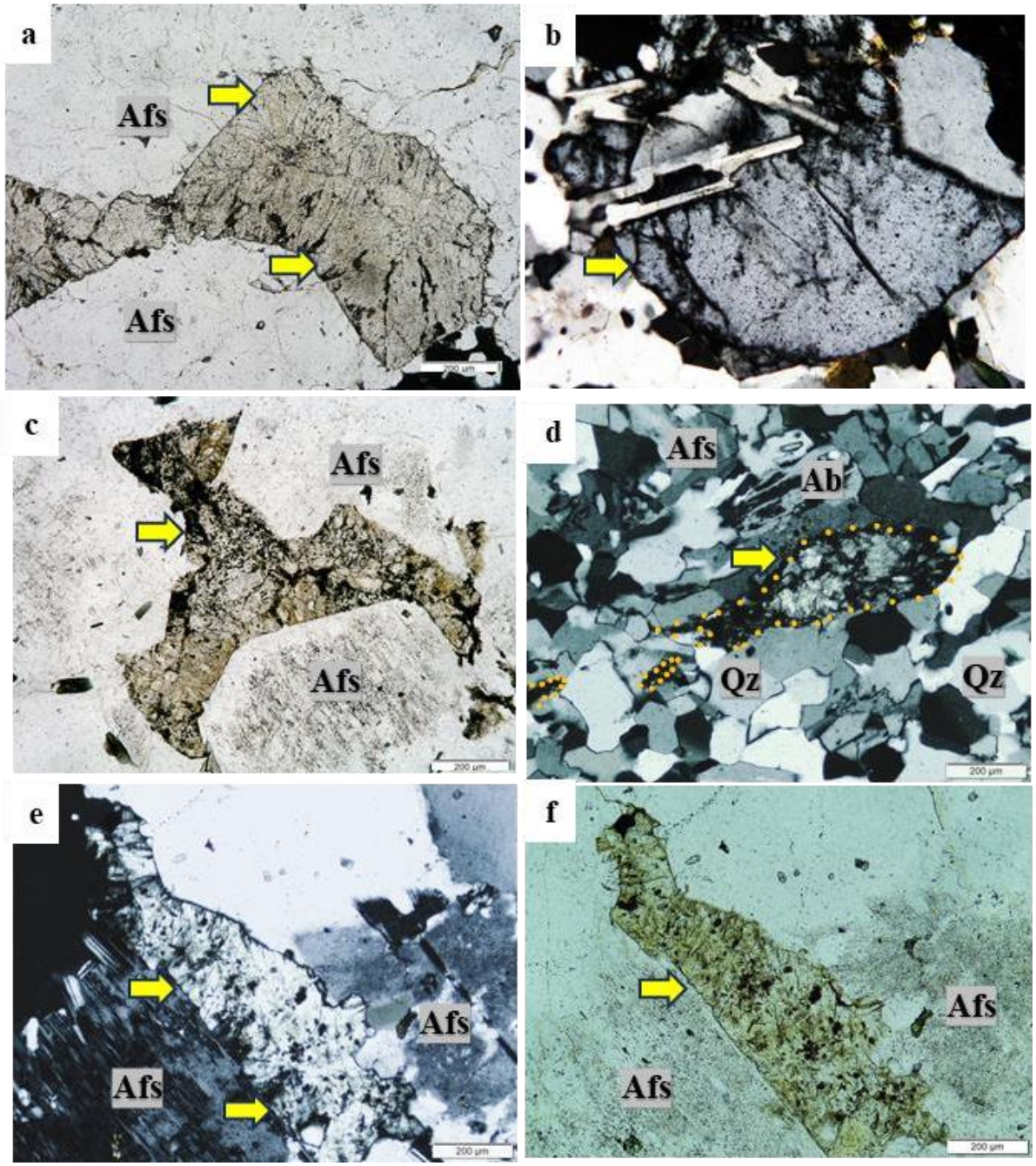

Fig 3.3 Textural Types of Elpidite Crystals in Thin Sections (a, b, c) Euhedral crystals of elpidite, representative of textural type I (Elp). (d) Vein-like aggregate of interstitial elpidite crystals among grains of quartz (Qz), alkali feldspar (Afs), and albite, representative of textural type III (Ab).(e, f) Aggregates of prismatic elpidite crystals interstitial to grains of quartz (Qz) and alkali feldspar (Afs), representative of textural type II.

Three textural types of elpidite were identified: (1) isolated subhedral to euhedral crystals with orthorhombic symmetry (Figs 3.4 and 3.5), (2) granular interstitial aggregates, and (3) vein-like aggregates aligned with the protomylonitic foliation. These types often coexist within single samples, particularly in hydrothermal alteration zones, where they show darker colors and may form pseudomorphs or be replaced by secondary minerals. Elpidite crystals range from 0.5 to 2.0 mm and are typically isolated and in contact with surrounding quartz and feldspar. In contrast, granular and vein-like aggregates exhibit slightly larger grains, between 1.0 and 2.0 mm, with distinct crystal boundaries (Fig 3.4).

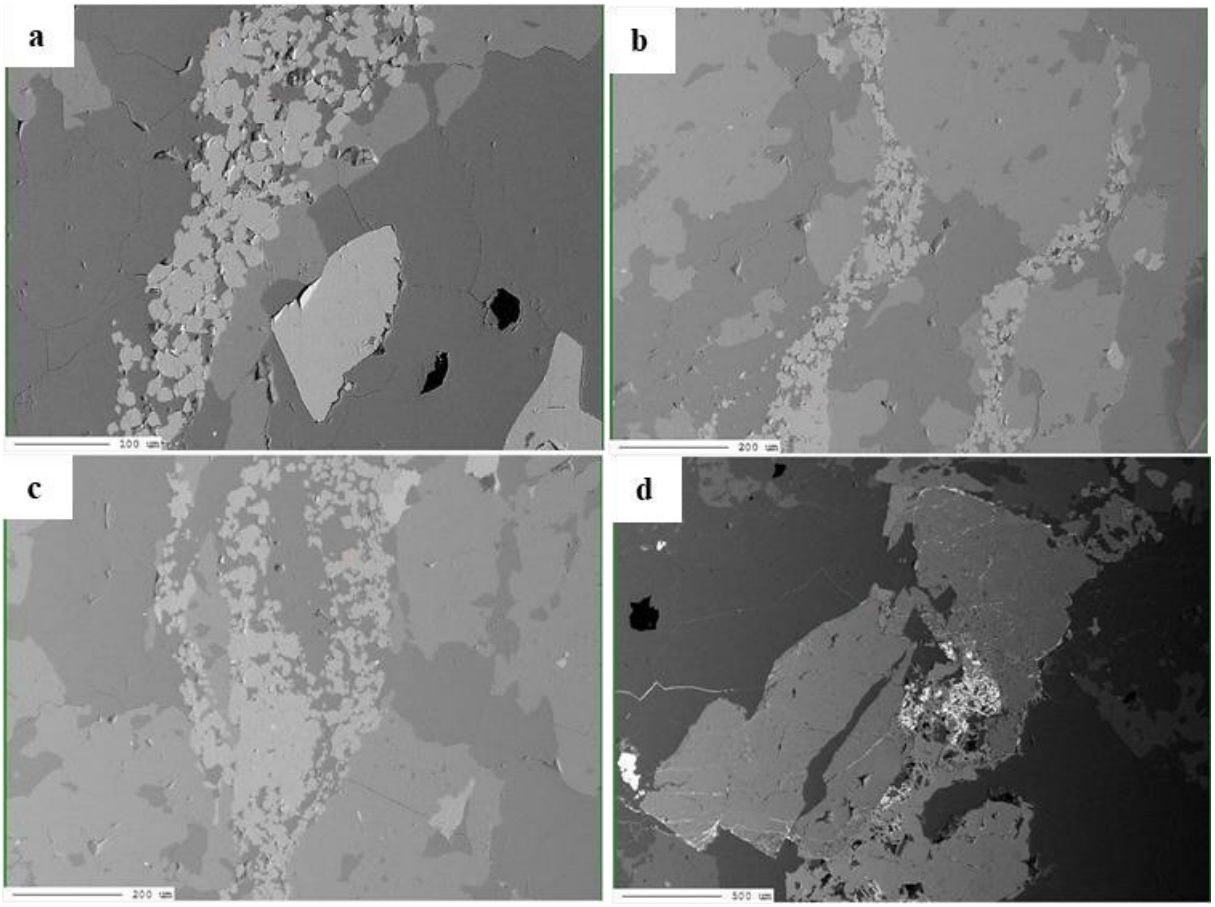

Fig 3.4 Backscattered Electron Images in Compositional Mode of Vein-like (a, b) and Granular (c, d) Aggregates of Elpidite Crystals from Samples MR-03 and MR-26

In some samples, elpidite coexists with (Na,K)-zirconosilicates. (Na,K)ZrS-I, found in sample MR-38, features euhedral crystals and pseudomorphs with monoclinic symmetry, high relief, low birefringence (δ~0.007), and concentric zoning, often enveloped by aegirine (Vilalva, 2007). (Na,K)ZrS-II, primarily in sample MR-26, consists of euhedral to subhedral crystals with tabular habit, orthorhombic symmetry and concentric zoning, distinguished from elpidite by its biaxial (-) optical character.

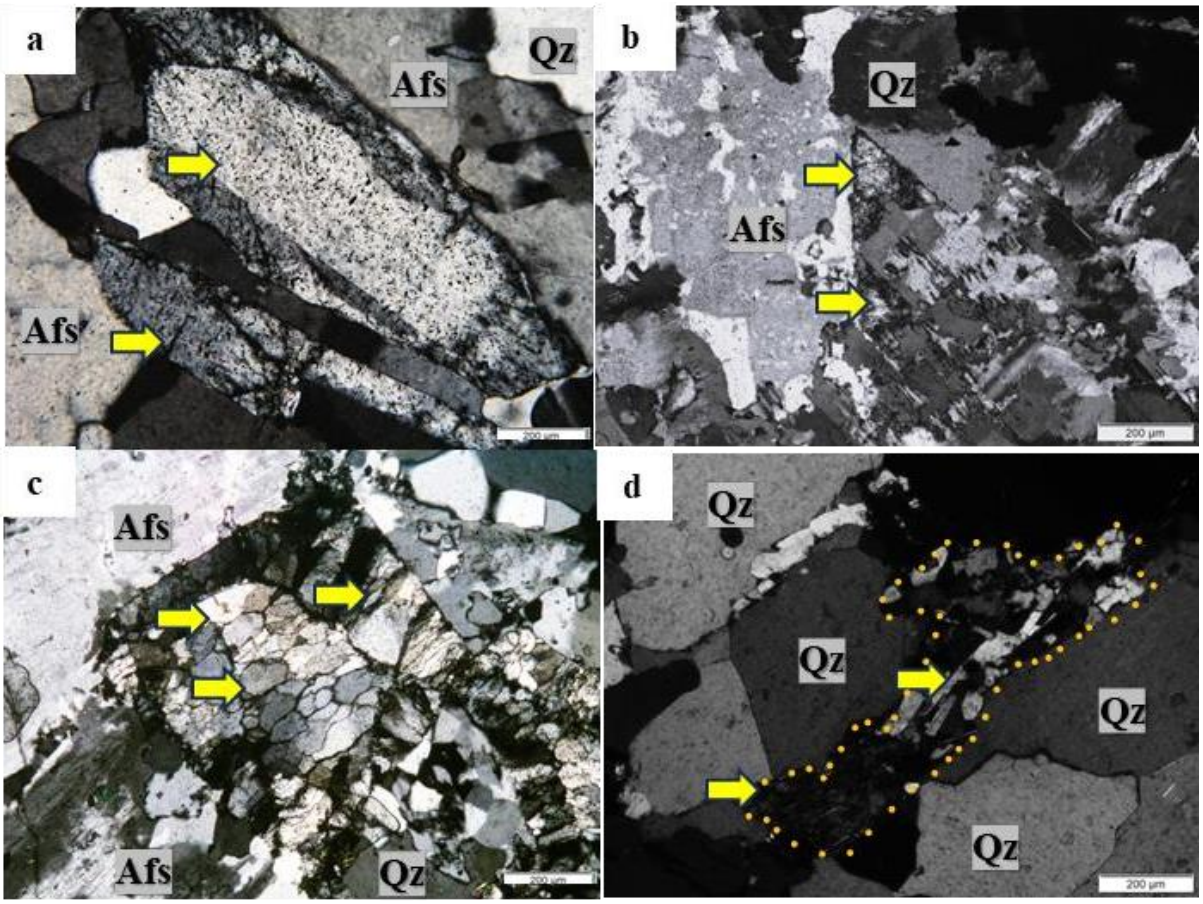

Fig 3.5 Detailed Visualization of Elpidite and (Na,K)-Zirconosilicate Phases (highlighted by the yellow arrow) (a, b) Display subhedral elpidite crystals (Elp), highlighting their distinct crystal forms and contacts with neighboring minerals. (c, d) Show aggregates of prismatic elpidite crystals interstitial to grains of quartz (Qz) and alkali feldspar (Afs). The boundaries between the elpidite grains are well-defined, underscoring their structured placement within the matrix

Textural analysis suggests elpidite and (Na,K)ZrS types crystallized during late-magmatic to post-magmatic stages. The vein-like aggregates paralleling the foliation likely formed earlier than granular interstitial ones, along with other Ti-Zr-bearing minerals. Euhedral crystals indicate late to post-magmatic crystallization, with (Na,K)ZrS-II typically forming during post-magmatic phases, along with albite, aegirine-augite, and REE-bearing minerals, following the submagmatic nature of the foliation (cf. Vilalva & Vlach, 2014; Vilalva et al., 2016). The crystallization sequence based on textural relationships is illustrated in Figure 3.6.

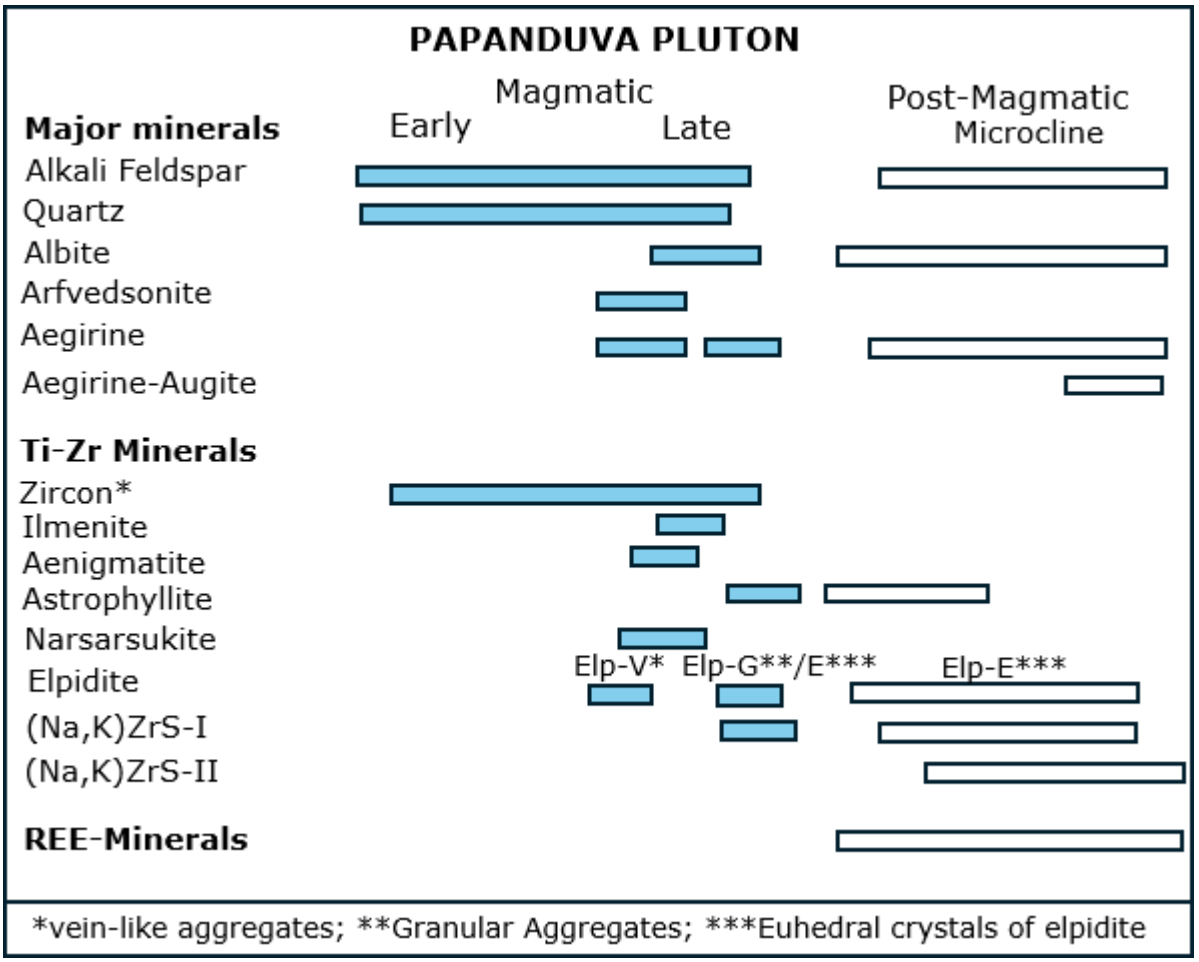

Fig 3.6 Interpreted crystallization sequence for the studied samples of the Papanduva plutons showing the mineral assemblages at early, late- and post-magmatic stages. Note that elpidite generations are grouped in elp-V, Elp-G, or Elp-E textural types

4.2 Major element compositional variations

4.2.1 Elpidite

Papanduva elpidite exhibits relatively uniform major element compositions, with variations mainly observed for Zr, Al and K (Fig 3.7): ZrO_2 content varies between 17.4 and 27.8 wt.% (0.856 - 1.438 cpfu), with the highest values found in euhedral crystals and vein-like aggregates of sample MR-21 (Fig 7). Notably, Na_2O (8.8-10.32 wt.%; 1.723 - 2.038 cpfu) and CaO contents (<0.01 - 0.24 wt.%; 0.026 cpfu) remain constant across all elpidite types. Euhedral crystals show slight enrichment in K_2O (up to 0.33 wt.%; 0.044 cpfu) compared to the other elpidite types (0.2 - 0.24 wt.%; 0.026 - 0.032 cpfu), whereas Al_2O_3 content increases significantly from vein-like aggregates (up to 0.13 wt.%; 0.015 cpfu) to euhedral crystals (up to 1.3 wt%.; 0.17 cpfu) and granular aggregates (up to 1.73 wt.%; 0.206 cpfu). The total elemental analysis range (86-95 wt.%) is consistent with the structural incorporation of three H_2O molecules.

Average structural formulas for each textural type are:

Type I (euhedral crystals): $(Na_{1.925}K_{0.017})_{\sum=1.943}\ Zr_{1.011}Si_6O_{15}\cdot 3H_2O$

Type II (granular aggregates): $(Na_{1.942}K_{0.01}Ca_{0.009})_{\sum=1.961}\ Zr_{1.014}\ Si_6O_{15}\cdot 3H_2O$

Type III (vein-like aggregates): $(Na_{1.879}K_{0.017}Ca_{0.009})_{\sum=1.904}Zr_{1.132}Si_6O_{15}\cdot 3H_2O$

The elpidite [B] site also accommodates minor Ti, Hf, REE, Y, and other trace elements. An excess of Zr (>1.0 cpfu) was observed, likely compensating for Si deficiency in the tetrahedral [T] site. This substitution mechanism was not directly considered, assuming the [T] site is considered solely filled by Si. The [A] site, hosting mainly Na, K and Ca, approaches the ideal stoichiometric value of 2.0 cpfu.

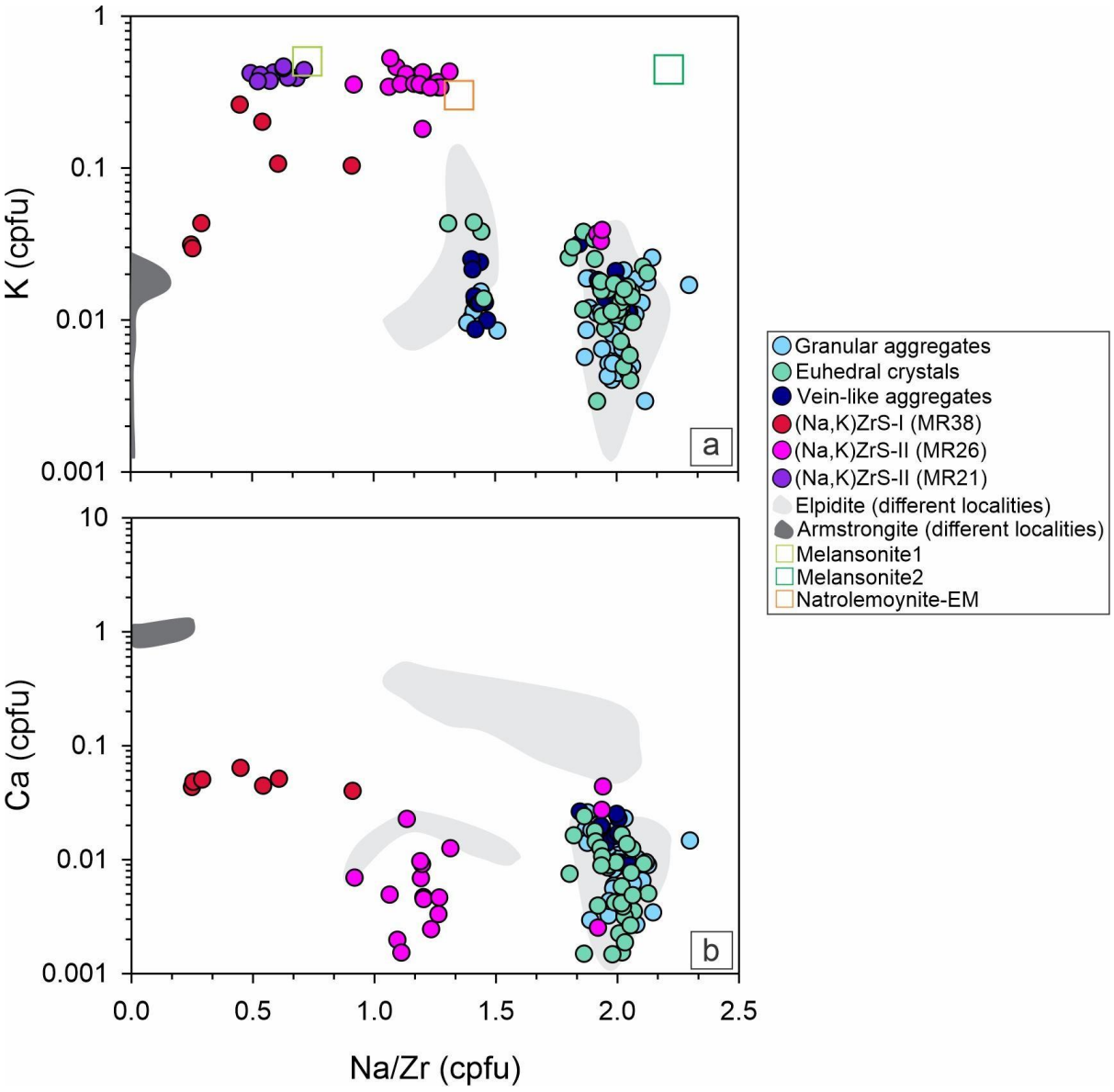

Fig 3.7 Binary diagrams correlating Na/Zr with (a) K and (b) Ca, presenting the composition of granular aggregates, euhedral crystals and vein-like aggregates of elpidite, (Na,K)ZrS-I from sample MR-38, and (Na,K)ZrS-II from samples MR-21 and MR-26 from the Papanduva Pluton, correlating with elpidite and armstrongite from different localities, as follows. Elpidite: Cegielka, 2022; Bonin, 1988; Bernarde, 2020; Vlasov, 1966; Birkett et al., 1992; Roelofsen & Veblen, 1999; Kynicky et al., 2011; Cametti et al., 2016; Salvi & Williams-Jones, 1995. Armstrongite: Roelofsen & Veblen, 1999; Gysi et al., 2015; Kynicky et al., 2011; Birkett et al., 1992; Mesto et al., 2014; Vladykin et al., 1973; Vladykin and Kovalenko, 2006; Jambor et al., 1987 and Jambor et al., 1988. Melansonite 1 data from Gore & McDonald 2023, melansonite 2 and natromelansonite data from Lykova et al. 2024

4.2.2 (Na, K)-Zirconosilicates-I and II

(Na,K)ZrS-I crystals and pseudomorphs from sample MR38 exhibit distinct compositional zones indicative of intense hydrothermal alteration (Fig 3.8). These are enriched in CaO (0.24 – 0.43 wt.%; 0.03 to 0.048 cpfu) and K_2O (0.19% to 1.48 wt.%; 0.022 to 0.196 cpfu) compared to unaltered regions. Conversely, Na_2O content shows a significant decrease (down to 1.31 - 4.13 wt%; 0.234 to 0.921 cpfu). ZrO_2 remains relatively constant (18.04% and 22.16 wt.%; 0.932 to 1.015 cpfu), while SiO_2 increases up to 65.25 wt.%. These compositional changes cause the altered zones to deviate from the typical elpidite compositions in Figure 7. The average structural formula is:

$$(Na_{0.46}K_{0.083}Ca_{0.037})_{\sum=0.58}\,Zr_{0.967}Si_6O_{15}{\cdot}nH_2O, \text{ where } n \geq 3$$

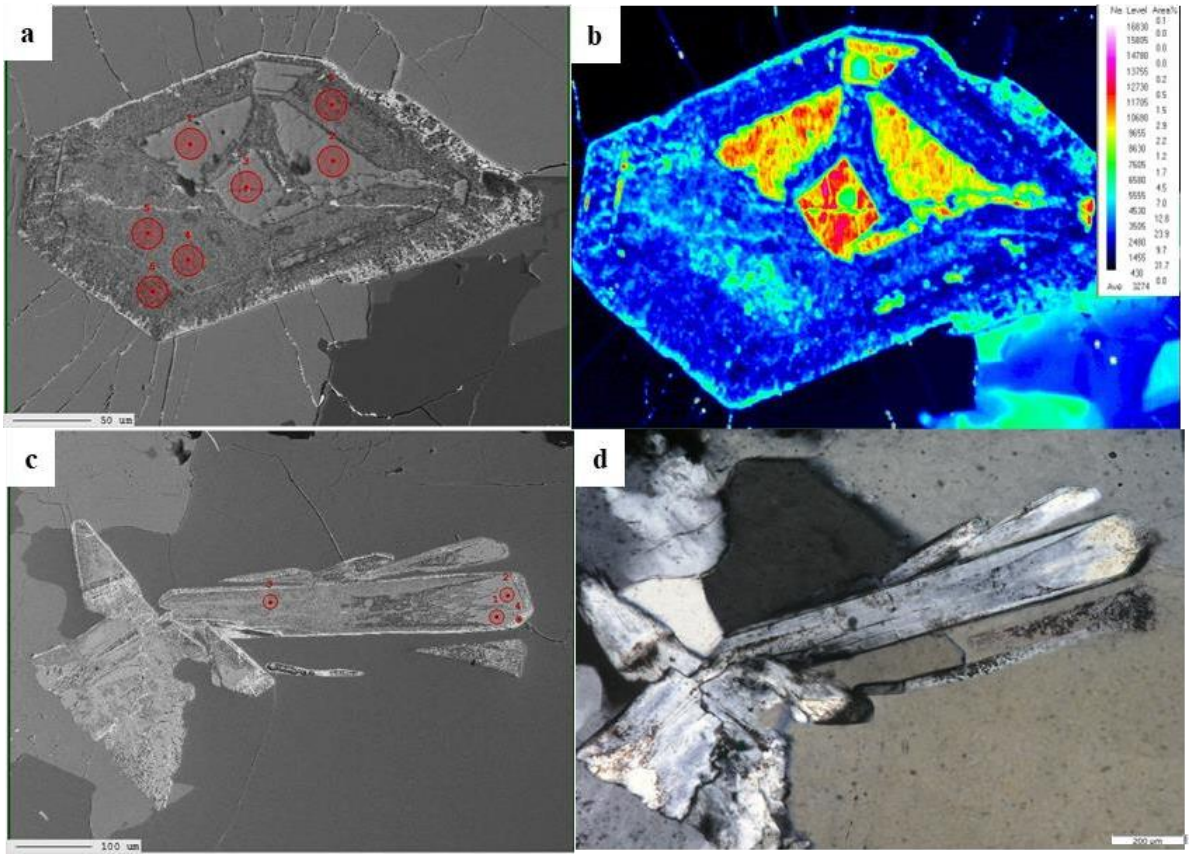

Fig 3.8 (a) Backscattered electron image in compositional mode of a pseudomorph with euhedral outlines of (K,Na)ZrS-I, partially included in aegirine, in sample MR38. Altered zones are characterized by higher K (and Ca) contents. White veins at the edges are enriched in Zr. Note also the radial fractures in aegirine filled with Zr-rich phases. (b) Backscattered electron image in compositional mode of euhedral pseudomorphs of elpidite of textural type 1 among quartz and alkali feldspar crystals in sample MR38. Analytical points 3 and 4 show relative depletion in Na and Si.(c) Detailed view of the pseudomorphs depicted in (b) under an electron microscope (crossed polarizers)

(Na,K)ZrS-II is characterized by higher K_2O contents, and exhibits distinct compositional variations between samples MR-26 and MR-21 (Fig. 3.7). In sample MR-26, K_2O crystals contents ranging from 0.19 to 3.14 wt.% (0.033 to 0.528 cpfu), Na_2O, from 3.48% to 8.93 wt.% (0.884 to 0.0235 cpfu), and ZrO2 from 13.89% to 18.35 wt.% (0.887 to 1.216 cpfu). Additionally, lower chemical analysis closure (87 - 90 wt.%) suggests reduced water content in these crystals. This observation aligns with Grigor'eva et al. (2011), who propose that K cations preferentially occupy water molecule sites in the zirconosilicate structure, leading to decreased water content

In contrast, (Na,K)ZrS-II crystals from MR-21 exhibit higher ZrO_2 content (17.31-22.77 wt.%, 1.156-1.507 cpfu), the highest observed in this study. K_2O content remains substantial (2.08-2.66 wt.%, 0.373-0.466 cpfu), while Na_2O content decreases (2.69-3.24 wt.%, 0.713-0.862 cpfu) (Fig. 3.7). CaO values are negligible. Notably, crystals from MR-21 exhibit a maximum analysis closure of 87%, indicating potentially higher water content relative to MR-26 crystals.

The average structural formula are:

MR-26: $(Na_{1.325}K_{0.324}Ca_{0.008})_{\sum=1.657}\,Zr_{1.018}Si_8O_{19}{\cdot}nH_2O$, where $n \geq 3$

MR-21: $(Na_{0.794}K_{0.414})_{\sum=1.208}\,Zr_{1.33}Si_8O_{19}{\cdot}nH_2O$, where $n \geq 3$

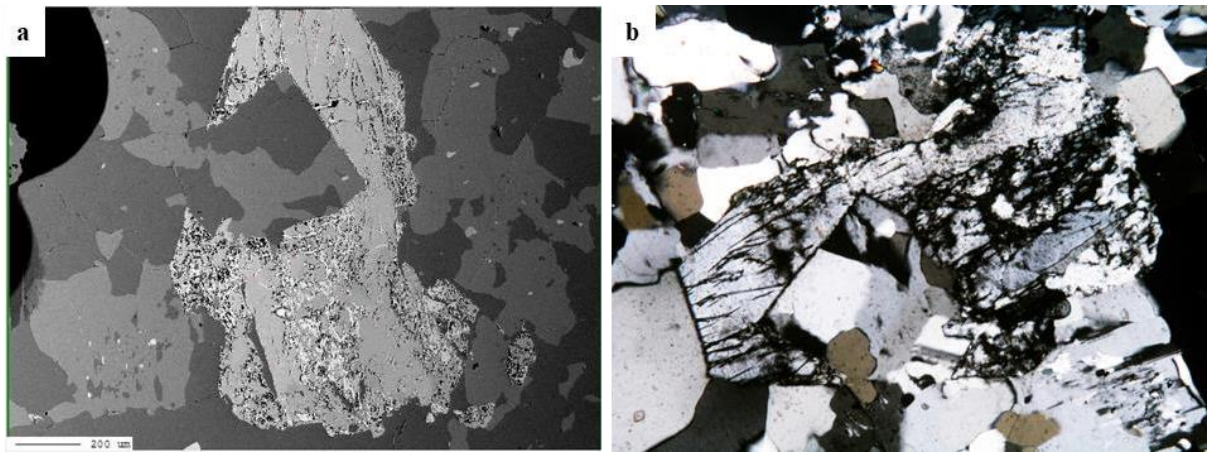

Fig 3.9 (a) Backscattered electron image in compositional mode of a euhedral crystal with prismatic habit and orthorhombic symmetry of (K,Na)ZrS-II from sample MR26. Note the altered parts in the

central zone of the crystal, appearing as lighter shades. (b) Detail of the crystal depicted in (a) under a petrographic microscope (crossed polarizers). Note the straight contact with quartz crystals

4.3 Trace element compositions

Trace element (TE) and rare-earth element (REE) compositions of elpidite types are presented in Figure 3.10 alongside the zircon patterns from the Papanduva massive facies. Compared to zircon, elpidite exhibits depletion in most elements except Ba, Pb, and Sr, which are enriched in all types, with vein-like and granular aggregates showing the highest concentrations (Figs. 3.10a & 3.10c). Similarly, elpidite is REE-depleted compared to zircon (Figs, 3.10b, 3.10d, 3.10f) and displays LREE depletion and HREE enrichment with a positive Eu anomaly (La/Yb < 0.932; Eu/Eu* = 0.116-1.565). Euhedral elpidite (Fig. 3.10f) has the lowest median REE contents (539 ppm), while higher LREE (comparable to zircon) are found in granular aggregates (271ppm; Fig. 3.10d) and HREE in vein-like ones (1971 ppm). Notably, two vein-like elpidite analyses exhibit LREE contents similar to zircon (Fig. 3.10b).

Zircon and elpidite show contrasting trends in HREE enrichment. Zircon displays a steady increase in HREE content (Yb/Gd)N ratios between 7.9 and 10.1 from Gd to Lu, reflecting its role as the primary host for HREEs during early magmatic stages. Conversely, elpidite shows a trend of relative HREE depletion (Yb/Gd)N between 0.6 and 6.5) throughout the HREE series.

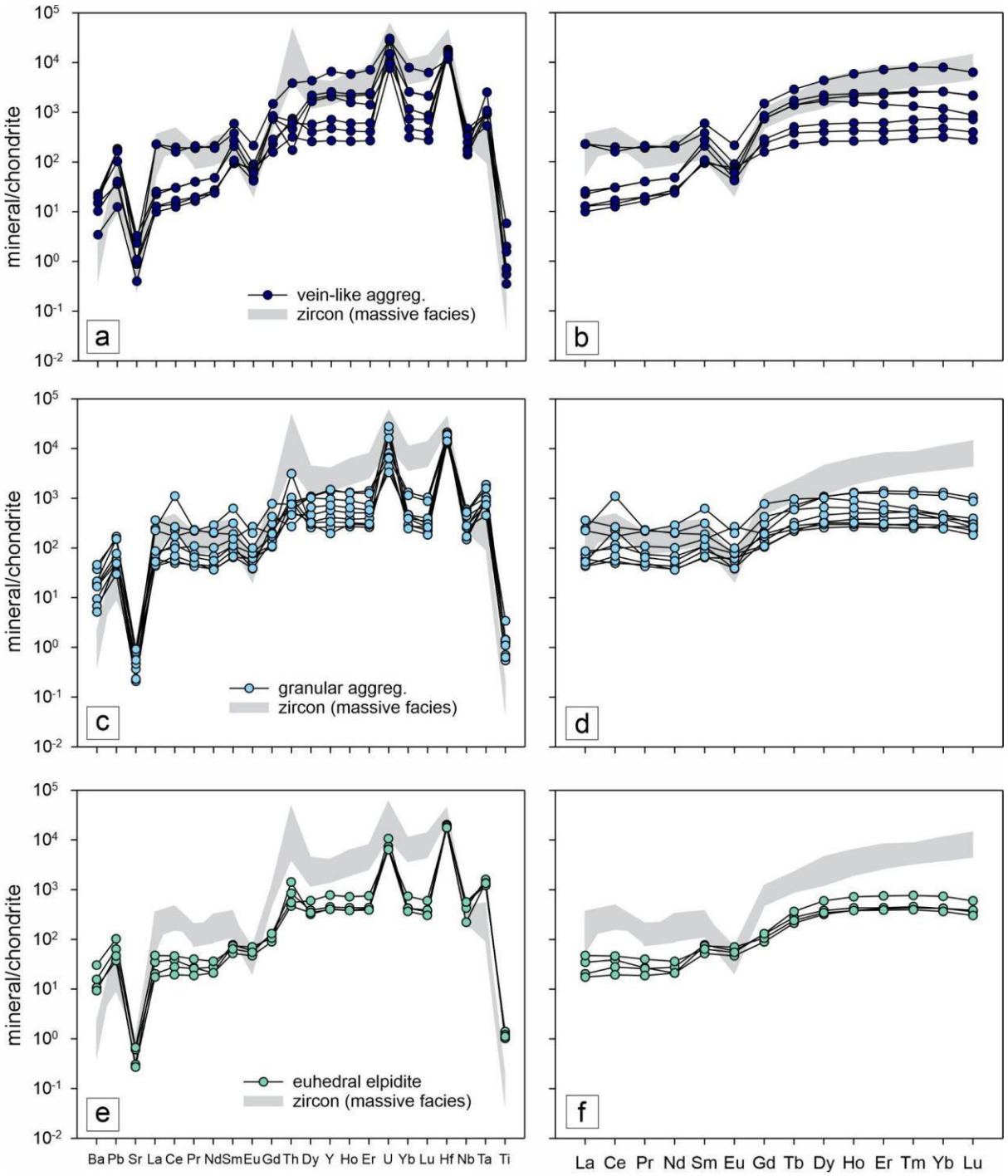

Fig 3.10 median (a) trace element and (b) REE distribution patterns for elpidite from the Papanduva pluton. The patterns of the zircon in the whole rock are also represented for comparison. Trace element concentrations normalised to the CI chondrite

Figure 3.11 reveals positive correlations of HREEs with Ca and K, and negative correlations with Na and Zr (measured during ablation experiments). This suggests that elpidite crystallization was influenced by the availability of these elements, possibly reflecting the influence of fluid-induced hydrothermal alteration on HREE mobility during late- to post-magmatic stages. Furthermore, these correlations are consistent with a coupled substitution mechanism (Fig 3.12) expressed as:

$$Zr^{4+} + 2Na^{+} \rightarrow Ca^{2+} + K^{+} + HREE^{3+} \qquad \text{Eq.3.1}$$

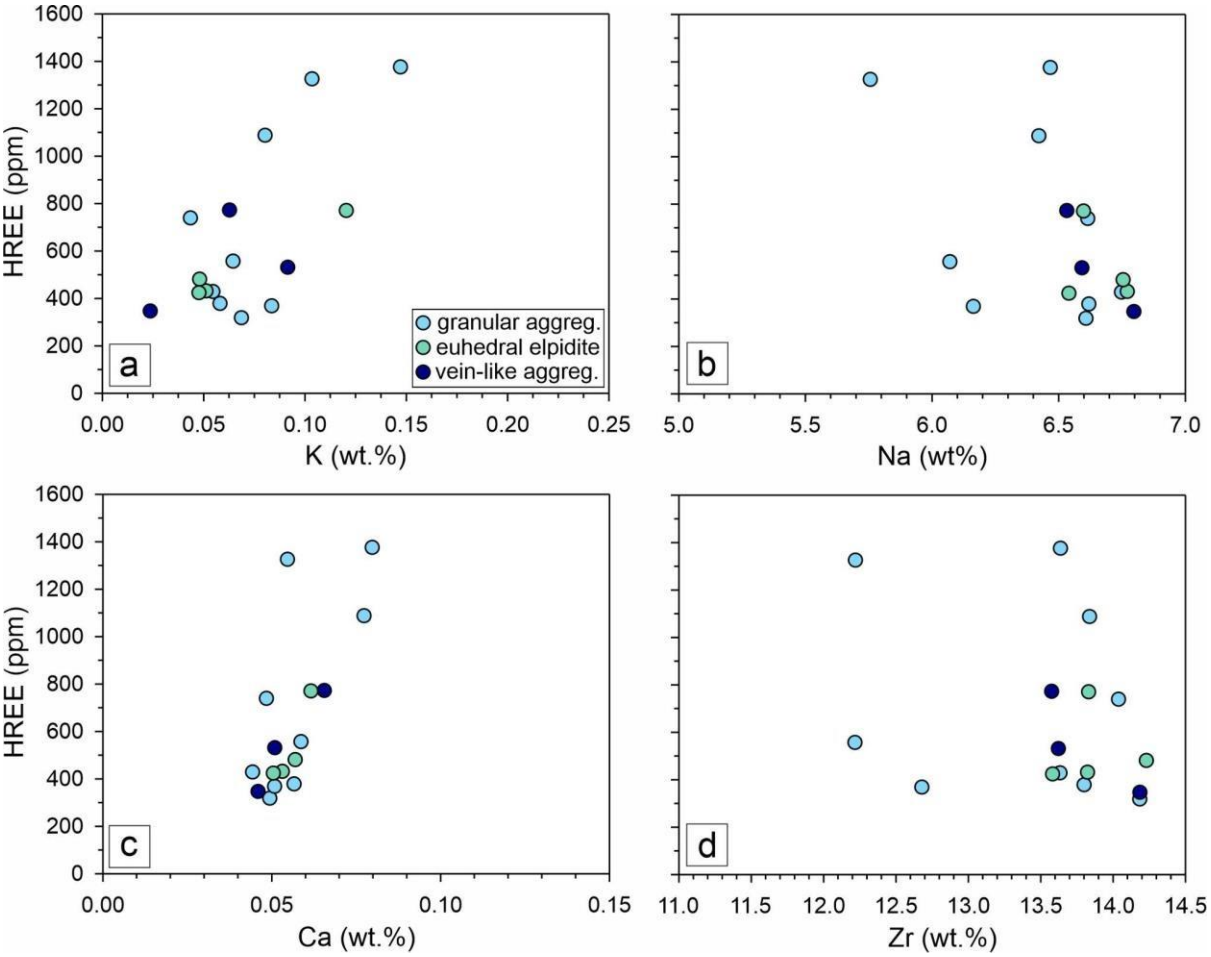

Fig 3.11 Binary diagrams showing the correlation between heavy rare earth elements (HREE) and the contents of (a)K, (b) Na, (c)Ca, and (d) Zr in elpidites from the Papanduva Pluton. The legend indicates three types of aggregates: granular aggregates (light blue circles), euhedral elpidite (green circles), and vein-like aggregates (dark blue circles)

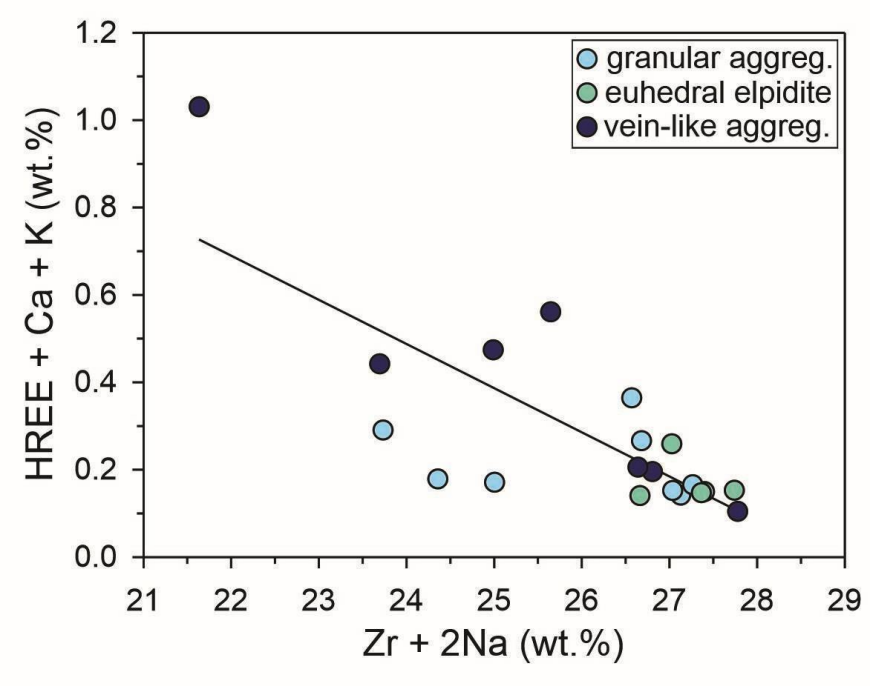

Fig 3.1 Binary diagram between HREE+Ca+K (wt.%) and Zr + 2 Na (wt.%) showing the coupled substitution mechanism between the elements in elpidite crystals from the Papanduva Pluton

5. Discussion

5.1 Compositional Variations of Papanduva Zirconosilicates and Comparison with Other Occurrences

To understand the relationships among zirconosilicates in the Papanduva Pluton, we employed binary and ternary elemental variation diagrams, integrating data from the literature on elpidite and other relevant zirconosilicates (Bonin, 1988; Roelofsen and Veblen, 1999; Salvi & Williams-Jones, 1995; Kynicky et al., 2011; Gysi et al., 2015; Cegielka, 2022). The binary diagrams (Figure 3.7) show that the composition of elpidite from the Papanduva Pluton largely aligns with those documented elsewhere. Both euhedral and aggregate forms of elpidite display overlapping compositions, indicating a consistent increase in K while Na levels remain steady, suggesting a specific evolutionary trajectory in mineral composition relevant to their crystallization environment and processes.

Notably, the Zr-rich crystals from sample MR-21 exhibit compositions similar to elpidite in peralkaline granites and pegmatites from the Khan Bogd Complex, Mongolia (Kynicky et al., 2011), particularly in terms of K and Na, yet they lack the typical Ca enrichment observed in Khan Bogd samples. The Papanduva elpidite shows minimal variation in Ca content, contrasting with other occurrences where calcium enrichment, parallel to decreasing Na, shifts compositions toward the armstrongite endmember. This has prompted some authors to propose a potential solid solution between elpidite and armstrongite (Roelofsen and Veblen,

1999; Mesto et al., 2014; Bernard, 2020). However, this view is contested by Bogdanov et al. (2021), who note that the structural formula of the second endmember, although similar to armstrongite, crystallizes in the C2/m space group, indicating a fundamentally different structural type.

The coherence in composition among different forms of elpidite from the Papanduva Pluton, both in euhedral and aggregate forms, as well as in comparative literature instances, underscores a consistent trend of increasing potassium while maintaining stable sodium levels. This compositional consistency supports interpretations of their crystallization environment and processes.

Papanduva (Na,K) zirconosilicates are characterized by higher K and lower Na contents, with Ca levels comparable to those of elpidite (Figure 3.7). Grigor'eva et al. (2011) suggest that in elpidite, K may preferentially replace water molecules within the crystal structure rather than substituting for Na, potentially explaining the observed reduction in water content. The K contents in (Na,K)ZrS-II are nearly constant, aligning closely with the compositions of melansonite (Gore & McDonald, 2023) and natrolemoynite (McDonald & Chao, 2001; Figure 3.7a), and exhibit a slight increase in Ca concurrent with Na depletion, as observed in other elpidite samples (Figure 3.7b). Conversely, (Na,K)ZrS-I from sample MR-38 shows intermediate K levels with a generally positive correlation with Na, indicating a compositional continuum with armstrongite and suggesting a transitional phase that bridges the gap between lower and higher K contents.

Figure 3.13 illustrates average REE patterns for Papanduva elpidite compared to elpidite from the Khan Bogd Complex (KBC), Mongolia (Kynicky et al., 2011). In both locations, rocks precipitating elpidite lack primary zircon. Papanduva elpidite exhibits lower REE contents, particularly in light REEs (LREE), with a marked enrichment in heavy REEs (HREE) over LREE, as demonstrated by the upward trend from LREEs to HREEs. Conversely, KBC elpidite maintains a relatively stable and consistent LREE pattern, with smoother transitions and more pronounced Eu anomalies. Notably, HREE enrichment correlates with an increase in Ca content, alongside K in Papanduva, suggesting that hydrothermal activity predominantly drives REE remobilization (see also Bernard, 2020).

Kynicky et al. (2011) describe the KBC formation environment as influenced by a combination of extreme fractional crystallization and hydrothermal alteration. This process involved alkali feldspar, quartz, and ferromagnesian silicates, enhancing the peralkalinity index and Zr content. Post-magmatic alterations, significant in remobilizing high field strength elements (HFSE) as observed in other peralkaline complexes (e.g., Boily & Williams-Jones,

1994; Schmitt et al., 2002), involved the release of silica-saturated orthomagmatic fluids interacting with a calcic, CO_2–F-rich fluid, altering the geochemical signatures of the minerals. This alteration resulted in the replacement of the primary magmatic phase of elpidite by Ca-rich zirconosilicates such as armstrongite and gittinsite, along with calcite, fluorocarbonates, and fluorite. Similarly, calcic metasomatism involving CO_2–F-rich fluids has been proposed as the primary mechanism for the replacement of elpidite and remobilization of HFSE and REE at the Strange Lake Complex (Salvi & Williams-Jones, 1995, 2006; Roelofsen & Veblen, 1999; Gysi et al., 2016).

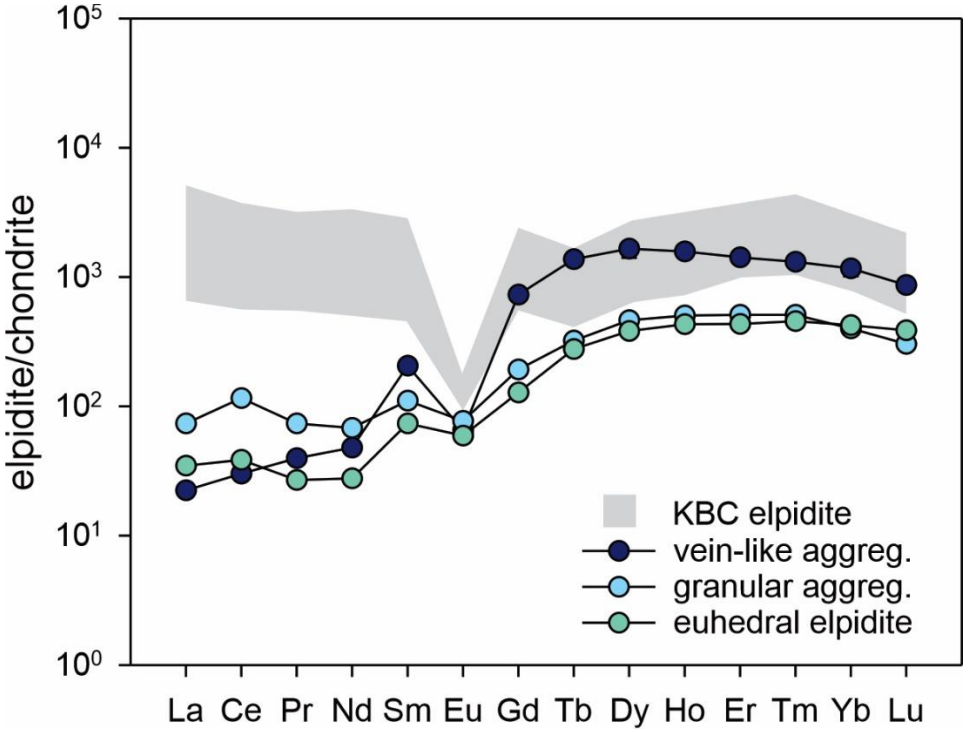

Fig 3.2 Binary diagram illustrating average REE patterns for elpidite from Papanduva compared to elpidite from the Khan Bogd Complex (KBC), Mongolia (Kynicky et al., 2011).

The ternary plot Zr vs. Na vs. 10K (Fig. 3.14) compares the chemical compositions of elpidite from Papanduva to other localities. The Papanduva elpidite plots towards the Na vertex, aligning with analyses from the literature and nearing the ideal end-member composition. In contrast, the (Na,K)ZrS-II compositions show Zr depletion and a significant shift towards the K vertex, indicating substantial alteration in K content relative to Na and Zr. However, a significant gap exists in the diagram, with few crystals populating this intermediate space, suggesting a limited extent of solid solution between Na and K. Furthermore, both elpidite and (Na,K)ZrS-II from sample MR-21 are distinctly Zr-enriched, displaying a positive correlation between Na and K.

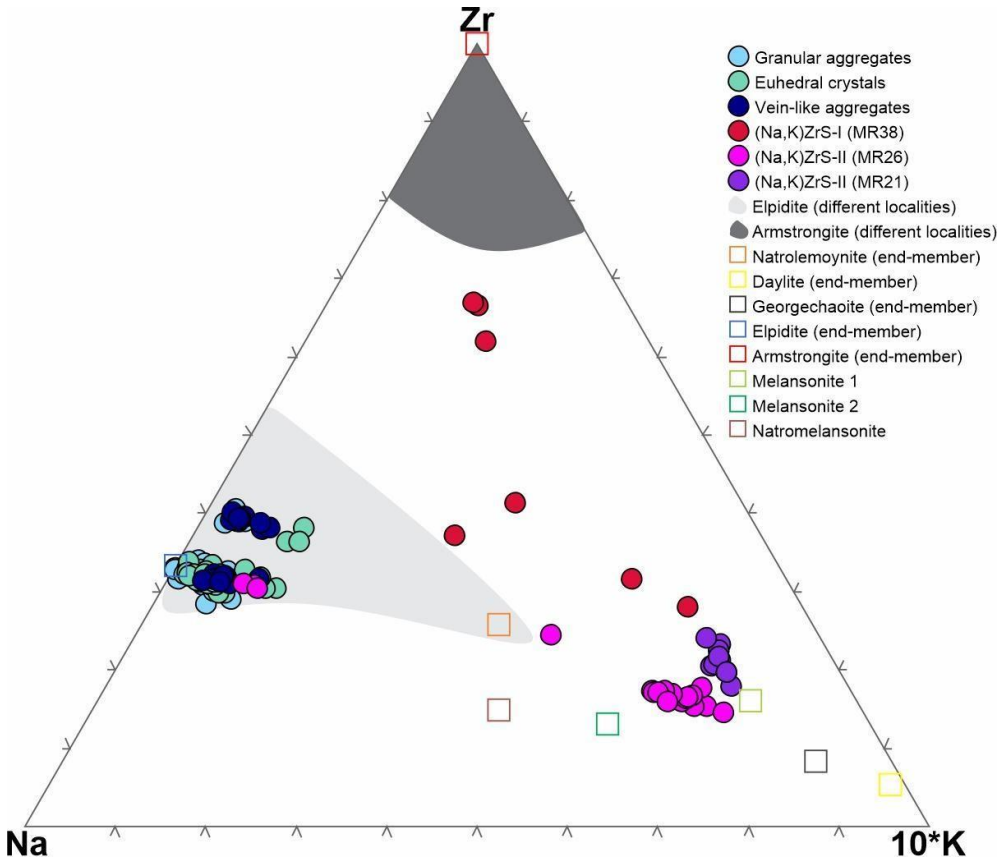

Fig 3.3 Ternary diagram (Zr vs.Na. vs 10K) showing the composition of granular aggregates, euhedral crystals and vein-like aggregates of elpidite, (Na,K)ZrS-I from sample MR-38, and (Na,K)ZrS-II from

samples MR-21 and MR-26 from the Papanduva Pluton, as well as end-members of zirconosilicates and elpidite and armstrongite from different localities, as follows. Elpidite: Cegielka, 2022; Bonin (1988); Bernarde, 2020; Vlasov, 1966; Birkett et al., 1992; Roelofsen & Veblen, 1999; Kynicky et al., 2011; Cametti et al., 2016; Salvi & Williams-Jones, 1995. Armstrongite: Roelofsen & Veblen, 1999; Gysi et al., 2015; Kynicky et al., 2011; Birkett et al., 1992; Mesto et al., 2014; Vladykin et al., 1973; Vladykin and Kovalenko, 2006; Jambor et al., 1987 and Jambor et al., 1988. Melansonite 1 data from Gore & McDonald 2022, melansonite 2 and natromelansonite data from Lykova et al. 2024

Unlike other zirconosilicates, (Na,K)ZrS-I from sample MR-38 demonstrates a trend of decreasing K and increasing Zr under relatively stable Na contents (and negligible Ca), an irregular behavior likely due to extensive alteration. This alteration complicates its placement within typical compositional trends observed in less altered samples, as evidenced in Figure 8.

5.2 Zirconosilicate Formation and Evolution in the Papanduva Pluton

In the Papanduva Pluton, elpidite is the primary carrier of heavy rare earth elements (HREEs) in the foliated facies, while zircon serves this role in the massive facies. This mineralogical distinction underscores the different evolutionary paths of these facies. The massive facies, characterized by zircon dominance, shows higher strontium (Sr) and barium (Ba) contents compared to the elpidite-dominated foliated facies. Such a pattern, coupled with the relative depletion of calcium (Ca) and europium (Eu) among other REEs, was observed in the Khan Bogd Complex (KBC) by Kynicky et al. (2011). They interpreted this as evidence that the granites of the main phase, featuring elpidite, evolved from the same magma as the porphyritic unit with zircon presence, through the fractionation of potassium feldspar and calcium-rich albite.

However, the more evolved foliated facies in the Papanduva pluton are distinguished by increases in light rare earth elements (LREE), HREE, zirconium (Zr), and other high field strength elements (HFSE), alongside a rise in peralkalinity during the late-magmatic stages. This suggests factors other than fractional crystallization driving this enrichment. Notably, the lower LREE contents of the Papanduva elpidite compared to those from KBC suggest early removal of LREEs by accessory minerals such as narsarsukite, astrophyllite, nacareniobsite, and chevkinite (Vilalva et al., 2013; 2016). Moreover, Papanduva elpidite displays a trend of relative HREE depletion across the HREE series when compared to zircon. This likely reflects competition with other minerals like arfvedsonite and aegirine, which have significant HREE contents (124 ppm and 138 ppm, respectively; Vilalva et al., 2016), and a Y-bearing silicate, tentatively identified as gerenite-(Y) (up to 823 ppm; Vilalva et al., 2013), crystallizing during the late- to post-magmatic stages.

Similar trends are observed in A-type granites in Suzhou, China, and El-Sibai, Egypt, where decreasing Sr and Ba contents and increasing Zr and niobium (Nb) contents are noted, alongside a "flattening" of the chondrite-normalized REE profile and a reduction of Eu in more evolved magmatic members. These trends point to the segregation of accessory phases enriched in LREE (such as allanite or monazite) and the complexing of HFSE with fluorine (F) as explanations for the observed enrichments in Zr, Nb, and HREE (Charoy & Raimbault, 1994). Abdel-Rahman & El-Kibbi (2001) propose a similar petrogenetic scenario but suggest that HREE enrichment at El-Sibai is also due to the complexing of these elements with sodium (Na) and F in the melt, which presumably leads to the crystallization of arfvedsonite.

Furthermore, studies of minor elements in elpidite by Kynicky et al. (2011) reveal significant calcium metasomatism, resulting in high-Ca varieties of elpidite that exhibit similar REE patterns to low-Ca species but with elevated concentrations. This pattern of REE remobilization suggests that active hydrothermal processes are a primary factor influencing elemental distributions in these minerals. In the Papanduva elpidite, Figure 3.11 shows that HREEs exhibit strong positive correlations with K and Ca and negative correlations with Na and Zr, indicating that the crystallization of elpidite and the incorporation of REEs are closely linked to the availability of alkali elements and the specific geochemical environment during formation.

Two main interpretations arise from the observed REE patterns in the elpidite types within the Papanduva Pluton. The first suggests that variations are due to chemical competition with other mineral phases assimilating REEs, while the second posits that these fluctuations are also influenced by remobilizations promoted by hydrothermal activities. The presence of post-magmatic crystals and pseudomorphs after (Na,K)ZrS supports the latter hypothesis, indicating the percolation of likely potassium-rich hydrothermal fluids during the final crystallization stages. Further evidence is provided by Vlach & Vilalva (2023), who studied narsarsukite in the foliated facies and observed intergrowths with (Na,K)ZrS, suggesting potential co-precipitation during the magmatic stage or post-magmatic exsolution induced by fluids. This process depleted the narsarsukite in zirconium, leading to the precipitation of the zirconosilicate. Considering the textural and chemical data, the former scenario appears more plausible for explaining the observed decrease in zirconium in the (Na,K)ZrS, and the chemical competition observed.

Conversely, elpidite in late- to post-magmatic assemblages with arfvedsonite (up to 124 ppm HREE), aegirine (up to 138 ppm HREE), and generite (up to 823 ppm), indicates significant competition for the HREE budget, potentially decreasing REE values in elpidite. Marr et al. (1998) and Currie & Zaleski (1985) note that elpidite is a saturating phase only at

low temperatures (approximately 600°C at 100 MPa) and is replaced by vlasovite (not present in the Papanduva pluton) and zircon (± quartz) with increasing temperature. These observations align with estimates by Vilalva et al. (2016) for late-magmatic (<650°C) and post-magmatic (<500°C) stages (at 100 MPa) for the foliated facies, based on amphibole and clinopyroxene compositions.

This brings up a pivotal question: Is the increase in potassium activity during the late and post-magmatic stages in the Papanduva Pluton solely a result of decreasing sodium activity, as would be typical in an agpaitic-like crystallization sequence, or is it influenced by the presence of hydrothermal/metasomatic fluids, likely rich in potassium? This potassium may originate from the late to post-magmatic replacement of primary potassium-bearing minerals (like arfvedsonite and K-feldspar) during fluid-rock interactions, a feature common across all lithotypes of Papanduva (Vilalva & Vlach, 2014; Vilalva et al., 2016), as no evidence of external influx has been identified.

Peralkaline granitic systems such as the Papanduva Pluton are less studied compared to syenitic suites, resulting in limited insights into their HFSE-rich silicate evolution. Here, elpidite is the prominent zirconium-bearing mineral, unlike other systems where dalyite might occur. The formation of elpidite, requiring higher silica activity, underscores the crucial role of silica in determining the stability and formation of various zirconium-bearing phases.

The physicochemical conditions during magma formation—pressure, temperature, oxygen fugacity (fO_2), silica activity ($aSiO_2$), peralkalinity (alkali activity), and liquid water activity (aH_2O)—significantly influence the crystallization of zircon-bearing (miaskitic-like) or alkali-zirconosilicate-bearing (agpaitic-like) mineral assemblages in alkaline granites. In the Papanduva Pluton, the transition from a zircon-bearing assemblage in the massive facies to an alkali zirconosilicate-bearing assemblage in the foliated facies is marked by an increase in fO_2, peralkalinity, fluorine, and 18O-rich conditions (Vilalva et al., 2016). This transition facilitates the formation of zirconosilicates like elpidite, which crystallize under higher fO_2 and lower sodium silicate activity ($aNa_2Si_2O_5$), in contrast to zircon, which forms under a wide range of fO_2 and low alkali activities.

5.3 Geochemical Evolution and Stability Fields in the Papanduva Pluton

Marks et al. (2011) introduce semiquantitative diagrams that delineate stability fields for various parageneses in peralkaline granites, emphasizing the activities of Na_2O and K_2O. The evolutionary trajectory for mineral assemblages in the Papanduva Pluton—transitioning from miaskitic-like in the massive facies to agpaitic-like in the foliated facies—appears more complex than that observed in other occurrences such as the Strange Lake (Canada) and the

Illímausaq (Greenland) complexes. This trajectory involves an initial increase in Na_2O activity under stable K_2O activity, followed by an increase in K_2O activity, leading to a positive slope between the stability fields of astrophyllite + elpidite and aenigmatite + elpidite, which are both present in the foliated facies.

To explore these stability fields and the inferred evolutionary path leading to the precipitation of different alkali zirconosilicates in this alkaline granitic system, we constructed a semiquantitative stability plot. This plot, correlating log(aNa_2O) vs. log(aK_2O), illustrates the stability regions for minerals such as zircon, aenigmatite, elpidite, and other relevant Na- and K-zirconosilicates, along with astrophyllite and narsarsukite, delineating the conditions under which they form and transform (Fig 3.15). The diagram, based on thermodynamic data within the simplified chemical system of Na_2O-K_2O-Al_2O_3-SiO_2-H_2O, utilizes Schreinemaker's analysis for accurate positioning and intersection of stability boundaries. The evolutionary path, depicted with arrows, illustrates the transition from early magmatic to post-magmatic phases, highlighting how changes in the chemical environment—specifically Na_2O and K_2O activities—drive this transition.

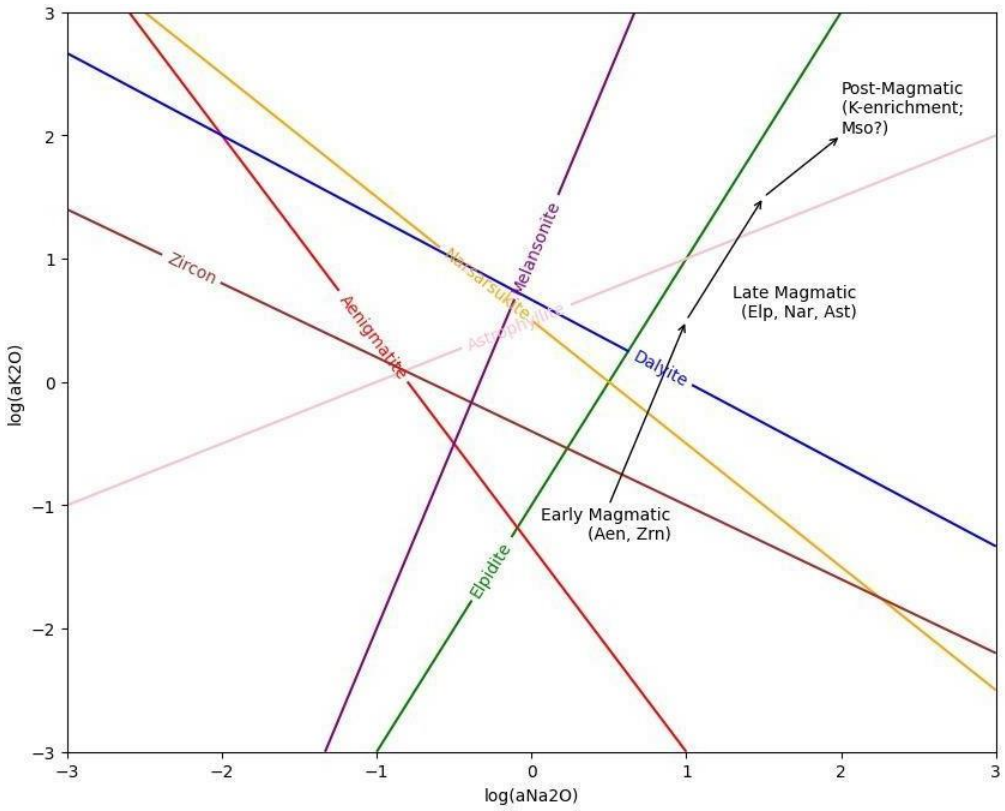

Fig 3.4 graph correlating log(aNa2O) vs. log(aK2O), illustrate the regions of stability for minerals such as zircon, aenigmatite, elpidite and other relevant Na and K zirconosilicates, This diagram, based on thermodynamic data within the simplified chemical system of Na2O-K2O-Al2O3-SiO2-H2O, uses Schreinemaker analysis for precise positioning and intersection of stability limits

During the main magmatic stage, zircon and aenigmatite crystallize in the massive facies as primary Zr-bearing phases under conditions of low oxygen fugacity (fO_2) and moderate Na_2O and K_2O activities. As the system evolves towards higher peralkalinity, fluorine, and fO_2, increasing Zr solubility in the melt, zircon is progressively replaced by elpidite through the reaction:

$$ZrSiO_4 + Na_2Si_2O_5 + 3SiO_2 + 3H_2O \rightarrow Na_2ZrSi_6O_{15}{\cdot}3H_2O. \quad \text{Eq.3.2}$$

This reaction illustrates the destabilization of zircon under high activities of Na2Si2O5 (indicative of peralkalinity) and excess silica in a hydrated magma. Concurrently, narsarsukite and astrophyllite stabilize, reflecting an increase in alkali activities. In the post-magmatic stages, as the system continues to cool and hydrothermal processes intensify, the circulation of K-rich fluids (also containing Ca) leads to the partial replacement of elpidite by (Na,K)-zirconosilicates, represented in Figure 3.15 by dalyite ($K_2ZrSi_6O_{15}$) and melansonite ($NaKZrSi_8O_{19}{\cdot}5H_2O$). Given that zirconosilicates and other rare alkali- and HFSE-bearing minerals are restricted to the foliated facies, it is likely that sub-magmatic deformation facilitated the circulation of these potassium-rich fluids, promoting hydrothermal alteration and affecting the partitioning of HFSE and REE budgets, as suggested by Vilalva et al. (2013, 2016).

These insights suggest the following general reactions for the formation of (Na,K)ZrS-I and II from a precursor zirconosilicate, ideally elpidite, during post-magmatic stages, within the simplified chemical system Na_2O-K_2O-Al_2O_3-SiO_2-H_2O:

(Na,K)ZrS-I:

$$Na_2ZrSi_6O_{15}.3H_2O + K^+_{(aq)} + Ca^{2+}_{(aq)} + (n-3)H_2O \rightarrow (NaKCa)ZrSi_6O_{15}.nH_2O_{(S)} + 2Na^+_{(aq)} \quad \text{Eq.3.3}$$

(Na,K)ZrS-II:

$$2Na_2ZrSi_6O_{15}.3H_2O + 2K^+_{(aq)} + 2Ca^{2+}_{(aq)} + 4SiO_2(n-6)H_2O \rightarrow (NaKCa)_2ZrSi_8O_{19}.nH_2O_{(S)} + 4Na^+_{(aq)}$$
$$\text{Eq.3.4}$$

Alternatively, the formation of (Na,K)ZrS-I and II directly from hydrothermal fluids can be explained by:

(Na,K)ZrS-I:

$$Zr^{4+}_{(aq)} + Na^+_{(aq)} + K^+_{(aq)} + Ca^{2+}_{(aq)} + 6SiO_{2(aq)} + (3+n)H_2O \rightarrow (NaKCa)ZrSi_6O_{15}.nH_2O_{(S)} \quad \text{Eq.3.5}$$

(Na,K)ZrS-II:

$$2Zr^{4+}_{(aq)}+2Na^{+}_{(aq)}+2K^{+}_{(aq)}+2Ca^{2+}_{(aq)}+16SiO_{2(aq)}+(3+n)H_2O \rightarrow (NaKCa)_2ZrSi_8O_{19}.nH_2O_{(S)}$$

Eq.3.6

6. Conclusions

This study provides a comprehensive analysis of elpidite and associated (Na,K)-zirconosilicates within the Papanduva Pluton, revealing insights into the late- to post-magmatic evolution of peralkaline granites. The main conclusions are listed below:

1. Elpidite is identified as the primary Zr-bearing mineral in the more evolved, foliated lithofacies of the Papanduva Pluton, accompanied by post-magmatic (Na,K)ZrS-I and (Na,K)ZrS-II phases. This transition from zircon to these zirconosilicates reflects changes in physicochemical conditions, including increased peralkalinity and silica activity during magmatic evolution.

2. The study identified three distinct textural types of elpidite: isolated euhedral crystals, granular interstitial aggregates, and vein-like aggregates. Each textural type exhibits specific major element variations, while (Na,K)ZrS-I and (Na,K)ZrS-II phases show distinct compositional and textural characteristics indicative of their formation and alteration processes.

3. Major element compositions of elpidite are relatively uniform, with notable variations in Zr, Al, and K contents linked to textural differences and alteration processes. (Na,K)ZrS-I and (Na,K)ZrS-II exhibit distinct compositional zones, with significative variations in K, Na and Ca, indicative of intense hydrothermal alteration. (Na,K)ZrS-I, with intermediate, and (Na,K)ZrS-II, with higher K_2O contents, reflect different stages and intensities of hydrothermal alteration.

4. Trace element and rare earth element (REE) analyses reveal that elpidite is enriched in Ba, Pb, and Sr while being depleted in most REEs compared to zircon. It shows significant heavy REE (HREE) enrichment and a positive Eu anomaly, indicating its role in HREE distribution during late to post-magmatic stages.

5. Textural analysis suggests that elpidite and (Na,K)ZrS types crystallized during late-magmatic to post-magmatic stages. The vein-like aggregates paralleling the foliation likely formed earlier than granular interstitial ones, along with other Ti-Zr-bearing minerals. Euhedral crystals indicate late to post-magmatic crystallization, with (Na,K)ZrS-II typically forming during post-magmatic phases, along with albite, aegirine-augite, and REE-bearing minerals, following the submagmatic nature of the foliation.

6. The study emphasizes the importance of both magmatic and post-magmatic processes in the formation and evolution of zirconosilicates, providing valuable insights into Zr behavior, melt evolution, and mineral stability in peralkaline granitic systems.

7. Hydrothermal fluids, likely K-rich, played a crucial role in the post-magmatic alteration of elpidite, leading to the formation of secondary (Na,K)-zirconosilicates. The interaction with these fluids, likely facilitated by sub-magmatic deformation, caused significant hydrothermal alteration, chemical remobilization (including HFSE and REE) and element incorporation, forming (Na,K)ZrS-I and (Na,K)ZrS-II from a precursor zirconosilicate, ideally elpidite.

Acknowledgements

The authors thank the Fundação de Amparo à Pesquisa do Estado de São Paulo (FAPESP) for financial support (19-117343-4) and the Brazilian National Council for Scientific and Technological Development (CNPq 130482/2023-4) for supporting the research grant.

References

Abdel-Rahman, A.M.; El-Kibbi, M (2001) Anorogenic magmatism: chemical evolution of the Mount El-Sibai A-type complex (Egypt), and implications for the origin of within-plate felsic magmas. Geol. Mag. 138, 67-85.

Andersen, T.; Carr, P.; Erambert, M (2012) Late magmatic mineral assemblages with siderite and zirconian pyroxene and amphibole in the anorogenic Mt Gibraltar microsyenite, New South Walles, Austrália, and their petrological implications. Lithos,151,46-56.

Andrade, S. (2016). Análises por LA-ICPMS em zircões de rochas graníticas da Faixa Ribeira no Estado de São Paulo – SE Brasil: Implicações genéticas e geocronológicas. Doctoral's Thesis, University of SãoPaulo, São Paulo, Brazil, 361 pp.

Basei M.A.S., Brito Neves B.B., Siga Jr. O., Babinski M., Pimentel M.M., Tassinari C.C.G., Hollanda M.H.B., Nutman A., Cordani U.G. (2010) Contribution of SHRIMP U–Pb zircon geochronology to unravelling the evolution of Brazilian Neoproterozoic fold belts. Precambrian Research, 183:112-144.

Bernard, C. (2020) Concentration and fractionation of Rare Earth Elements in alkaline complexes: the role of fluids.Tese de Doutorado, Universidade de Toulouse.

Birkett, T. C., Miller, R. R., Roberts, A. C., and Mariano, A. N. (1992) Zirconium-bearing minerals of the Strange Lake intrusive complex, Quebec-Labrador. *The Canadian Mineralogist*, *30*(1), 191–205.

Bogdanov, A., Kaneva E., Shendrik, R (2021) New Insights into the Crystal Chemistry of Elpidite, $Na_2Zr[Si_6O_{15}]\cdot 3H_2O$ and $(Na_{1+Y}Ca_{x1-X-Y})\Sigma=2Zr[Si_6O_{15}]\cdot(3-X)H_2O$, and Ab Initio Modeling of IR Spectra. Materials, 14, 2160.

Boily M, Williams-Jones AE. (1994) The role of magmatic and hydrothermal processes in the chemical evolution of the Strange Lake plutonic complex, Quebec-Labrador. Contrib Mineral Petrol 118:33–47.

Bonin, B. (1988) Peralkaline granites in Corsica: Some petrological and geochemical constraints. *Rendiconti della Società italiana di Mineralogia e Petrologia*, *43*(2), 281–306.

Borst, A. M.; Friss, H., Andersen, T.; Nielsen, T. F. D.; Waight, T. E.; Smit, M. A. (2016) Zirconosilicates in the kakortokites of the Ilímaussaq complex, South Greenland: Implications for fluid evolution and high-field-strength and rare-earth element mineralization in agpaitic systems. Mineralogical Magazine, 80: 5-30.

Cametti, G.; Armbruster, T.; Nagashima, M. (2016) Dehydration and thermal stability of elpidite: An in-situ single crystal X-ray diffraction study. Microporous Mesoporous Mater. *227*, 81–87.

Cannillo, E.; Rossi, G.; Ungaretti, L. (1973) The Crystal Structure of Elpidite. American Mineralogist, 58, 106-109.

Cegielka, M.; Baginski, B.; Macdonaldi, R.; Belkin, H. E.; Kotowski, J. Upton, B. G.J. (2022) Zirconium silicates in a peralkaline granite: a record of the interplay of magmatic and hydrothermal processes (Ilímaussaq complex, Greenland). Acta Geologica Polonica, 72, 235-245.

Charoy B and Raimbault L. (1994) Zr-, Th-, and REE-rich biotite differentiates in the A-type granite pluton of Suzhou (Eastern China): the key role of fluorine. J Petrol 35: 919-962.

Currie., K. L; Zaleski, E. (1985) The relative stability of Elpidite and Vlasovite: a P-T indicator for peralkaline rocks. Canadian Mineralogist, 23, 577-582.

Day, M. C., & Hawthorne, F. C. A (2020) structure hierarchy for silicate minerals: Chain, ribbon, and tube silicates. Mineralogical Magazine, 84(2), 165-244.

Estrade, G. Salvi, S.; Béziat. (2018) Crystallization and destabilization of eudialyte-group mineralsin peralkaline granite and pegmatite: a case study from the Ambohimirahavavy complex, Madagascar. Mineralogical Magazine, 82, 375–399.

Gore, T.E. and McDonald, A.M. (2023) Melansonite, $(Na,\square)\square_2KZrSi_8O_{19}\cdot 5H_2O$, a new member of the rhodesite group, from Mont Saint-Hilaire, Québec, Canada: Characterization, crystal-structure determination, and origin. The Canadian Journal of Mineralogy and Petrology, 61, 387–400.

Grigor'eva, A. A.; Zubkova, N. V.; Pekov, I. V.; Kolitsch, U.; Pushchavosky, D. Yu.; Vigasina, M. F.; Giester, G.; Dordevic', T.; Tillmans, E.; Chukanov, N. V. Crystal (2011) Chemistry of Elpidite from Khan Bogdo (Mongolia) and It's K- and Rb-Exchanged Forms. Structure of Inorganic Compounds, 56, 832-841.

Gualda, G. A. R.; Vlach, S. R. F. (2007ª) The Serra da Graciosa A-type Granites and Syenites, Southern Brazil. Part 1: regional setting and geological characterization. Anais da Academia Brasileira de Ciências, 79: 405-430.

Gysi A. P.; Williams-Jones A. E.; Collins P. (2015) Lithogeochemical vectors for hydrothermal processes in the Strange Lake peralkaline granitic REE-Zr–Nb deposit. Econ Geol 111, 1241–1276.

Jambor, J. L., Roberts, A.C., Grice, J. D., (1987) Armstrongite from the Strange Lake Alkalic Complex, on the Quebec – Labrador Boundary, Canada. Powder Diffraction, 2, 244.

Johnsen, O.; Ferraris, G.; Gault, R. A.; Grice, J. D.; Kampf, A. R.;PEKOV, I. V. (2003) The nomenclature of Eudialyte-group minerals. The Canadian Mineralogist, 41, 785-794.

Keppler, H. (1993) Influence of fluorine on the enrichment of high field strength trace elements in granitic rocks. Contributions to Mineralogy and Petrology, 111, 113-121.

Kynicky J.; Chakhmouradian A. R.; Xu C. (2011) Distribution and evolution of zirconium mineralization in peralkaline granites nd associated pegmatites of the Khan Bogd complex, southern Mongolia. Can Mineral 49:947–965.

Linthout, K. (1984) Alkali-zirconosilicates in peralkaline rocks. Contributions to Mineralogy and Petrology, 86, 155-158.

Lykova I, Rowe R, Poirier G, Friis H, Barnes S. (2024) Natromelansonite, Na3Zr[Si7AlO19]·4–5H2O, a new member of the rhodesite mero-plesiotype series from Mont Saint-Hilaire, Quebec, Canada. *Mineralogical Magazine*. 88(2),195-202.

Marks, M. A. W.; Hettman, K.; Schilling, J.; Frost, B. R.; Markl, G. (2011) The Mineralogical Diversity of Alkaline Igneous Rocks: Critical Factors for the Transition from Miaskitic to Agpaitic Phase Assemblages. Journal of Petrology, 52, 439-455.

Marks, M. A. W.; Markl, G. (2017) A global review on agpaitic rocks. Earth-Science Reviews, 173, 229-258.

Marr, R.A., Baker, D.R., and Williams-Jones, A.E (1998) Chemical controls on the solubility of Zr-bearing phases in simplified peralkaline melts and application to the Strange Lake Intrussion, Quebec-Labrador: The Canadian Mineralogist, v. 36, p. 1001–1008.

McDonald A. M., Chao G. Y. (2001) Natrolemoynite, a new hydrated sodium zirconosilicate from Mont Saint-Hilaire, Quebec: description and structure determination, The Canadian Mineralogist, 39, 1295-1306.

Mesto, E., Kaneva, E., Schingaro, E., Vladykin, N., Lacalamita, M., and Scordari, F. (2014) Armstrongite from Khan Bogdo (Mongolia): Crystal structure determination and implications for zeolite-like cation exchange properties. American Mineralogist, 99(11-12), 2424–2432.

Oliveira, A. L. S. (2019) ELPIDITA, UM ÁLCALI-ZIRCONOSSILICATO DO PLÚTON PAPANDUVA (PRSC): ASPECTOS TEXTURAIS, QUIMISMO E IMPLICAÇÕES PETROLÓGICAS. Trabalho de Conclusão de Curso - Departamento de Geologia, Universidade Federal do Rio Grande do Norte.

QUIROZ-VALLE, F. R., Lino, L. M., Citroni, S., Basei, M. A. S., Hueck, M., Vlach, S.R.F., Becker-Kerber, B., Prado, G. (2023) Paleovolcanology, geochemistry, and zircon U-Pb-Hf isotopes of the volcano-sedimentary sequences from the Ediacaran Campo Alegre-Corupá Basin, southern Brazil: linking volcanism and tectonics during Western Gondwana consolidation. Gondwana Research, v. 115, p. 128-154.

Roelofsen, J. N., and Veblen, D. R. (1999) Relationships among zirconosilicates: Examination by cathodoluminescence and transmission electron microscopy. Mineralogy and Petrology, 67(1-2), 71–84.

Salvi S, William-Jones A. (1995) Zirconosilicate phase relations in the Strange Lake (Lac Brisson) pluton, Quebec-Labrador, Canada: American Mineralogist. Am Mineral 80, 1031–1040.

Salvi S, William-Jones A. (2006) Alteration, HFSE mineralisation and hydrocarbon formation in peralkaline igneous systems: Insights from the Strange Lake Pluton, Canada. Lithos, 91 (1-4), 19-34.

Schmitt, A.K., Trumbull, R.B., Dulski, P., Emmermann, R. (2002) Zr–Nb–REE mineralization in peralkaline granites from the Amis complex, Brandberg (Namibia): evidence for magmatic pre-enrichment from melt inclusions. Economic Geology 97, 399–413.

Siachoque, A.; Vilalva, F. C. J., Vlach, S.R.F. (2022) Astrophyllite in peralkaline granites from the Graciosa Province (S-SE Brazil): Insights for magmatic vs. post-magmatic crystallization environments. Lithos, 432-433.

Vilalva, F. C. J. (2007) Petrografia e mineralogia de granitos peralcalinos: o Plúton Papanduva, Complexo Morro Redondo (PR/SC). Dissertação de Mestrado, Instituto de Geociências, Universidade de São Paulo, São Paulo, 323 p.

Vilalva, F. C. J., & Vlach, S. R. F. (2010) Major-and trace-element composition of REE-rich turkestanite from peralkaline granites of the Morro Redondo Complex, Graciosa Province, south Brazil. Mineralogical Magazine, 74: 645-658.

Vilalva, F. C. J.; Vlach, S. R. F. (2014) Geology, petrography and geochemistry of the A-type granites from the Morro Redondo Complex (PR-SC), southern Brazil, Graciosa Province. Anais da Academia Brasileira de Ciências, 86, 85-116.

Vilalva, F. C. J.; Vlach, S. R. F.; Simonetti, A. (2013) Nacareniobsite-(Ce) And Britholite-(Ce) In Peralkaline Granites From The Morro Redondo Complex, Graciosa Province, Southern Brazil: Occurrence and Compositional Data. The Canadian Mineralogist, 51: 313-332.

Vilalva F.C.J., Vlach S.R.F. and Simonetti A. (2016) Chemical and O-isotope compositions of amphiboles and clinopyroxenes from A-type granites of the Papanduva Pluton, South Brazil: Insights into late- to post-magmatic evolution of peralkaline systems. Chemical Geology, 420, 186–199.

Vilalva F.C.J., Simonetti A. and Vlach S.R.F. (2019) Insights on the origin of the Graciosa A-type granites and syenites (Southern Brazil) from zircon U–Pb geochronology, chemistry, and Hf and O isotope compositions. Lithos, 340– 341, 20–33.

Vlach S.R.F., Siga O., Harara O.M.M., Gualda G. A.R., Basei M.A.S and Vilalva F.C.J. (2011) Crystallization ages of the A-type magmatism of the Graciosa Province (Southern Brazil): Constraints from zircon U–Pb (ID–TIMS) dating of coeval K-rich gabbro–dioritic rocks. Journal of South American Earth Sciences, 32, 407–415.

Vlach, S.R.F., Vilalva, F, C. J. (2023) Narsarsukite in peralkaline granites from the Papanduva Pluton, Graciosa Province, south Brazil: insights from textural and chemical features. Mineralogical Magazine.

Vladykin, N. V., Kovalenko, V. I., Kashaev, A. A., Sapozhnikov, A. N. and Pisarskaya, V. A. (1973) Dokl. A/tad. Nauk S.S.S.R. 209, 1185-1188.

Vladykin, N.V., and Kovalenko, V.I. (2006) Zirconium silicates. Armstrongite. In M.I. Novgorodova, Ed., Minerals of Mongolia, p. 250–256. Fersman Mineralogical Museum, RAS, Moscow.

Vlasov, K. A.; Kuz'menko, M. Z.; Es'kova, E. M (1966) *The Lovozero Alkali Massif.* Oliver and Boyd, Edinburg, 627 p.

Zubkova N.V., Nikolova R.P., Chukanov N.V., Kostov-Kytin V.V., Pekov I.V., Varlamov D.A., Larikova T.S., Kazheva O.N., Chervonnaya N.A., Shilov G.V. (2019) Crystal Chemistry and Properties of Elpidite and Its Ag-Exchanged Forms. *Minerals.* 9, 420.

4. CONSIDERAÇÕES FINAIS

O Plúton Papanduva oferece um cenário ideal para investigar processos magmáticos e pós-magmáticos em sistemas alcalinos supersaturados. Esta dissertação de Mestrado foca na caracterização da elpidita e dos zirconossilicatos nas litofácies mais evoluídas do plúton, buscando desvendar os mecanismos que controlaram a formação e evolução desses minerais. Os resultados destacam a importância das interações magmáticas e hidrotermais na geração de diversidade mineralógica em sistemas graníticos alcalinos.

Com base na composição química (elementos maiores e traços) e nas características texturais da elpidita e (Na,K)-zirconossilicatos em álcali-feldspato granitos do Plúton Papanduva observa-se que a cristalização e evolução química da elpidita no Plúton Papanduva é marcada por uma série de processos tardi- a pós-magmáticos, incluindo variações nas atividades de álcalis e interações hidrotermais. Devido a variações na atividade de álcalis e presença de H_2O, as paragêneses miasquíticas (litofácies maciça) e agpaíticas (litofácies foliada), estão associadas à presença de diferentes minerais portadores do elemento Zr, sendo o zircão a principal fase hospedeira na litofácies maciça e os zirconossilicatos na litofácies foliada do plúton.

A elpidita cristaliza-se em três tipos texturais distintos: (1) cristais subédricos a euédricos; (2) agregados granulares; e (3) agregados venulares. Análises químicas (elementos maiores) desses grupos mostram composições uniformes de elementos principais, mas com variações em Zr, Al e K. Os agregados venulares formaram-se antes dos intersticiais granulares, e os cristais euédricos indicam cristalização tardia a pós-magmática.

O Plúton Papanduva também abriga zirconossilicatos distintos, caracterizados por teores mais altos de K e menores de Na e Zr, os quais foram denominados (Na,K)ZrS-I e II. Além disso, algumas dessas fases indicam uma diminuição na quantidade de H_2O, pois nos primeiros estágios de troca iônica na elpidita, os cátions de K ocupam ordenadamente o local de uma molécula de água na cavidade mais volumosa, em vez de ocupar o sítio do Na, resultando na diminuição de água estrutural. As fases (NaK)ZrS-II e (NaK)ZrS-I apresentam características texturais e composicionais específicas, refletindo uma evolução química complexa durante a

cristalização. (Na, K) ZrS-II formaram-se durante fases pós-magmáticas, junto com albita, aegirina-augita e outros minerais acessórios portadores que competem pelos conteúdos de elementos terras-raras (ETR).

A análise de elementos traços na elpidita revela uma concentração menor para a maioria dos elementos comparada ao zircão, com enriquecimentos em Ba, Pb e Sr. O zircão e a elpidita mostram tendências contrastantes no enriquecimento de ETR pesados, com o zircão sendo o hospedeiro primário durante estágios magmáticos iniciais.

Os padrões de ETR nas variedades de elpidita do Pluton Papanduva indicam que a distribuição desses elementos é resultado da competição com outras fases minerais e, principalmente, de processos de remobilização associados à atividade hidrotermal. A presença de cristais pós-magmáticos e pseudomorfos de (Na,K)ZrS confirma a percolação de fluidos hidrotermais ricos em potássio durante os estágios finais de cristalização, os quais influenciaram significativamente a distribuição dos ETRs na elpidita

No Plúton Papanduva, a transição de assembléias com zircão na fácies maciça para zirconossilicatos alcalinos na fácies foliada é marcada principalmente por um aumento em $fO2$, peralcalinidade (definida por $a Na_2O$ e $a K_2O$) e flúor. Inicialmente, há um aumento $a Na_2O$ sob condições estáveis de $a K_2O$, seguido por aumento desta última, criando um gradiente positivo entre os campos de estabilidade de astrofilita + elpidita e aenigmatita + elpidita na fácies foliada.

Durante o estágio magmático principal, zircão e aenigmatita cristalizam na fácies maciça sob baixa f_{O2} e atividades moderadas de Na_2O e K_2O. Com a evolução para maior peralcalinidade, flúor e f_{O2}, a solubilidade do Zr aumenta, levando à substituição progressiva do zircão pela elpidita. Simultaneamente, narsarsukita e astrofilita se estabilizam, refletindo maior atividade alcalina. Nas fases pós-magmáticas, o resfriamento e a intensificação dos processos hidrotermais promovem a circulação de fluidos ricos em K (e Ca), substituindo parcialmente a elpidita por (Na,K)-zirconossilicatos.

Considerando que zirconossilicatos e outros álcali-minerais raros contendo HFSE estão restritos à fácies foliada, conclui-se que a deformação submagmática que afeta esta fácies facilitou a circulação de fluidos hidrotermais ricos em potássio,

promovendo a alteração hidrotermal e afetando a partição de HFSE e ETR, conforme sugerido por Vilalva et al. (2013, 2016).

Por fim, para futuros trabalhos, indica-se fazer as análises de traços dos zirconossilicatos de Na e K, além do aprofundamento com inclusões fluidas e isótopos estáveis de oxigênio para melhor investigar a origem e evolução desses minerais nos estágios tardi- a pós-magmáticos e sua importância em sistemas peralcalinos supersaturados.

REFERÊNCIAS BIBLIOGRÁFICAS

A.

Andersen T.; Erambert M.; Larsen A.O.; Selbekk R.S.(2010) Petrology of nepheline syenite pegmatites in the Oslo Rift, Norway: zirconium silicate mineral assemblages as indicators of alkalinity and volatile fugacity in mildly agpaitic magma. Journal of Petrology. 51(11),:2303-2325

Andreeva, I.A.(2016) Genesis and mechanisms of formation of rare-metal peralkaline granites of the Khaldzan Buregtey massif, Mongolia: evidence from melt inclusions. Petrology, 24, 462–476.

B.

Buch, T. (2018) Caracterização mineralógica e geoquímica de ocorrências de Elementos Terras Raras no Maciço Granítico Ouro Fino, Rondônia, Brasil. Dissertação de Mestrado, Instituto de Geociências, Universidade de Brasília, Brasília, 54 p.

C.

Chukanov N.V., Rastsvetaeva R.K., Rozenberg K.A., Aksenov S.M., Pekov I.V., Belakovskiy D.I., Kristiansen R. Ilyukhinite, (2015) IMA 2015-065. CNMNC Newsletter No. 28, December 2015, page 1860; Mineralogical Magazine, 79, 1859-1864.

E.

Enrich, G. E. R., Ruberti, E., Azzone, R. G., & Gomes, C. D. B. (2016) Eudialyte-group minerals from the Monte de Trigo alkaline suite, Brazil: composition and petrological implications. Brazilian Journal of Geology, 46, 411-426.

F.

Frost, B. R.; Frost, C. D. (2008) Uma classificação geoquímica para rochas ígneas feldspáticas. Jornal de Petrologia, 49, 1955-1969.

G.

Gomes, C. D. B., Azzone, R. G., Enrich, G. E. R., Guarino, V., & Ruberti, E. (2021) Agpaitic Alkaline Rocks in Southern Brazilian Platform: A Review. Minerals, 11(9), 934.

Guarino, V., de'Gennaro, R., Melluso, L., Ruberti, E., & Azzone, R. G. (2019) The Transition from miaskitic to agpaitic rocks, as highlighted by the accessory phase assemblages in the Passa Quatro alkaline complex (southeastern Brazil). The Canadian Mineralogist, 57(3), 339-361.

K.

Khomyakov, A. P. (1995) Mineralogy of Hyperagpaitic Alkaline Rocks. Geological Maganize.

Kostov-Kytin V.V.;Kerestedjian T.N. (2020) Rietveld analysis of elpidite framework flexibility using in situ powder XRD data of thermally treated samples. Minerals. 10, 639.

L.

Le Maitre, R. W. (ed.).(2003) Igneous Rocks: a classification and glossary of therms. 2. Ed. Cambridge University Press, Cambridge.

M.

Marr, R. A.; Wood, S. A. (1992) Preliminary petrogenetic grids for sodium and calcium zirconosilicate minerals in felsic peralkaline rocks: the SiO_2-Na_2ZrO_3 and SiO_2-$CaZrO_3$ pseudobinary systems. American Mineralogist, 77, 810-820.

Melluso, L., Guarino, V., Lustrino, M., Morra, V., & De' Gennaro, (2017) R.The REE- and HFSE-bearing phases in the Itatiaia alkaline complex (Brazil) and geochemical evolution of feldspar-rich felsic melts. Mineralogical Magazine, 81(2), 217-250.

Migdisov A, Williams-Jones A. E.; Brugger J, Caporuscio F. A. (2016) Hydrothermal transport, deposition, and fractionation of the REE: experimental data and thermodynamic calculations. Chem Geol 439,13–42.

R.

Rastsvetaeva R.K. & Chukanov N.V. (2012) Classification of eudialytegroup minerals. Geology of Ore Deposits, 54(7), 487-497.

S.

Schilling J., Marks M., Wenzel T., Markl G. (2009) Reconstruction of magmatic to subsolidus processes in an agpaitic system using eudialyte textures and composition: a case study from Tamazeght, Morocco. The Canadian Mineralogist, 47(2):351-365.

Siégel, C.; Bryan, S.E.; Allen, C.M.; Gust, D.A. (2018) Use and abuse of zircon-based thermometers: a critical review and a recommended approach to identifiy antecrystic zircons. Earth Sciences Reviews,176. 87–116.

Sørensen H. (2006) The Ilímaussaq alkaline complex, South Greenland-an overview of 200 years of research and an outlook. Medd om Grønl Geosci 45, 10–31.

U.

Ulbrich H.H., Vlach S.R.F., Demaiffe D., Ulbrich M.N.C. (2005) Structure and origin of the Poços de Caldas alkaline massif. In: Comin-Chiaramonti P., Gomes C.B. (eds.). Mesozoic to Cenozoic alkaline magmatism in the Brazilian Platform. São Paulo: Edusp/Fapesp, p. 367-418.

V.

Vasyukova O.V.; Williams-Jones A.E.; (2019) Closed system fluid-mineral-mediated trace element behaviour in peralkaline rare metal pegmatites: evidence from Strange Lake. Chem Geol 505, 86–99.

W.

Watson, E. B.; (1983) Harrison, T. M. Zircon saturation revisited: temperature and composition effects in a variety of crustal magma types. Earth and Planetary Science Letters. 64 (2), 295-304.

ANEXOS

ANEXO I – TABELA DE DADOS EPMA

mineral	elpidita	elpidita	elpidita	elpidita	elpidita	elpidita	elpidita	elpidita	elpidita	elpidita	elpidita	elpidita	elpidita	elpidita	elpidita	elpidita
Sample	MR03_c1						Mr03_c2a				MR03_c2b					
Point ID	1	2	3	4	5	6	1	2	3	4	1	2	3	4	5	6
obs.	gran. aggreg.	gran. aggreg.	gran. aggreg.	gran. aggreg.	gran. aggreg.	gran. aggreg.	gran. aggreg.	gran. aggreg.	gran. aggreg.	gran. aggreg.	gran. aggreg.	gran. aggreg.	gran. aggreg.	gran. aggreg.	gran. aggreg.	gran. aggreg.
SiO_2	57.57	58.66	58.82	58.30	58.20	58.24	58.25	58.84	58.66	58.66	59.40	58.53	58.55	58.32	57.99	58.60
TiO_2	0.07	0.02	b.d.l	0.02	0.05	b.d.l	b.d.l	0.06	0.02	0.04	b.d.l	0.01	0.03	0.07	0.04	0.05
ZrO_2	19.34	19.06	19.99	19.71	19.75	19.88	19.67	19.37	19.44	20.22	17.37	18.93	18.75	18.30	19.15	19.68
HfO_2	0.31	0.40	0.30	0.37	0.37	0.43	0.34	0.38	0.33	0.34	0.33	0.43	0.37	0.33	0.34	0.42
ThO_2	b.d.l	b.d.l	b.d.l	0.06	b.d.l	b.d.l	b.d.l	b.d.l	b.d.l	b.d.l	b.d.l	0.04	b.d.l	0.04	b.d.l	b.d.l
Al_2O_3	0.44	0.61	0.20	0.09	0.28	0.03	0.06	0.05	0.03	0.02	1.73	0.21	0.06	0.75	0.09	b.d.l
FeO	0.10	0.05	0.09	0.15	0.04	0.04	0.03	0.06	b.d.l	0.02	0.17	0.14	0.16	0.50	0.14	0.05
CaO	0.10	0.06	0.03	0.05	0.03	0.08	0.05	0.02	b.d.l	0.00	0.14	0.08	0.09	0.03	b.d.l	b.d.l
Na_2O	9.67	10.08	9.49	9.84	9.75	9.87	10.10	10.12	10.07	10.06	10.04	10.12	9.82	9.88	9.70	9.84
K_2O	0.07	0.10	0.09	0.12	0.09	0.10	0.08	0.08	0.07	0.04	0.13	0.14	0.14	0.20	0.12	0.05
PbO	b.d.l	b.d.l	b.d.l	b.d.l	b.d.l	b.d.l	b.d.l	b.d.l	b.d.l	b.d.l	b.d.l	b.d.l	b.d.l	b.d.l	b.d.l	b.d.l
MgO	b.d.l	b.d.l	b.d.l	b.d.l	b.d.l	b.d.l	b.d.l	b.d.l	b.d.l	b.d.l	b.d.l	b.d.l	b.d.l	b.d.l	b.d.l	b.d.l
V_2O_5	b.d.l	b.d.l	b.d.l	b.d.l	b.d.l	b.d.l	b.d.l	b.d.l	b.d.l	b.d.l	b.d.l	b.d.l	b.d.l	b.d.l	b.d.l	b.d.l
P_2O_5	b.d.l	b.d.l	b.d.l	b.d.l	b.d.l	b.d.l	b.d.l	b.d.l	b.d.l	b.d.l	b.d.l	b.d.l	b.d.l	b.d.l	b.d.l	b.d.l
Nb_2O_5	b.d.l	b.d.l	b.d.l	0.04	0.02	b.d.l	b.d.l	b.d.l	b.d.l	b.d.l	b.d.l	0.03	0.01	0.01	b.d.l	0.10
Ta_2O_5	b.d.l	b.d.l	b.d.l	b.d.l	b.d.l	b.d.l	b.d.l	b.d.l	b.d.l	b.d.l	b.d.l	b.d.l	b.d.l	b.d.l	b.d.l	b.d.l
UO_2	b.d.l	b.d.l	b.d.l	b.d.l	b.d.l	b.d.l	b.d.l	b.d.l	b.d.l	b.d.l	b.d.l	b.d.l	b.d.l	b.d.l	b.d.l	b.d.l
MnO	b.d.l	b.d.l	b.d.l	b.d.l	b.d.l	b.d.l	b.d.l	b.d.l	b.d.l	b.d.l	b.d.l	b.d.l	b.d.l	b.d.l	b.d.l	b.d.l
Cr_2O_3	b.d.l	b.d.l	b.d.l	b.d.l	b.d.l	b.d.l	b.d.l	b.d.l	b.d.l	b.d.l	b.d.l	b.d.l	b.d.l	b.d.l	b.d.l	b.d.l
La_2O_3	b.d.l	b.d.l	b.d.l	b.d.l	b.d.l	b.d.l	b.d.l	b.d.l	b.d.l	b.d.l	b.d.l	b.d.l	b.d.l	b.d.l	b.d.l	b.d.l
Ce_2O_3	b.d.l	b.d.l	b.d.l	b.d.l	b.d.l	b.d.l	b.d.l	b.d.l	b.d.l	b.d.l	b.d.l	b.d.l	b.d.l	b.d.l	b.d.l	b.d.l
Nd_2O_3	b.d.l	b.d.l	b.d.l	b.d.l	b.d.l	b.d.l	b.d.l	b.d.l	b.d.l	b.d.l	b.d.l	b.d.l	b.d.l	b.d.l	b.d.l	b.d.l
Gd_2O_3	0.21	0.02	0.08	b.d.l	0.19	b.d.l	b.d.l	b.d.l	b.d.l	0.14	0.06	0.02	0.03	b.d.l	b.d.l	b.d.l
Dy_2O_3	n.a	b.d.l	b.d.l	b.d.l	b.d.l	0.07	b.d.l	0.04	0.05	0.05	0.15	b.d.l	b.d.l	b.d.l	b.d.l	0.10
Yb_2O_3	0.14	b.d.l	0.07	b.d.l	0.08	0.02	b.d.l	0.09	b.d.l	0.01	b.d.l	0.02	0.21	0.03	0.02	0.06
Y_2O_3	0.16	b.d.l	0.12	0.14	0.11	0.33	0.17	0.07	0.04	0.05	0.18	0.18	0.23	0.16	0.15	0.13
Total	88.18	89.07	89.29	88.91	88.95	89.07	88.74	89.17	88.72	89.66	89.70	88.87	88.45	88.61	87.74	89.08
Cl	n.a	n.a	n.a	n.a	n.a	n.a	n.a	n.a	n.a	n.a	n.a	n.a	n.a	n.a	n.a	n.a
F	b.d.l	0.02	0.02	b.d.l	0.05	b.d.l	b.d.l	b.d.l	0.04	b.d.l	0.11	0.07	b.d.l	0.01	0.04	0.07
H_2O*	10.13	10.13	10.13	10.13	10.13	10.13	10.13	10.13	10.13	10.13	10.13	10.13	10.13	10.13	10.13	10.13
Total 2	98.34	99.22	99.43	99.03	99.13	99.20	98.87	99.30	98.88	99.79	99.93	99.07	98.58	98.74	97.90	99.28

**conteúdo fixo baseado na fórmula estequiométrica ideal*

na = não analisado

bdl = abaixo do limite de detecção

mineral	elpidita	elpidita	elpidita	elpidita	elpidita	elpidita	elpidita	elpidita	elpidita	elpidita	elpidita	elpidita	elpidita	elpidita	elpidita	elpidita
Sample	MR03_c1						Mr03_c2a				MR03_c2b					
Point ID	1	2	3	4	5	6	1	2	3	4	1	2	3	4	5	6
obs.	gran. aggreg.	gran. aggreg.	gran. aggreg.	gran. aggreg.	gran. aggreg.	gran. aggreg.	gran. aggreg.	gran. aggreg.	gran. aggreg.	gran. aggreg.	gran. aggreg.	gran. aggreg.	gran. aggreg.	gran. aggreg.	gran. aggreg.	gran. aggreg.
	proporções catiônicas com base em 6 Si e 15 oxigênios															
Si	6.000	6.000	6.000	6.000	6.000	6.000	6.000	6.000	6.000	6.000	6.000	6.000	6.000	6.000	6.000	6.000
Ti	0.003	0.001	0.000	0.001	0.002	0.000	0.000	0.002	0.001	0.002	0.000	0.000	0.001	0.003	0.002	0.002
Zr	0.983	0.951	0.994	0.989	0.993	0.999	0.988	0.963	0.970	1.009	0.856	0.946	0.937	0.918	0.966	0.983
Hf	0.009	0.012	0.009	0.011	0.011	0.013	0.010	0.011	0.010	0.010	0.010	0.013	0.011	0.010	0.010	0.012
Th	0.000	0.000	0.000	0.001	0.000	0.000	0.000	0.000	0.000	0.000	0.000	0.001	0.000	0.001	0.000	0.000
Al	0.054	0.074	0.024	0.011	0.034	0.003	0.007	0.006	0.004	0.003	0.206	0.025	0.007	0.090	0.011	0.000
Fe	0.009	0.004	0.008	0.013	0.003	0.004	0.003	0.005	0.000	0.002	0.014	0.012	0.013	0.043	0.012	0.004
Ca	0.011	0.007	0.003	0.006	0.003	0.009	0.006	0.003	0.000	0.000	0.015	0.009	0.010	0.003	0.001	0.000
Na	1.954	1.999	1.877	1.963	1.949	1.972	2.017	2.001	1.997	1.995	1.966	2.011	1.951	1.971	1.946	1.953
K	0.009	0.013	0.012	0.016	0.012	0.013	0.010	0.011	0.010	0.005	0.017	0.018	0.019	0.026	0.016	0.007
Pb	0.000	0.000	0.000	0.000	0.000	0.000	0.000	0.000	0.000	0.000	0.000	0.000	0.000	0.000	0.000	0.000
Mg	0.000	0.000	0.000	0.000	0.000	0.000	0.000	0.000	0.000	0.000	0.000	0.000	0.000	0.000	0.000	0.000
V	0.000	0.000	0.000	0.000	0.000	0.000	0.000	0.000	0.000	0.000	0.000	0.000	0.000	0.000	0.000	0.000
P	0.000	0.000	0.000	0.000	0.000	0.000	0.000	0.000	0.000	0.000	0.000	0.000	0.000	0.000	0.000	0.000
Nb	0.000	0.001	0.000	0.002	0.001	0.000	0.000	0.000	0.000	0.000	0.000	0.001	0.001	0.000	0.000	0.005
Ta	0.000	0.000	0.000	0.000	0.000	0.000	0.000	0.000	0.000	0.000	0.000	0.000	0.000	0.000	0.000	0.000
U	0.000	0.000	0.000	0.000	0.000	0.000	0.000	0.000	0.000	0.000	0.000	0.000	0.000	0.000	0.000	0.000
Mn	0.000	0.000	0.000	0.000	0.000	0.000	0.000	0.000	0.000	0.000	0.000	0.000	0.000	0.000	0.000	0.000
Cr	0.000	0.000	0.000	0.000	0.000	0.000	0.000	0.000	0.000	0.000	0.000	0.000	0.000	0.000	0.000	0.000
La	0.000	0.000	0.000	0.000	0.000	0.000	0.000	0.000	0.000	0.000	0.000	0.000	0.000	0.000	0.000	0.000
Ce	0.000	0.000	0.000	0.000	0.000	0.000	0.000	0.000	0.000	0.000	0.000	0.000	0.000	0.000	0.000	0.000
Nd	0.000	0.000	0.000	0.000	0.000	0.000	0.000	0.000	0.000	0.000	0.000	0.000	0.000	0.000	0.000	0.000
Gd	0.008	0.001	0.003	0.000	0.007	0.000	0.000	0.000	0.000	0.005	0.002	0.001	0.001	0.000	0.000	0.000
Dy	0.000	0.000	0.000	0.000	0.000	0.002	0.000	0.001	0.002	0.002	0.005	0.000	0.000	0.000	0.000	0.003
Yb	0.005	0.000	0.002	0.000	0.003	0.001	0.000	0.003	0.000	0.000	0.000	0.001	0.007	0.001	0.001	0.002
Y	0.005	0.000	0.004	0.004	0.004	0.010	0.005	0.002	0.001	0.002	0.005	0.006	0.007	0.005	0.005	0.004

mineral	elpidita	elpidita	elpidita	elpidita	elpidita	elpidita	elpidita	elpidita	elpidita	elpidita	elpidita	elpidita	elpidita	elpidita	elpidita	elpidita
Sample	MR26_c2							MR26_c3							MR26_c4	
Point ID	1	2	3	4	5	6	7	1	2	3	4	5	6	7	1	2
obs.	gran. aggreg.	gran. aggreg.	gran. aggreg.	gran. aggreg.	gran. aggreg.	gran. aggreg.	gran. aggreg.	gran. aggreg.	gran. aggreg.	gran. aggreg.	gran. aggreg.	gran. aggreg.	gran. aggreg.	gran. aggreg.	gran. aggreg.	gran. aggreg.
SiO_2	59.62	58.94	58.84	58.34	59.15	59.92	58.70	58.20	58.49	58.87	58.69	59.16	59.00	59.49	58.95	59.10
TiO_2	0.06	0.11	0.26	0.10	0.14	0.12	0.10	0.01	0.11	0.18	0.16	0.07	b.d.l	0.07	0.08	0.04
ZrO_2	19.60	19.71	19.75	20.02	19.12	19.74	20.43	19.69	19.35	19.62	19.52	19.64	19.96	19.61	19.60	20.08
HfO_2	0.35	0.33	0.41	0.42	0.38	0.46	0.48	0.34	0.40	0.47	0.49	0.52	0.44	0.46	0.42	0.53
ThO_2	0.02	b.d.l	b.d.l	0.04	b.d.l	0.03	0.06	b.d.l	0.005	b.d.l	0.06	0.01	b.d.l	b.d.l	b.d.l	b.d.l
Al_2O_3	0.04	0.03	0.02	0.03	0.02	0.02	0.05	0.14	0.09	0.06	0.04	0.05	0.01	0.03	0.02	0.05
FeO	0.05	0.06	0.08	0.05	0.04	0.00	0.44	0.13	0.03	0.06	0.08	b.d.l	0.07	0.05	b.d.l	0.07
CaO	0.09	0.06	0.18	0.17	0.09	0.12	0.13	0.17	0.10	0.12	0.09	0.10	0.05	0.08	0.08	0.04
Na_2O	10.07	10.23	9.53	9.41	10.18	9.63	9.64	9.89	9.50	9.97	10.01	9.78	9.95	9.88	10.09	9.93
K_2O	0.04	0.04	0.09	0.04	0.02	0.05	0.07	0.07	0.08	b.d.l	b.d.l	0.03	0.06	0.03	0.03	0.04
PbO	b.d.l	b.d.l	b.d.l	b.d.l	b.d.l	b.d.l	b.d.l	b.d.l	b.d.l	b.d.l	b.d.l	b.d.l	b.d.l	b.d.l	b.d.l	b.d.l
MgO	b.d.l	b.d.l	b.d.l	b.d.l	b.d.l	b.d.l	b.d.l	b.d.l	b.d.l	b.d.l	b.d.l	b.d.l	b.d.l	b.d.l	b.d.l	b.d.l
V_2O_5	b.d.l	b.d.l	b.d.l	b.d.l	b.d.l	b.d.l	b.d.l	b.d.l	b.d.l	b.d.l	b.d.l	b.d.l	b.d.l	b.d.l	b.d.l	b.d.l
P_2O_5	b.d.l	b.d.l	b.d.l	b.d.l	b.d.l	b.d.l	b.d.l	b.d.l	b.d.l	b.d.l	b.d.l	b.d.l	b.d.l	b.d.l	b.d.l	b.d.l
Nb_2O_5	b.d.l	0.01	b.d.l	b.d.l	b.d.l	b.d.l	b.d.l	0.20	b.d.l	b.d.l	0.06	b.d.l	0.01	0.06	b.d.l	b.d.l
Ta_2O_5	b.d.l	b.d.l	b.d.l	b.d.l	b.d.l	b.d.l	b.d.l	b.d.l	b.d.l	b.d.l	b.d.l	b.d.l	b.d.l	b.d.l	b.d.l	b.d.l
UO_2	b.d.l	b.d.l	b.d.l	b.d.l	b.d.l	b.d.l	b.d.l	b.d.l	b.d.l	b.d.l	b.d.l	b.d.l	b.d.l	b.d.l	b.d.l	b.d.l
MnO	b.d.l	b.d.l	b.d.l	b.d.l	b.d.l	b.d.l	b.d.l	b.d.l	b.d.l	b.d.l	b.d.l	b.d.l	b.d.l	b.d.l	b.d.l	b.d.l
Cr_2O_3	b.d.l	b.d.l	b.d.l	b.d.l	b.d.l	b.d.l	b.d.l	b.d.l	b.d.l	b.d.l	b.d.l	b.d.l	b.d.l	b.d.l	b.d.l	b.d.l
La_2O_3	b.d.l	b.d.l	b.d.l	b.d.l	b.d.l	b.d.l	b.d.l	b.d.l	b.d.l	b.d.l	b.d.l	b.d.l	b.d.l	b.d.l	b.d.l	b.d.l
Ce_2O_3	b.d.l	b.d.l	b.d.l	b.d.l	b.d.l	b.d.l	b.d.l	b.d.l	b.d.l	b.d.l	b.d.l	b.d.l	b.d.l	b.d.l	b.d.l	b.d.l
Nd_2O_3	b.d.l	b.d.l	b.d.l	b.d.l	b.d.l	b.d.l	b.d.l	b.d.l	b.d.l	b.d.l	b.d.l	b.d.l	b.d.l	b.d.l	b.d.l	b.d.l
Gd_2O_3	0.13	b.d.l	0.04	0.03	b.d.l	b.d.l	b.d.l	b.d.l	0.17	b.d.l	b.d.l	b.d.l	0.10	0.12	0.05	0.12
Dy_2O_3	0.02	b.d.l	b.d.l	0.07	0.01	b.d.l	b.d.l	b.d.l	0.25	b.d.l	b.d.l	b.d.l	0.14	0.07	b.d.l	0.05
Yb_2O_3	0.16	0.05	0.07	0.08	b.d.l	0.03	0.03	0.05	0.01	0.07	0.06	b.d.l	0.05	0.05	0.04	0.06
Y_2O_3	0.16	0.08	0.08	0.13	0.16	0.22	0.12	0.05	0.28	0.09	0.07	0.39	0.20	0.18	0.19	0.28
Total	90.43	89.65	89.34	88.93	89.32	90.33	90.26	88.95	88.86	89.52	89.32	89.75	90.05	90.17	89.56	90.38
Cl	n.a	n.a	n.a	n.a	n.a	n.a	n.a	n.a	n.a	n.a	n.a	n.a	n.a	n.a	n.a	n.a
F	b.d.l	0.07	0.02	b.d.l	b.d.l	b.d.l	b.d.l	0.11	b.d.l	0.07	0.07	b.d.l	b.d.l	b.d.l	0.04	b.d.l
H_2O*	10.13	10.13	10.13	10.13	10.13	10.13	10.13	10.13	10.13	10.13	10.13	10.13	10.13	10.13	10.13	10.13
Total 2	100.55	99.85	99.48	99.05	99.44	100.46	100.38	99.19	98.98	99.71	99.52	99.87	100.18	100.30	99.73	100.51

na = não analisado

bdl = abaixo do limite de detecção

mineral	elpidita	elpidita	elpidita	elpidita	elpidita	elpidita	elpidita	elpidita	elpidita	elpidita	elpidita	elpidita	elpidita	elpidita	elpidita	elpidita
Sample	MR26_c2							MR26_c3							MR26_c4	
Point ID	1	2	3	4	5	6	7	1	2	3	4	5	6	7	1	2
obs.	gran. aggreg.	gran. aggreg.	gran. aggreg.	gran. aggreg.	gran. aggreg.	gran. aggreg.	gran. aggreg.	gran. aggreg.	gran. aggreg.	gran. aggreg.	gran. aggreg.	gran. aggreg.	gran. aggreg.	gran. aggreg.	gran. aggreg.	gran. aggreg.
Si	6.000	6.000	6.000	6.000	6.000	6.000	6.000	6.000	6.000	6.000	6.000	6.000	6.000	6.000	6.000	6.000
Ti	0.002	0.005	0.011	0.004	0.006	0.005	0.004	0.001	0.005	0.008	0.007	0.003	0.000	0.003	0.004	0.002
Zr	0.962	0.978	0.982	1.004	0.946	0.964	1.018	0.990	0.968	0.975	0.973	0.971	0.990	0.964	0.973	0.994
Hf	0.010	0.010	0.012	0.012	0.011	0.013	0.014	0.010	0.012	0.014	0.014	0.015	0.013	0.013	0.012	0.015
Th	0.000	0.000	0.000	0.001	0.000	0.001	0.001	0.000	0.000	0.000	0.001	0.000	0.000	0.000	0.000	0.000
Al	0.005	0.004	0.003	0.004	0.002	0.002	0.007	0.017	0.011	0.007	0.004	0.006	0.002	0.003	0.003	0.006
Fe	0.005	0.005	0.007	0.005	0.003	0.000	0.038	0.011	0.003	0.005	0.007	0.000	0.006	0.004	0.000	0.006
Ca	0.010	0.006	0.020	0.018	0.009	0.012	0.014	0.019	0.011	0.013	0.010	0.011	0.006	0.009	0.009	0.004
Na	1.965	2.019	1.884	1.876	2.002	1.870	1.910	1.977	1.889	1.970	1.984	1.923	1.962	1.932	1.991	1.955
K	0.005	0.005	0.011	0.006	0.003	0.006	0.009	0.009	0.011	0.000	0.000	0.004	0.008	0.004	0.005	0.005
Pb	0.000	0.000	0.000	0.000	0.000	0.000	0.000	0.000	0.000	0.000	0.000	0.000	0.000	0.000	0.000	0.000
Mg	0.000	0.000	0.000	0.000	0.000	0.000	0.000	0.000	0.000	0.000	0.000	0.000	0.000	0.000	0.000	0.000
V	0.000	0.000	0.000	0.000	0.000	0.000	0.000	0.000	0.000	0.000	0.000	0.000	0.000	0.000	0.000	0.000
P	0.000	0.000	0.000	0.000	0.000	0.000	0.000	0.000	0.000	0.000	0.000	0.000	0.000	0.000	0.000	0.000
Nb	0.000	0.001	0.000	0.000	0.000	0.000	0.000	0.009	0.000	0.000	0.003	0.000	0.000	0.003	0.000	0.000
Ta	0.000	0.000	0.000	0.000	0.000	0.000	0.000	0.000	0.000	0.000	0.000	0.000	0.000	0.000	0.000	0.000
U	0.000	0.000	0.000	0.000	0.000	0.000	0.000	0.000	0.000	0.000	0.000	0.000	0.000	0.000	0.000	0.000
Mn	0.000	0.000	0.000	0.000	0.000	0.000	0.000	0.000	0.000	0.000	0.000	0.000	0.000	0.000	0.000	0.000
Cr	0.000	0.000	0.000	0.000	0.000	0.000	0.000	0.000	0.000	0.000	0.000	0.000	0.000	0.000	0.000	0.000
La	0.000	0.000	0.000	0.000	0.000	0.000	0.000	0.000	0.000	0.000	0.000	0.000	0.000	0.000	0.000	0.000
Ce	0.000	0.000	0.000	0.000	0.000	0.000	0.000	0.000	0.000	0.000	0.000	0.000	0.000	0.000	0.000	0.000
Nd	0.000	0.000	0.000	0.000	0.000	0.000	0.000	0.000	0.000	0.000	0.000	0.000	0.000	0.000	0.000	0.000
Gd	0.005	0.000	0.001	0.001	0.000	0.000	0.000	0.000	0.006	0.000	0.000	0.000	0.004	0.004	0.002	0.004
Dy	0.001	0.000	0.000	0.002	0.000	0.000	0.000	0.000	0.008	0.000	0.000	0.000	0.005	0.002	0.000	0.002
Yb	0.005	0.002	0.002	0.003	0.000	0.001	0.001	0.002	0.000	0.002	0.002	0.000	0.002	0.002	0.001	0.002
Y	0.005	0.003	0.002	0.004	0.005	0.007	0.004	0.002	0.009	0.003	0.002	0.012	0.006	0.005	0.006	0.009

mineral	elpidita	elpidita	elpidita	elpidita	elpidita	elpidita	elpidita	elpidita	elpidita	elpidita	elpidita	elpidita	elpidita	elpidita	elpidita	elpidita
Sample									MR38_c4							
Point ID	3	4	5	6	7	8	9	10	1	2	3	4	6			
obs.	gran. aggreg.	gran. aggreg.	gran. aggreg.	gran. aggreg.	gran. aggreg.	gran. aggreg.	gran. aggreg.	gran. aggreg.	gran. aggreg.	gran. aggreg.	gran. aggreg.	gran. aggreg.	gran. aggreg.	gran. aggreg.	gran. aggreg.	gran. aggreg.
SiO_2	58.84	59.22	57.82	59.14	57.68	58.95	58.01	58.28	58.19	59.16	58.73	59.29	56.41	55.18	57.03	56.70
TiO_2	0.03	0.08	0.05	0.05	0.03	0.07	0.04	0.16	0.16	0.15	0.25	0.18	b.d.l	b.d.l	b.d.l	b.d.l
ZrO_2	19.42	19.34	20.02	19.26	19.22	19.72	19.98	19.27	19.54	19.10	19.34	19.69	26.20	25.62	25.04	24.92
HfO_2	0.33	0.39	0.43	0.47	0.53	0.46	0.25	0.27	0.50	0.42	0.44	0.50	b.d.l	b.d.l	b.d.l	b.d.l
ThO_2	0.04	b.d.l	b.d.l	0.04	b.d.l	0.01	b.d.l	0.03	b.d.l	0.06	b.d.l	b.d.l	b.d.l	b.d.l	b.d.l	b.d.l
Al_2O_3	0.02	0.02	0.38	0.05	0.18	0.02	0.21	0.03	0.09	0.02	0.04	0.05	b.d.l	b.d.l	b.d.l	b.d.l
FeO	b.d.l	0.04	0.25	0.09	0.05	0.00	0.22	0.12	0.12	0.10	0.05	0.15	b.d.l	0.10	0.02	0.01
CaO	0.11	0.12	0.16	0.10	0.17	0.08	0.23	0.13	0.21	0.12	0.14	0.08	b.d.l	b.d.l	b.d.l	b.d.l
Na_2O	9.94	9.55	9.53	9.80	9.36	9.84	9.43	9.73	9.97	9.86	9.67	9.71	9.25	9.09	9.15	9.03
K_2O	0.09	0.03	0.14	0.05	0.08	0.04	0.14	0.09	0.16	0.09	0.09	0.13	0.08	0.08	0.10	0.11
PbO	b.d.l	b.d.l	b.d.l	b.d.l	b.d.l	b.d.l	b.d.l	b.d.l	b.d.l	b.d.l	b.d.l	b.d.l	b.d.l	b.d.l	b.d.l	b.d.l
MgO	b.d.l	b.d.l	b.d.l	b.d.l	b.d.l	b.d.l	b.d.l	b.d.l	b.d.l	b.d.l	b.d.l	b.d.l	b.d.l	b.d.l	b.d.l	b.d.l
V_2O_5	b.d.l	b.d.l	b.d.l	b.d.l	b.d.l	b.d.l	b.d.l	b.d.l	b.d.l	b.d.l	b.d.l	b.d.l	b.d.l	b.d.l	b.d.l	b.d.l
P_2O_5	b.d.l	b.d.l	b.d.l	b.d.l	b.d.l	b.d.l	b.d.l	b.d.l	b.d.l	b.d.l	b.d.l	b.d.l	b.d.l	b.d.l	b.d.l	b.d.l
Nb_2O_5	0.01	0.02	b.d.l	b.d.l	b.d.l	b.d.l	0.06	0.19	b.d.l	0.01	0.01	b.d.l	b.d.l	b.d.l	b.d.l	b.d.l
Ta_2O_5	b.d.l	b.d.l	b.d.l	b.d.l	b.d.l	b.d.l	b.d.l	b.d.l	b.d.l	b.d.l	b.d.l	b.d.l	b.d.l	b.d.l	b.d.l	b.d.l
UO_2	b.d.l	b.d.l	b.d.l	b.d.l	b.d.l	b.d.l	b.d.l	b.d.l	b.d.l	b.d.l	b.d.l	b.d.l	b.d.l	b.d.l	b.d.l	b.d.l
MnO	b.d.l	b.d.l	b.d.l	b.d.l	b.d.l	b.d.l	b.d.l	b.d.l	b.d.l	b.d.l	b.d.l	b.d.l	b.d.l	b.d.l	b.d.l	b.d.l
Cr_2O_3	b.d.l	b.d.l	b.d.l	b.d.l	b.d.l	b.d.l	b.d.l	b.d.l	b.d.l	b.d.l	b.d.l	b.d.l	b.d.l	b.d.l	b.d.l	b.d.l
La_2O_3	b.d.l	b.d.l	b.d.l	b.d.l	b.d.l	b.d.l	b.d.l	b.d.l	b.d.l	b.d.l	b.d.l	b.d.l	b.d.l	b.d.l	b.d.l	b.d.l
Ce_2O_3	b.d.l	b.d.l	b.d.l	b.d.l	b.d.l	b.d.l	b.d.l	b.d.l	b.d.l	b.d.l	b.d.l	b.d.l	b.d.l	b.d.l	b.d.l	b.d.l
Nd_2O_3	b.d.l	b.d.l	b.d.l	b.d.l	b.d.l	b.d.l	b.d.l	b.d.l	b.d.l	b.d.l	b.d.l	b.d.l	b.d.l	b.d.l	b.d.l	b.d.l
Gd_2O_3	b.d.l	0.17	0.17	0.04	0.08	0.06	0.12	b.d.l	b.d.l	b.d.l	b.d.l	b.d.l	b.d.l	b.d.l	b.d.l	b.d.l
Dy_2O_3	0.13	0.10	0.08	b.d.l	b.d.l	b.d.l	0.11	b.d.l	b.d.l	0.00	b.d.l	b.d.l	b.d.l	b.d.l	b.d.l	b.d.l
Yb_2O_3	0.07	b.d.l	0.21	0.11	0.13	0.02	b.d.l	b.d.l	b.d.l	b.d.l	b.d.l	0.01	b.d.l	b.d.l	b.d.l	b.d.l
Y_2O_3	0.25	0.26	0.27	0.22	0.41	0.32	0.12	0.05	0.07	b.d.l	0.01	0.06	b.d.l	b.d.l	b.d.l	b.d.l
Total	89.28	89.34	89.53	89.42	87.92	89.58	88.93	88.35	89.01	89.08	88.76	89.83	91.93	90.07	91.34	90.78
Cl	n.a	n.a	n.a	n.a	n.a	n.a	n.a	n.a	n.a	n.a	n.a	n.a	n.a	n.a	n.a	n.a
F	0.12	b.d.l	b.d.l	0.02	b.d.l	b.d.l	b.d.l	0.06	0.05	b.d.l	0.01	0.01	b.d.l	b.d.l	b.d.l	b.d.l
H_2O*	10.13	10.13	10.13	10.13	10.13	10.13	10.13	10.13	10.13	10.13	10.13	10.13	9.00	9.00	9.00	9.00
Total 2	99.52	99.47	99.65	99.57	98.04	99.71	99.06	98.54	99.18	99.21	98.90	99.97	100.93	99.07	100.34	99.78

na = não analisado

bdl = abaixo do limite de detecção

mineral	elpidita	elpidita	elpidita	elpidita	elpidita	elpidita	elpidita	elpidita	elpidita	elpidita	elpidita	elpidita	elpidita	elpidita	elpidita	elpidita
Sample									MR38_c4							
Point ID	3	4	5	6	7	8	9	10	1	2	3	4	6			
obs.	gran. aggreg.	gran. aggreg.	gran. aggreg.	gran. aggreg.	gran. aggreg.	gran. aggreg.	gran. aggreg.	gran. aggreg.	gran. aggreg.	gran. aggreg.	gran. aggreg.	gran. aggreg.	gran. aggreg.	gran. aggreg.	gran. aggreg.	gran. aggreg.
Si	6.000	6.000	6.000	6.000	6.000	6.000	6.000	6.000	6.000	6.000	6.000	6.000	6.000	6.000	6.000	6.000
Ti	0.001	0.003	0.002	0.002	0.001	0.003	0.002	0.007	0.007	0.006	0.011	0.008	0.000	0.000	0.000	0.000
Zr	0.966	0.955	1.013	0.953	0.975	0.979	1.008	0.967	0.982	0.945	0.963	0.972	1.359	1.358	1.285	1.286
Hf	0.010	0.011	0.013	0.014	0.016	0.013	0.007	0.008	0.015	0.012	0.013	0.014	0.000	0.000	0.000	0.000
Th	0.001	0.000	0.000	0.001	0.000	0.000	0.000	0.001	0.000	0.001	0.000	0.000	0.000	0.000	0.000	0.000
Al	0.002	0.003	0.047	0.006	0.023	0.003	0.025	0.004	0.011	0.002	0.004	0.006	0.000	0.000	0.000	0.000
Fe	0.000	0.004	0.022	0.007	0.004	0.000	0.019	0.011	0.011	0.009	0.004	0.013	0.000	0.009	0.002	0.001
Ca	0.012	0.013	0.018	0.011	0.019	0.008	0.026	0.014	0.023	0.013	0.015	0.008	0.000	0.000	0.000	0.000
Na	1.965	1.876	1.917	1.928	1.888	1.942	1.891	1.942	1.993	1.939	1.915	1.905	1.907	1.917	1.866	1.853
K	0.012	0.004	0.019	0.007	0.011	0.005	0.019	0.012	0.021	0.011	0.011	0.016	0.010	0.012	0.014	0.015
Pb	0.000	0.000	0.000	0.000	0.000	0.000	0.000	0.000	0.000	0.000	0.000	0.000	0.000	0.000	0.000	0.000
Mg	0.000	0.000	0.000	0.000	0.000	0.000	0.000	0.000	0.000	0.000	0.000	0.000	0.000	0.000	0.000	0.000
V	0.000	0.000	0.000	0.000	0.000	0.000	0.000	0.000	0.000	0.000	0.000	0.000	0.000	0.000	0.000	0.000
P	0.000	0.000	0.000	0.000	0.000	0.000	0.000	0.000	0.000	0.000	0.000	0.000	0.000	0.000	0.000	0.000
Nb	0.001	0.001	0.000	0.000	0.000	0.000	0.003	0.009	0.000	0.001	0.000	0.000	0.000	0.000	0.000	0.000
Ta	0.000	0.000	0.000	0.000	0.000	0.000	0.000	0.000	0.000	0.000	0.000	0.000	0.000	0.000	0.000	0.000
U	0.000	0.000	0.000	0.000	0.000	0.000	0.000	0.000	0.000	0.000	0.000	0.000	0.000	0.000	0.000	0.000
Mn	0.000	0.000	0.000	0.000	0.000	0.000	0.000	0.000	0.000	0.000	0.000	0.000	0.000	0.000	0.000	0.000
Cr	0.000	0.000	0.000	0.000	0.000	0.000	0.000	0.000	0.000	0.000	0.000	0.000	0.000	0.000	0.000	0.000
La	0.000	0.000	0.000	0.000	0.000	0.000	0.000	0.000	0.000	0.000	0.000	0.000	0.000	0.000	0.000	0.000
Ce	0.000	0.000	0.000	0.000	0.000	0.000	0.000	0.000	0.000	0.000	0.000	0.000	0.000	0.000	0.000	0.000
Nd	0.000	0.000	0.000	0.000	0.000	0.000	0.000	0.000	0.000	0.000	0.000	0.000	0.000	0.000	0.000	0.000
Gd	0.000	0.006	0.006	0.001	0.003	0.002	0.005	0.000	0.000	0.000	0.000	0.000	0.000	0.000	0.000	0.000
Dy	0.004	0.003	0.003	0.000	0.000	0.000	0.004	0.000	0.000	0.000	0.000	0.000	0.000	0.000	0.000	0.000
Yb	0.002	0.000	0.007	0.004	0.004	0.001	0.000	0.000	0.000	0.000	0.000	0.000	0.000	0.000	0.000	0.000
Y	0.008	0.008	0.008	0.007	0.013	0.010	0.004	0.001	0.002	0.000	0.000	0.002	0.000	0.000	0.000	0.000

mineral	elpidita	elpidita	elpidita	elpidita	elpidita	elpidita	elpidita	elpidita	elpidita	elpidita	elpidita	elpidita	elpidita
Sample			MR38_c2a		MR38_c3						MR43_1_C1		
Point ID			1	2	1	2	3	4	5	6	1	2	3
obs.	gran. aggreg.	gran. aggreg.	euhedral crystal	euhedral crystal	euhedral crystal	euhedral crystal	euhedral crystal	euhedral crystal	euhedral crystal	euhedral crystal	euhedral crystal	euhedral crystal	euhedral crystal
SiO_2	56.88	56.68	58.96	59.34	59.15	57.56	54.17	57.56	55.13	56.89	58.66	58.98	59.25
TiO_2	b.d.l	b.d.l	0.03	0.09	0.14	0.17	0.16	0.06	0.12	0.17	0.12	0.10	0.17
ZrO_2	26.93	24.34	19.12	18.91	19.46	18.93	19.92	18.77	20.80	18.81	19.58	20.24	19.04
HfO_2	b.d.l	b.d.l	0.41	0.19	0.46	0.55	0.48	0.45	0.50	0.39	0.40	0.34	0.33
ThO_2	b.d.l	b.d.l	0.03	b.d.l	b.d.l	0.02	b.d.l	0.07	b.d.l	0.03	b.d.l	0.05	b.d.l
Al_2O_3	b.d.l	b.d.l	0.07	0.07	0.05	0.05	1.30	0.07	0.20	0.10	b.d.l	b.d.l	0.01
FeO	b.d.l	0.08	0.24	0.18	0.31	0.15	0.25	0.14	0.09	0.16	0.01	0.02	0.06
CaO	b.d.l	b.d.l	0.22	0.16	0.08	0.11	0.12	0.05	0.06	0.11	0.05	b.d.l	0.05
Na_2O	9.38	9.23	8.96	9.07	10.32	9.81	9.57	10.04	9.43	9.13	9.97	9.94	9.66
K_2O	0.07	0.06	0.29	0.26	0.17	0.12	0.18	0.15	0.19	0.13	0.08	0.07	0.12
PbO	b.d.l	b.d.l	b.d.l	b.d.l	b.d.l	b.d.l	b.d.l	b.d.l	b.d.l	b.d.l	b.d.l	b.d.l	b.d.l
MgO	b.d.l	b.d.l	b.d.l	b.d.l	b.d.l	b.d.l	b.d.l	b.d.l	b.d.l	b.d.l	b.d.l	b.d.l	b.d.l
V_2O_5	b.d.l	b.d.l	b.d.l	b.d.l	b.d.l	b.d.l	b.d.l	b.d.l	b.d.l	b.d.l	b.d.l	b.d.l	b.d.l
P_2O_5	b.d.l	b.d.l	b.d.l	b.d.l	b.d.l	b.d.l	b.d.l	b.d.l	b.d.l	b.d.l	b.d.l	b.d.l	b.d.l
Nb_2O_5	b.d.l	b.d.l	0.23	0.31	0.04	0.00	0.05	b.d.l	b.d.l	0.03	b.d.l	b.d.l	0.00
Ta_2O_5	b.d.l	b.d.l	b.d.l	b.d.l	b.d.l	b.d.l	b.d.l	b.d.l	b.d.l	b.d.l	b.d.l	b.d.l	b.d.l
UO_2	b.d.l	b.d.l	b.d.l	b.d.l	b.d.l	b.d.l	b.d.l	b.d.l	b.d.l	b.d.l	b.d.l	b.d.l	b.d.l
MnO	b.d.l	b.d.l	b.d.l	b.d.l	b.d.l	b.d.l	b.d.l	b.d.l	b.d.l	b.d.l	b.d.l	b.d.l	b.d.l
Cr_2O_3	b.d.l	b.d.l	b.d.l	b.d.l	b.d.l	b.d.l	b.d.l	b.d.l	b.d.l	b.d.l	b.d.l	b.d.l	b.d.l
La_2O_3	b.d.l	b.d.l	b.d.l	b.d.l	b.d.l	b.d.l	b.d.l	b.d.l	b.d.l	b.d.l	b.d.l	b.d.l	b.d.l
Ce_2O_3	b.d.l	b.d.l	b.d.l	b.d.l	b.d.l	b.d.l	b.d.l	b.d.l	b.d.l	b.d.l	b.d.l	b.d.l	b.d.l
Nd_2O_3	b.d.l	b.d.l	b.d.l	b.d.l	b.d.l	b.d.l	b.d.l	b.d.l	b.d.l	b.d.l	b.d.l	b.d.l	b.d.l
Gd_2O_3	b.d.l	b.d.l	b.d.l	b.d.l	b.d.l	0.11	b.d.l	0.02	b.d.l	0.15	b.d.l	0.04	b.d.l
Dy_2O_3	b.d.l	b.d.l	b.d.l	b.d.l	b.d.l	b.d.l	0.11	0.07	b.d.l	b.d.l	0.15	b.d.l	b.d.l
Yb_2O_3	b.d.l	b.d.l	b.d.l	0.12	0.01	b.d.l	b.d.l	0.02	b.d.l	0.10	0.07	0.10	0.13
Y_2O_3	b.d.l	b.d.l	0.20	0.06	0.06	0.03	0.07	0.09	0.09	b.d.l	0.07	0.02	0.22
Total	93.26	90.39	88.76	88.78	90.26	87.61	86.38	87.55	86.61	86.20	89.18	89.89	89.05
Cl	n.a	n.a	n.a	n.a	n.a	n.a	n.a	n.a	n.a	n.a	n.a	n.a	n.a
F	b.d.l	b.d.l	b.d.l	b.d.l	b.d.l	0.03	0.03	b.d.l	0.10	0.06	0.07	0.04	0.15
H_2O*	9.00	9.00	10.13	10.13	10.13	10.13	10.13	10.13	10.13	10.13	10.13	10.13	10.13
Total 2	102.26	99.39	98.88	98.90	100.39	97.77	96.54	97.68	96.84	96.38	99.37	100.05	99.33

na = não analisado

bdl = abaixo do limite de detecção

mineral	elpidita	elpidita	elpidita	elpidita	elpidita	elpidita	elpidita	elpidita	elpidita	elpidita	elpidita	elpidita	elpidita
Sample			MR38_c2a		MR38_c3						MR43_1_C1		
Point ID			1	2	1	2	3	4	5	6	1	2	3
obs.	gran. aggreg.	gran. aggreg.	euhedral crystal	euhedral crystal	euhedral crystal	euhedral crystal	euhedral crystal	euhedral crystal	euhedral crystal	euhedral crystal	euhedral crystal	euhedral crystal	euhedral crystal
Si	6.000	6.000	6.000	6.000	6.000	6.000	6.000	6.000	6.000	6.000	6.000	6.000	6.000
Ti	0.000	0.000	0.001	0.004	0.006	0.008	0.007	0.003	0.006	0.007	0.005	0.004	0.007
Zr	1.385	1.256	0.949	0.932	0.963	0.962	1.076	0.954	1.104	0.967	0.977	1.004	0.940
Hf	0.000	0.000	0.012	0.006	0.013	0.016	0.015	0.013	0.015	0.012	0.012	0.010	0.010
Th	0.000	0.000	0.001	0.000	0.000	0.001	0.000	0.002	0.000	0.001	0.000	0.001	0.000
Al	0.000	0.000	0.009	0.008	0.006	0.006	0.170	0.008	0.026	0.012	0.001	0.000	0.001
Fe	0.000	0.007	0.021	0.015	0.026	0.013	0.023	0.012	0.008	0.014	0.001	0.002	0.005
Ca	0.000	0.000	0.024	0.018	0.009	0.012	0.014	0.005	0.007	0.013	0.005	0.000	0.006
Na	1.919	1.895	1.768	1.778	2.030	1.983	2.055	2.029	1.990	1.867	1.977	1.961	1.897
K	0.010	0.009	0.038	0.034	0.022	0.015	0.025	0.020	0.026	0.017	0.011	0.009	0.015
Pb	0.000	0.000	0.000	0.000	0.000	0.000	0.000	0.000	0.000	0.000	0.000	0.000	0.000
Mg	0.000	0.000	0.000	0.000	0.000	0.000	0.000	0.000	0.000	0.000	0.000	0.000	0.000
V	0.000	0.000	0.000	0.000	0.000	0.000	0.000	0.000	0.000	0.000	0.000	0.000	0.000
P	0.000	0.000	0.000	0.000	0.000	0.000	0.000	0.000	0.000	0.000	0.000	0.000	0.000
Nb	0.000	0.000	0.010	0.014	0.002	0.000	0.003	0.000	0.000	0.001	0.000	0.000	0.000
Ta	0.000	0.000	0.000	0.000	0.000	0.000	0.000	0.000	0.000	0.000	0.000	0.000	0.000
U	0.000	0.000	0.000	0.000	0.000	0.000	0.000	0.000	0.000	0.000	0.000	0.000	0.000
Mn	0.000	0.000	0.000	0.000	0.000	0.000	0.000	0.000	0.000	0.000	0.000	0.000	0.000
Cr	0.000	0.000	0.000	0.000	0.000	0.000	0.000	0.000	0.000	0.000	0.000	0.000	0.000
La	0.000	0.000	0.000	0.000	0.000	0.000	0.000	0.000	0.000	0.000	0.000	0.000	0.000
Ce	0.000	0.000	0.000	0.000	0.000	0.000	0.000	0.000	0.000	0.000	0.000	0.000	0.000
Nd	0.000	0.000	0.000	0.000	0.000	0.000	0.000	0.000	0.000	0.000	0.000	0.000	0.000
Gd	0.000	0.000	0.000	0.000	0.000	0.004	0.000	0.001	0.000	0.006	0.000	0.001	0.000
Dy	0.000	0.000	0.000	0.000	0.000	0.000	0.004	0.002	0.000	0.000	0.005	0.000	0.000
Yb	0.000	0.000	0.000	0.004	0.000	0.000	0.000	0.001	0.000	0.004	0.002	0.003	0.004
Y	0.000	0.000	0.006	0.002	0.002	0.001	0.002	0.003	0.003	0.000	0.002	0.001	0.007

mineral	elpidita	elpidita	elpidita	elpidita	elpidita	elpidita	elpidita	elpidita	elpidita	elpidita	elpidita	elpidita
Sample				MR43_1_C2a							MR43_3_C1	
Point ID	4	5	6	1	2	3	4	5	6	7	1	2
obs.	euhedral crystal	euhedral crystal	euhedral crystal	euhedral crystal	euhedral crystal	euhedral crystal	euhedral crystal	euhedral crystal	euhedral crystal	euhedral crystal	euhedral crystal	euhedral crystal
SiO_2	59.00	58.97	58.88	59.33	59.16	58.96	59.48	58.80	59.54	59.12	59.29	59.76
TiO_2	0.12	0.08	0.13	0.01	0.03	0.06	0.04	0.05	0.09	0.08	0.01	0.07
ZrO_2	19.85	20.24	20.04	19.95	18.91	19.67	19.42	19.49	19.13	19.60	19.32	19.30
HfO_2	0.45	0.34	0.49	0.34	0.29	0.39	0.35	0.37	0.38	0.39	0.41	0.33
ThO_2	b.d.l	0.03	b.d.l	b.d.l	b.d.l	b.d.l	0.02	0.04	b.d.l	b.d.l	b.d.l	0.08
Al_2O_3	0.03	0.03	0.02	0.04	0.06	0.03	0.06	0.06	0.05	0.04	0.02	0.03
FeO	0.02	0.02	0.01	0.06	0.01	0.02	b.d.l	0.06	0.07	0.01	0.04	0.00
CaO	0.03	0.01	b.d.l	0.04	0.01	0.08	0.07	0.09	0.03	0.04	0.02	0.10
Na_2O	10.32	9.48	9.78	9.63	9.60	9.71	10.04	9.77	9.76	9.97	9.75	9.40
K_2O	0.07	0.09	0.08	0.02	0.09	0.12	0.03	0.08	0.04	0.10	0.09	0.12
PbO	b.d.l	b.d.l	b.d.l	b.d.l	b.d.l	b.d.l	b.d.l	b.d.l	b.d.l	b.d.l	b.d.l	b.d.l
MgO	b.d.l	b.d.l	b.d.l	b.d.l	b.d.l	b.d.l	b.d.l	b.d.l	b.d.l	b.d.l	b.d.l	b.d.l
V_2O_5	b.d.l	b.d.l	b.d.l	b.d.l	b.d.l	b.d.l	b.d.l	b.d.l	b.d.l	b.d.l	b.d.l	b.d.l
P_2O_5	b.d.l	b.d.l	b.d.l	b.d.l	b.d.l	b.d.l	b.d.l	b.d.l	b.d.l	b.d.l	b.d.l	b.d.l
Nb_2O_5	b.d.l	b.d.l	0.02	b.d.l	0.02	b.d.l	b.d.l	0.02	0.01	b.d.l	b.d.l	b.d.l
Ta_2O_5	b.d.l	b.d.l	b.d.l	b.d.l	b.d.l	b.d.l	b.d.l	b.d.l	b.d.l	b.d.l	b.d.l	b.d.l
UO_2	b.d.l	b.d.l	b.d.l	b.d.l	b.d.l	b.d.l	b.d.l	b.d.l	b.d.l	b.d.l	b.d.l	b.d.l
MnO	b.d.l	b.d.l	b.d.l	b.d.l	b.d.l	b.d.l	b.d.l	b.d.l	b.d.l	b.d.l	b.d.l	b.d.l
Cr_2O_3	b.d.l	b.d.l	b.d.l	b.d.l	b.d.l	b.d.l	b.d.l	b.d.l	b.d.l	b.d.l	b.d.l	b.d.l
La_2O_3	b.d.l	b.d.l	b.d.l	b.d.l	b.d.l	b.d.l	b.d.l	b.d.l	b.d.l	b.d.l	b.d.l	b.d.l
Ce_2O_3	b.d.l	b.d.l	b.d.l	b.d.l	b.d.l	b.d.l	b.d.l	b.d.l	b.d.l	b.d.l	b.d.l	b.d.l
Nd_2O_3	b.d.l	b.d.l	b.d.l	b.d.l	b.d.l	b.d.l	b.d.l	b.d.l	b.d.l	b.d.l	b.d.l	b.d.l
Gd_2O_3	0.14	0.19	0.01	0.06	0.11	0.12	0.08	0.04	b.d.l	0.13	0.03	0.04
Dy_2O_3	0.14	b.d.l	b.d.l	0.07	0.16	b.d.l	b.d.l	0.06	b.d.l	b.d.l	b.d.l	b.d.l
Yb_2O_3	0.05	0.02	0.02	0.20	0.13	0.04	0.11	0.09	b.d.l	0.10	0.01	0.11
Y_2O_3	0.07	b.d.l	0.03	0.42	0.50	0.46	0.44	0.48	0.33	0.41	0.44	0.56
Total	90.29	89.51	89.53	90.17	89.08	89.67	90.14	89.51	89.43	89.99	89.42	89.90
Cl	n.a	n.a	n.a	n.a	n.a	n.a	n.a	n.a	n.a	n.a	n.a	n.a
F	0.15	b.d.l	b.d.l	b.d.l	0.03	b.d.l	0.09	0.03	b.d.l	0.06	b.d.l	0.05
H_2O*	10.13	10.13	10.13	10.13	10.13	10.13	10.13	10.13	10.13	10.13	10.13	10.13
Total 2	100.56	99.64	99.65	100.29	99.23	99.79	100.36	99.66	99.55	100.17	99.55	100.08

na = não analisado

bdl = abaixo do limite de detecção

mineral	elpidita	elpidita	elpidita	elpidita	elpidita	elpidita	elpidita	elpidita	elpidita	elpidita	elpidita	elpidita
Sample				MR43_1_C2a							MR43_3_C1	
Point ID	4	5	6	1	2	3	4	5	6	7	1	2
obs.	euhedral crystal	euhedral crystal	euhedral crystal	euhedral crystal	euhedral crystal	euhedral crystal	euhedral crystal	euhedral crystal	euhedral crystal	euhedral crystal	euhedral crystal	euhedral crystal
Si	6.000	6.000	6.000	6.000	6.000	6.000	6.000	6.000	6.000	6.000	6.000	6.000
Ti	0.005	0.003	0.006	0.000	0.001	0.003	0.002	0.002	0.004	0.004	0.000	0.003
Zr	0.984	1.004	0.996	0.984	0.935	0.976	0.955	0.970	0.940	0.970	0.953	0.945
Hf	0.013	0.010	0.014	0.010	0.008	0.011	0.010	0.011	0.011	0.011	0.012	0.009
Th	0.000	0.001	0.000	0.000	0.000	0.000	0.000	0.001	0.000	0.000	0.000	0.002
Al	0.003	0.004	0.003	0.004	0.007	0.004	0.007	0.007	0.007	0.005	0.002	0.003
Fe	0.002	0.002	0.001	0.005	0.001	0.002	0.000	0.005	0.006	0.001	0.003	0.000
Ca	0.004	0.001	0.000	0.004	0.002	0.009	0.008	0.009	0.003	0.004	0.002	0.011
Na	2.035	1.870	1.932	1.888	1.888	1.916	1.964	1.933	1.907	1.962	1.913	1.830
K	0.010	0.012	0.011	0.003	0.012	0.016	0.004	0.011	0.005	0.013	0.012	0.016
Pb	0.000	0.000	0.000	0.000	0.000	0.000	0.000	0.000	0.000	0.000	0.000	0.000
Mg	0.000	0.000	0.000	0.000	0.000	0.000	0.000	0.000	0.000	0.000	0.000	0.000
V	0.000	0.000	0.000	0.000	0.000	0.000	0.000	0.000	0.000	0.000	0.000	0.000
P	0.000	0.000	0.000	0.000	0.000	0.000	0.000	0.000	0.000	0.000	0.000	0.000
Nb	0.000	0.000	0.001	0.000	0.001	0.000	0.000	0.001	0.000	0.000	0.000	0.000
Ta	0.000	0.000	0.000	0.000	0.000	0.000	0.000	0.000	0.000	0.000	0.000	0.000
U	0.000	0.000	0.000	0.000	0.000	0.000	0.000	0.000	0.000	0.000	0.000	0.000
Mn	0.000	0.000	0.000	0.000	0.000	0.000	0.000	0.000	0.000	0.000	0.000	0.000
Cr	0.000	0.000	0.000	0.000	0.000	0.000	0.000	0.000	0.000	0.000	0.000	0.000
La	0.000	0.000	0.000	0.000	0.000	0.000	0.000	0.000	0.000	0.000	0.000	0.000
Ce	0.000	0.000	0.000	0.000	0.000	0.000	0.000	0.000	0.000	0.000	0.000	0.000
Nd	0.000	0.000	0.000	0.000	0.000	0.000	0.000	0.000	0.000	0.000	0.000	0.000
Gd	0.005	0.007	0.000	0.002	0.004	0.004	0.003	0.001	0.000	0.005	0.001	0.001
Dy	0.005	0.000	0.000	0.002	0.006	0.000	0.000	0.002	0.000	0.000	0.000	0.000
Yb	0.002	0.001	0.001	0.007	0.004	0.001	0.004	0.003	0.000	0.003	0.000	0.003
Y	0.002	0.000	0.001	0.013	0.015	0.014	0.013	0.015	0.010	0.013	0.014	0.017

mineral	elpidita	elpidita	elpidita	elpidita	elpidita	elpidita	elpidita	elpidita	elpidita	elpidita	elpidita	elpidita
Sample							MR43_3_C2					
Point ID	3	4	5	6	7	8	1	2	3	4	5	6
obs.	euhedral crystal	euhedral crystal	euhedral crystal	euhedral crystal	euhedral crystal	euhedral crystal	euhedral crystal	euhedral crystal	euhedral crystal	euhedral crystal	euhedral crystal	euhedral crystal
SiO_2	59.18	59.34	59.07	58.88	59.35	58.90	58.76	59.03	58.84	58.92	58.47	59.20
TiO_2	0.03	0.11	0.10	0.08	b.d.l	0.10	0.12	0.24	0.06	0.06	0.09	0.11
ZrO_2	19.22	18.80	19.02	19.29	18.96	19.11	19.86	19.07	19.60	19.90	20.19	19.78
HfO_2	0.44	0.39	0.31	0.30	0.42	0.42	0.50	0.55	0.47	0.42	0.46	0.52
ThO_2	0.04	b.d.l	b.d.l	b.d.l	b.d.l	0.03	b.d.l	0.02	b.d.l	0.02	b.d.l	0.04
Al_2O_3	0.07	0.04	0.07	0.01	0.05	0.05	b.d.l	0.02	0.01	0.02	0.01	0.03
FeO	0.10	0.11	0.16	b.d.l	0.05	0.05	0.09	b.d.l	0.03	b.d.l	0.03	0.02
CaO	0.15	0.01	0.15	0.13	0.08	0.04	0.04	0.02	b.d.l	0.04	0.01	0.02
Na_2O	8.80	9.67	9.65	9.89	9.22	9.56	10.07	9.85	9.99	10.32	10.05	10.10
K_2O	0.23	0.13	0.06	0.11	0.14	0.13	0.10	0.05	0.11	0.11	0.09	0.12
PbO	b.d.l	b.d.l	b.d.l	b.d.l	b.d.l	b.d.l	b.d.l	b.d.l	b.d.l	b.d.l	b.d.l	b.d.l
MgO	b.d.l	b.d.l	b.d.l	b.d.l	b.d.l	b.d.l	b.d.l	b.d.l	b.d.l	b.d.l	b.d.l	b.d.l
V_2O_5	b.d.l	b.d.l	b.d.l	b.d.l	b.d.l	b.d.l	b.d.l	b.d.l	b.d.l	b.d.l	b.d.l	b.d.l
P_2O_5	b.d.l	b.d.l	b.d.l	b.d.l	b.d.l	b.d.l	b.d.l	b.d.l	b.d.l	b.d.l	b.d.l	b.d.l
Nb_2O_5	b.d.l	b.d.l	b.d.l	0.03	b.d.l	0.01	b.d.l	b.d.l	b.d.l	b.d.l	b.d.l	b.d.l
Ta_2O_5	b.d.l	b.d.l	b.d.l	b.d.l	b.d.l	b.d.l	b.d.l	b.d.l	b.d.l	b.d.l	b.d.l	b.d.l
UO_2	b.d.l	b.d.l	b.d.l	b.d.l	b.d.l	b.d.l	b.d.l	b.d.l	b.d.l	b.d.l	b.d.l	b.d.l
MnO	b.d.l	b.d.l	b.d.l	b.d.l	b.d.l	b.d.l	b.d.l	b.d.l	b.d.l	b.d.l	b.d.l	b.d.l
Cr_2O_3	b.d.l	b.d.l	b.d.l	b.d.l	b.d.l	b.d.l	b.d.l	b.d.l	b.d.l	b.d.l	b.d.l	b.d.l
La_2O_3	b.d.l	b.d.l	b.d.l	b.d.l	b.d.l	b.d.l	b.d.l	b.d.l	b.d.l	b.d.l	b.d.l	b.d.l
Ce_2O_3	b.d.l	b.d.l	b.d.l	b.d.l	b.d.l	b.d.l	b.d.l	b.d.l	b.d.l	b.d.l	b.d.l	b.d.l
Nd_2O_3	b.d.l	b.d.l	b.d.l	b.d.l	b.d.l	b.d.l	b.d.l	b.d.l	b.d.l	b.d.l	b.d.l	b.d.l
Gd_2O_3	0.09	b.d.l	0.08	b.d.l	0.07	b.d.l	b.d.l	b.d.l	0.07	b.d.l	b.d.l	0.07
Dy_2O_3	0.15	0.08	b.d.l	0.22	0.23	0.01	b.d.l	b.d.l	b.d.l	0.07	b.d.l	0.12
Yb_2O_3	0.13	0.21	0.12	0.07	0.09	0.02	0.03	b.d.l	0.06	0.13	0.01	0.06
Y_2O_3	0.59	0.37	0.65	0.45	0.61	0.31	0.02	0.01	0.05	0.10	0.05	0.02
Total	89.23	89.26	89.44	89.45	89.28	88.74	89.59	88.85	89.28	90.10	89.46	90.22
Cl	n.a	n.a	n.a	n.a	n.a	n.a	n.a	n.a	n.a	n.a	n.a	n.a
F	0.06	0.11	0.03	b.d.l	b.d.l	b.d.l	0.05	0.01	0.02	b.d.l	b.d.l	0.01
H_2O*	10.13	10.13	10.13	10.13	10.13	10.13	10.13	10.13	10.13	10.13	10.13	10.13
Total 2	99.41	99.49	99.59	99.57	99.40	98.87	99.76	98.99	99.43	100.22	99.59	100.35

na = não analisado

bdl = abaixo do limite de detecção

mineral	elpidita	elpidita	elpidita	elpidita	elpidita	elpidita	elpidita	elpidita	elpidita	elpidita	elpidita	elpidita
Sample							MR43_3_C2					
Point ID	3	4	5	6	7	8	1	2	3	4	5	6
obs.	euhedral crystal	euhedral crystal	euhedral crystal	euhedral crystal	euhedral crystal	euhedral crystal	euhedral crystal	euhedral crystal	euhedral crystal	euhedral crystal	euhedral crystal	euhedral crystal
Si	6.000	6.000	6.000	6.000	6.000	6.000	6.000	6.000	6.000	6.000	6.000	6.000
Ti	0.001	0.005	0.004	0.004	0.000	0.004	0.005	0.010	0.003	0.002	0.004	0.005
Zr	0.950	0.927	0.942	0.959	0.935	0.949	0.989	0.945	0.975	0.988	1.010	0.978
Hf	0.013	0.011	0.009	0.009	0.012	0.012	0.014	0.016	0.014	0.012	0.014	0.015
Th	0.001	0.000	0.000	0.000	0.000	0.001	0.000	0.000	0.000	0.000	0.000	0.001
Al	0.008	0.005	0.008	0.001	0.006	0.006	0.000	0.002	0.001	0.003	0.001	0.004
Fe	0.009	0.009	0.013	0.000	0.004	0.004	0.007	0.000	0.003	0.000	0.002	0.002
Ca	0.016	0.001	0.017	0.014	0.009	0.004	0.004	0.003	0.000	0.005	0.001	0.002
Na	1.730	1.896	1.900	1.954	1.807	1.888	1.994	1.941	1.975	2.038	2.000	1.985
K	0.030	0.017	0.007	0.014	0.018	0.017	0.013	0.006	0.014	0.014	0.011	0.016
Pb	0.000	0.000	0.000	0.000	0.000	0.000	0.000	0.000	0.000	0.000	0.000	0.000
Mg	0.000	0.000	0.000	0.000	0.000	0.000	0.000	0.000	0.000	0.000	0.000	0.000
V	0.000	0.000	0.000	0.000	0.000	0.000	0.000	0.000	0.000	0.000	0.000	0.000
P	0.000	0.000	0.000	0.000	0.000	0.000	0.000	0.000	0.000	0.000	0.000	0.000
Nb	0.000	0.000	0.000	0.001	0.000	0.001	0.000	0.000	0.000	0.000	0.000	0.000
Ta	0.000	0.000	0.000	0.000	0.000	0.000	0.000	0.000	0.000	0.000	0.000	0.000
U	0.000	0.000	0.000	0.000	0.000	0.000	0.000	0.000	0.000	0.000	0.000	0.000
Mn	0.000	0.000	0.000	0.000	0.000	0.000	0.000	0.000	0.000	0.000	0.000	0.000
Cr	0.000	0.000	0.000	0.000	0.000	0.000	0.000	0.000	0.000	0.000	0.000	0.000
La	0.000	0.000	0.000	0.000	0.000	0.000	0.000	0.000	0.000	0.000	0.000	0.000
Ce	0.000	0.000	0.000	0.000	0.000	0.000	0.000	0.000	0.000	0.000	0.000	0.000
Nd	0.000	0.000	0.000	0.000	0.000	0.000	0.000	0.000	0.000	0.000	0.000	0.000
Gd	0.003	0.000	0.003	0.000	0.003	0.000	0.000	0.000	0.002	0.000	0.000	0.003
Dy	0.005	0.003	0.000	0.007	0.008	0.000	0.000	0.000	0.000	0.002	0.000	0.004
Yb	0.004	0.007	0.004	0.002	0.003	0.001	0.001	0.000	0.002	0.004	0.000	0.002
Y	0.018	0.011	0.020	0.014	0.019	0.010	0.001	0.000	0.001	0.003	0.002	0.001

mineral	elpidita	elpidita	elpidita	elpidita	elpidita	elpidita	elpidita	elpidita	elpidita	elpidita	elpidita	elpidita
Sample	MR21				MR38_c5							
Point ID	2				1	2	3	4	5	6	7	8
obs.	euhedral crystal	euhedral crystal	euhedral crystal	euhedral crystal	vein-like aggreg.	vein-like aggreg.	vein-like aggreg.	vein-like aggreg.	vein-like aggreg.	vein-like aggreg.	vein-like aggreg.	vein-like aggreg.
SiO_2	57.46	56.59	57.12	57.50	59.61	58.80	59.06	59.26	57.52	58.79	59.10	58.23
TiO_2	n.a	n.a	n.a	n.a	0.19	0.12	0.13	0.12	0.11	0.12	0.14	0.38
ZrO_2	25.88	27.81	26.13	26.26	19.86	19.77	19.69	19.50	19.94	19.77	19.29	18.68
HfO_2	n.a	n.a	n.a	n.a	0.41	0.37	0.45	0.32	0.32	0.47	0.43	0.31
ThO_2	n.a	n.a	n.a	n.a	0.03	b.d.l	0.07	b.d.l	b.d.l	0.01	b.d.l	0.01
Al_2O_3	n.a	n.a	n.a	n.a	0.04	0.13	0.06	0.02	0.04	0.02	0.08	0.04
FeO	0.01	0.07	b.d.l	0.05	0.10	0.10	0.09	0.15	0.06	0.14	0.07	0.11
CaO	b.d.l	b.d.l	b.d.l	b.d.l	0.21	0.09	0.13	0.15	0.24	0.17	0.08	0.23
Na_2O	9.39	9.14	9.55	9.33	10.01	9.98	9.67	9.76	9.25	9.56	9.93	9.38
K_2O	0.29	0.32	0.10	0.33	0.11	0.12	0.11	0.11	0.24	0.14	0.09	0.16
PbO	b.d.l	b.d.l	b.d.l	b.d.l	b.d.l	b.d.l	b.d.l	b.d.l	b.d.l	b.d.l	b.d.l	b.d.l
MgO	b.d.l	b.d.l	b.d.l	b.d.l	b.d.l	b.d.l	b.d.l	b.d.l	b.d.l	b.d.l	b.d.l	b.d.l
V_2O_5	b.d.l	b.d.l	b.d.l	b.d.l	b.d.l	b.d.l	b.d.l	b.d.l	b.d.l	b.d.l	b.d.l	b.d.l
P_2O_5	b.d.l	b.d.l	b.d.l	b.d.l	b.d.l	b.d.l	b.d.l	b.d.l	b.d.l	b.d.l	b.d.l	b.d.l
Nb_2O_5	b.d.l	b.d.l	b.d.l	b.d.l	0.05	0.01	b.d.l	b.d.l	b.d.l	b.d.l	0.03	b.d.l
Ta_2O_5	b.d.l	b.d.l	b.d.l	b.d.l	b.d.l	b.d.l	b.d.l	b.d.l	b.d.l	b.d.l	b.d.l	b.d.l
UO_2	b.d.l	b.d.l	b.d.l	b.d.l	b.d.l	b.d.l	b.d.l	b.d.l	b.d.l	b.d.l	b.d.l	b.d.l
MnO	b.d.l	b.d.l	b.d.l	b.d.l	b.d.l	b.d.l	b.d.l	b.d.l	b.d.l	b.d.l	b.d.l	b.d.l
Cr_2O_3	b.d.l	b.d.l	b.d.l	b.d.l	b.d.l	b.d.l	b.d.l	b.d.l	b.d.l	b.d.l	b.d.l	b.d.l
La_2O_3	b.d.l	b.d.l	b.d.l	b.d.l	b.d.l	b.d.l	b.d.l	b.d.l	b.d.l	b.d.l	b.d.l	b.d.l
Ce_2O_3	b.d.l	b.d.l	b.d.l	b.d.l	b.d.l	b.d.l	b.d.l	b.d.l	b.d.l	b.d.l	b.d.l	b.d.l
Nd_2O_3	b.d.l	b.d.l	b.d.l	b.d.l	b.d.l	b.d.l	b.d.l	b.d.l	b.d.l	b.d.l	b.d.l	b.d.l
Gd_2O_3	b.d.l	b.d.l	b.d.l	b.d.l	b.d.l	b.d.l	0.04	0.04	0.15	0.10	b.d.l	b.d.l
Dy_2O_3	b.d.l	b.d.l	b.d.l	b.d.l	b.d.l	0.02	0.15	0.09	0.04	b.d.l	b.d.l	b.d.l
Yb_2O_3	b.d.l	b.d.l	b.d.l	b.d.l	0.06	0.12	0.11	0.19	0.04	0.13	b.d.l	b.d.l
Y_2O_3	b.d.l	b.d.l	b.d.l	b.d.l	0.02	0.00	0.04	0.07	0.03	0.05	0.02	0.12
Total	93.02	93.93	92.90	93.46	90.70	89.62	89.80	89.79	87.99	89.48	89.26	87.64
Cl	n.a	n.a	n.a	n.a	n.a	n.a	n.a	n.a	n.a	n.a	n.a	n.a
F	b.d.l	b.d.l	b.d.l	b.d.l	0.01	b.d.l	b.d.l	b.d.l	b.d.l	b.d.l	b.d.l	0.04
H_2O*	9.00	9.00	9.00	9.00	10.13	10.13	10.13	10.13	10.13	10.13	10.13	10.13
Total 2	102.02	102.93	101.90	102.46	100.84	99.75	99.93	99.91	98.11	99.61	99.38	97.80

na = não analisado

bdl = abaixo do limite de detecção

mineral	elpidita	elpidita	elpidita	elpidita	elpidita	elpidita	elpidita	elpidita	elpidita	elpidita	elpidita	elpidita
Sample	MR21				MR38_c5							
Point ID	2				1	2	3	4	5	6	7	8
obs.	euhedral crystal	euhedral crystal	euhedral crystal	euhedral crystal	vein-like aggreg.	vein-like aggreg.	vein-like aggreg.	vein-like aggreg.	vein-like aggreg.	vein-like aggreg.	vein-like aggreg.	vein-like aggreg.
Si	6.000	6.000	6.000	6.000	6.000	6.000	6.000	6.000	6.000	6.000	6.000	6.000
Ti	0.000	0.000	0.000	0.000	0.008	0.005	0.005	0.005	0.005	0.005	0.006	0.016
Zr	1.318	1.438	1.338	1.336	0.975	0.984	0.975	0.963	1.014	0.984	0.955	0.939
Hf	0.000	0.000	0.000	0.000	0.012	0.011	0.013	0.009	0.010	0.014	0.013	0.009
Th	0.000	0.000	0.000	0.000	0.001	0.000	0.002	0.000	0.000	0.000	0.000	0.000
Al	0.000	0.000	0.000	0.000	0.004	0.015	0.007	0.003	0.005	0.003	0.009	0.004
Fe	0.001	0.006	0.000	0.004	0.008	0.009	0.008	0.013	0.005	0.012	0.006	0.010
Ca	0.000	0.000	0.000	0.000	0.023	0.009	0.014	0.016	0.026	0.018	0.009	0.025
Na	1.901	1.879	1.945	1.887	1.954	1.974	1.905	1.916	1.871	1.892	1.955	1.874
K	0.038	0.043	0.014	0.044	0.014	0.015	0.014	0.015	0.032	0.018	0.011	0.021
Pb	0.000	0.000	0.000	0.000	0.000	0.000	0.000	0.000	0.000	0.000	0.000	0.000
Mg	0.000	0.000	0.000	0.000	0.000	0.000	0.000	0.000	0.000	0.000	0.000	0.000
V	0.000	0.000	0.000	0.000	0.000	0.000	0.000	0.000	0.000	0.000	0.000	0.000
P	0.000	0.000	0.000	0.000	0.000	0.000	0.000	0.000	0.000	0.000	0.000	0.000
Nb	0.000	0.000	0.000	0.000	0.002	0.000	0.000	0.000	0.000	0.000	0.001	0.000
Ta	0.000	0.000	0.000	0.000	0.000	0.000	0.000	0.000	0.000	0.000	0.000	0.000
U	0.000	0.000	0.000	0.000	0.000	0.000	0.000	0.000	0.000	0.000	0.000	0.000
Mn	0.000	0.000	0.000	0.000	0.000	0.000	0.000	0.000	0.000	0.000	0.000	0.000
Cr	0.000	0.000	0.000	0.000	0.000	0.000	0.000	0.000	0.000	0.000	0.000	0.000
La	0.000	0.000	0.000	0.000	0.000	0.000	0.000	0.000	0.000	0.000	0.000	0.000
Ce	0.000	0.000	0.000	0.000	0.000	0.000	0.000	0.000	0.000	0.000	0.000	0.000
Nd	0.000	0.000	0.000	0.000	0.000	0.000	0.000	0.000	0.000	0.000	0.000	0.000
Gd	0.000	0.000	0.000	0.000	0.000	0.000	0.001	0.001	0.006	0.004	0.000	0.000
Dy	0.000	0.000	0.000	0.000	0.000	0.001	0.005	0.003	0.001	0.000	0.000	0.000
Yb	0.000	0.000	0.000	0.000	0.002	0.004	0.004	0.006	0.001	0.004	0.000	0.000
Y	0.000	0.000	0.000	0.000	0.001	0.000	0.001	0.002	0.001	0.002	0.001	0.004

mineral	elpidita	elpidita	elpidita	elpidita	elpidita	elpidita	elpidita	elpidita	elpidita	elpidita	elpidita	elpidita
Sample			MR21(L1)									
Point ID	9	10	2									
obs.	vein-like aggreg.	vein-like aggreg.	vein-like aggreg.	vein-like aggreg.	vein-like aggreg.	vein-like aggreg.	vein-like aggreg.	vein-like aggreg.	vein-like aggreg.	vein-like aggreg.	vein-like aggreg.	vein-like aggreg.
SiO_2	59.13	59.91	58.09	58.61	58.65	57.12	58.62	57.32	57.85	59.18	58.16	58.76
TiO_2	0.23	0.21	n.a	n.a	n.a	n.a	n.a	n.a	n.a	n.a	n.a	n.a
ZrO_2	19.31	19.36	26.03	25.63	26.38	25.58	25.67	25.68	25.62	24.87	26.08	26.06
HfO_2	0.30	0.42	n.a	n.a	n.a	n.a	n.a	n.a	n.a	n.a	n.a	n.a
ThO_2	b.d.l	b.d.l	n.a	n.a	n.a	n.a	n.a	n.a	n.a	n.a	n.a	n.a
Al_2O_3	0.05	0.07	n.a	n.a	n.a	n.a	n.a	n.a	n.a	n.a	n.a	n.a
FeO	0.16	0.09	0.02	b.d.l	0.10	0.02	0.04	b.d.l	0.02	0.09	0.10	b.d.l
CaO	0.18	0.16	b.d.l	b.d.l	b.d.l	b.d.l	b.d.l	b.d.l	b.d.l	b.d.l	b.d.l	b.d.l
Na_2O	9.38	9.75	9.55	9.13	9.54	9.10	9.47	9.16	9.21	8.77	9.41	9.22
K_2O	0.13	0.14	0.10	0.10	0.18	0.11	0.08	0.07	0.10	0.19	0.10	0.17
PbO	b.d.l	b.d.l	b.d.l	b.d.l	b.d.l	b.d.l	b.d.l	b.d.l	b.d.l	b.d.l	b.d.l	b.d.l
MgO	b.d.l	b.d.l	b.d.l	b.d.l	b.d.l	b.d.l	b.d.l	b.d.l	b.d.l	b.d.l	b.d.l	b.d.l
V_2O_5	b.d.l	b.d.l	b.d.l	b.d.l	b.d.l	b.d.l	b.d.l	b.d.l	b.d.l	b.d.l	b.d.l	b.d.l
P_2O_5	b.d.l	b.d.l	b.d.l	b.d.l	b.d.l	b.d.l	b.d.l	b.d.l	b.d.l	b.d.l	b.d.l	b.d.l
Nb_2O_5	b.d.l	0.04	b.d.l	b.d.l	b.d.l	b.d.l	b.d.l	b.d.l	b.d.l	b.d.l	b.d.l	b.d.l
Ta_2O_5	b.d.l	b.d.l	b.d.l	b.d.l	b.d.l	b.d.l	b.d.l	b.d.l	b.d.l	b.d.l	b.d.l	b.d.l
UO_2	b.d.l	b.d.l	b.d.l	b.d.l	b.d.l	b.d.l	b.d.l	b.d.l	b.d.l	b.d.l	b.d.l	b.d.l
MnO	b.d.l	b.d.l	b.d.l	b.d.l	b.d.l	b.d.l	b.d.l	b.d.l	b.d.l	b.d.l	b.d.l	b.d.l
Cr_2O_3	b.d.l	b.d.l	b.d.l	b.d.l	b.d.l	b.d.l	b.d.l	b.d.l	b.d.l	b.d.l	b.d.l	b.d.l
La_2O_3	b.d.l	b.d.l	b.d.l	b.d.l	b.d.l	b.d.l	b.d.l	b.d.l	b.d.l	b.d.l	b.d.l	b.d.l
Ce_2O_3	b.d.l	b.d.l	b.d.l	b.d.l	b.d.l	b.d.l	b.d.l	b.d.l	b.d.l	b.d.l	b.d.l	b.d.l
Nd_2O_3	b.d.l	b.d.l	b.d.l	b.d.l	b.d.l	b.d.l	b.d.l	b.d.l	b.d.l	b.d.l	b.d.l	b.d.l
Gd_2O_3	b.d.l	0.04	b.d.l	b.d.l	b.d.l	b.d.l	b.d.l	b.d.l	b.d.l	b.d.l	b.d.l	b.d.l
Dy_2O_3	b.d.l	b.d.l	b.d.l	b.d.l	b.d.l	b.d.l	b.d.l	b.d.l	b.d.l	b.d.l	b.d.l	b.d.l
Yb_2O_3	0.05	b.d.l	b.d.l	b.d.l	b.d.l	b.d.l	b.d.l	b.d.l	b.d.l	b.d.l	b.d.l	b.d.l
Y_2O_3	0.05	0.03	b.d.l	b.d.l	b.d.l	b.d.l	b.d.l	b.d.l	b.d.l	b.d.l	b.d.l	b.d.l
Total	88.96	90.21	93.79	93.47	94.86	91.93	93.88	92.22	92.80	93.09	93.85	94.20
Cl	n.a	n.a	n.a	n.a	n.a	n.a	n.a	n.a	n.a	n.a	n.a	n.a
F	b.d.l	0.03	b.d.l	b.d.l	b.d.l	b.d.l	b.d.l	b.d.l	b.d.l	b.d.l	b.d.l	b.d.l
H_2O*	10.13	10.13	9.00	9.00	9.00	9.00	9.00	9.00	9.00	9.00	9.00	9.00
Total 2	99.09	100.36	102.79	102.47	103.86	100.93	102.88	101.22	101.80	102.09	102.85	103.20

na = não analisado

bdl = abaixo do limite de detecção

mineral	elpidita	elpidita	elpidita	elpidita	elpidita	elpidita	elpidita	elpidita	elpidita	elpidita	elpidita	elpidita
Sample			MR21(L1)									
Point ID	9	10	2									
obs.	vein-like aggreg.	vein-like aggreg.	vein-like aggreg.	vein-like aggreg.	vein-like aggreg.	vein-like aggreg.	vein-like aggreg.	vein-like aggreg.	vein-like aggreg.	vein-like aggreg.	vein-like aggreg.	vein-like aggreg.
Si	6.000	6.000	6.000	6.000	6.000	6.000	6.000	6.000	6.000	6.000	6.000	6.000
Ti	0.010	0.009	0.000	0.000	0.000	0.000	0.000	0.000	0.000	0.000	0.000	0.000
Zr	0.955	0.945	1.311	1.279	1.316	1.310	1.281	1.311	1.296	1.229	1.312	1.298
Hf	0.009	0.012	0.000	0.000	0.000	0.000	0.000	0.000	0.000	0.000	0.000	0.000
Th	0.000	0.000	0.000	0.000	0.000	0.000	0.000	0.000	0.000	0.000	0.000	0.000
Al	0.005	0.008	0.000	0.000	0.000	0.000	0.000	0.000	0.000	0.000	0.000	0.000
Fe	0.014	0.007	0.002	0.000	0.009	0.002	0.004	0.000	0.002	0.008	0.008	0.000
Ca	0.020	0.017	0.000	0.000	0.000	0.000	0.000	0.000	0.000	0.000	0.000	0.000
Na	1.845	1.893	1.912	1.812	1.892	1.853	1.880	1.860	1.853	1.723	1.883	1.825
K	0.017	0.018	0.013	0.013	0.024	0.014	0.010	0.009	0.013	0.025	0.013	0.021
Pb	0.000	0.000	0.000	0.000	0.000	0.000	0.000	0.000	0.000	0.000	0.000	0.000
Mg	0.000	0.000	0.000	0.000	0.000	0.000	0.000	0.000	0.000	0.000	0.000	0.000
V	0.000	0.000	0.000	0.000	0.000	0.000	0.000	0.000	0.000	0.000	0.000	0.000
P	0.000	0.000	0.000	0.000	0.000	0.000	0.000	0.000	0.000	0.000	0.000	0.000
Nb	0.000	0.002	0.000	0.000	0.000	0.000	0.000	0.000	0.000	0.000	0.000	0.000
Ta	0.000	0.000	0.000	0.000	0.000	0.000	0.000	0.000	0.000	0.000	0.000	0.000
U	0.000	0.000	0.000	0.000	0.000	0.000	0.000	0.000	0.000	0.000	0.000	0.000
Mn	0.000	0.000	0.000	0.000	0.000	0.000	0.000	0.000	0.000	0.000	0.000	0.000
Cr	0.000	0.000	0.000	0.000	0.000	0.000	0.000	0.000	0.000	0.000	0.000	0.000
La	0.000	0.000	0.000	0.000	0.000	0.000	0.000	0.000	0.000	0.000	0.000	0.000
Ce	0.000	0.000	0.000	0.000	0.000	0.000	0.000	0.000	0.000	0.000	0.000	0.000
Nd	0.000	0.000	0.000	0.000	0.000	0.000	0.000	0.000	0.000	0.000	0.000	0.000
Gd	0.000	0.001	0.000	0.000	0.000	0.000	0.000	0.000	0.000	0.000	0.000	0.000
Dy	0.000	0.000	0.000	0.000	0.000	0.000	0.000	0.000	0.000	0.000	0.000	0.000
Yb	0.002	0.000	0.000	0.000	0.000	0.000	0.000	0.000	0.000	0.000	0.000	0.000
Y	0.001	0.001	0.000	0.000	0.000	0.000	0.000	0.000	0.000	0.000	0.000	0.000

mineral	(Na,K)ZrS-I	(Na,K)ZrS-I	(Na,K)ZrS-I	(Na,K)ZrS-I	(Na,K)ZrS-I	(Na,K)ZrS-I	(Na,K)ZrS-I	(Na,K)ZrS-II	(Na,K)ZrS-II	(Na,K)ZrS-II	(Na,K)ZrS-II	(Na,K)ZrS-II	(Na,K)ZrS-II	(Na,K)ZrS-II
Sample	MR38_c1							MR26_c1						
Point ID	1	2	3	4	5	6	7	1	2	3	4	5	6	8
obs.	euhedral crystal	euhedral crystal	euhedral crystal	euhedral crystal	euhedral crystal	euhedral crystal	euhedral crystal							
SiO_2	65.25	64.82	63.85	57.85	57.46	52.16	56.78	61.56	60.68	61.02	61.10	61.09	60.72	60.77
TiO_2	0.15	0.09	0.10	0.11	0.10	0.09	0.05	0.03	0.04	0.01	b.d.l	b.d.l	0.08	0.02
ZrO_2	20.96	20.72	22.16	18.43	18.43	18.04	19.34	16.68	17.15	15.23	15.09	15.08	14.73	14.50
HfO_2	0.22	0.21	0.35	0.26	0.26	0.44	0.30	0.14	0.23	0.27	0.29	0.20	0.33	0.32
ThO_2	0.07	b.d.l	b.d.l	b.d.l	b.d.l	0.01	0.02	0.07	0.06	0.05	0.06	0.03	0.05	0.08
Al_2O_3	0.03	0.05	0.13	0.06	0.09	0.09	0.10	0.01	0.02	0.02	0.02	b.d.l	0.02	b.d.l
FeO	0.23	0.38	0.45	0.33	0.50	0.43	0.42	0.01	b.d.l	0.04	0.00	0.05	b.d.l	0.05
CaO	0.33	0.36	0.38	0.43	0.30	0.24	0.34	0.01	b.d.l	0.03	0.05	0.05	0.02	0.06
Na_2O	1.31	1.33	1.62	2.08	2.51	4.13	2.95	4.59	4.61	4.60	4.52	3.48	4.68	4.36
K_2O	0.20	0.19	0.27	1.48	1.13	0.53	0.59	2.78	3.14	1.08	2.48	2.12	2.19	2.09
PbO	b.d.l	b.d.l	b.d.l	b.d.l	b.d.l	b.d.l	b.d.l	n.a	n.a	n.a	n.a	n.a	n.a	n.a
MgO	b.d.l	b.d.l	b.d.l	b.d.l	b.d.l	b.d.l	b.d.l	n.a	n.a	n.a	n.a	n.a	n.a	n.a
V_2O_5	b.d.l	b.d.l	b.d.l	b.d.l	b.d.l	b.d.l	b.d.l	n.a	n.a	n.a	n.a	n.a	n.a	n.a
P_2O_5	b.d.l	b.d.l	b.d.l	b.d.l	b.d.l	b.d.l	b.d.l	n.a	n.a	n.a	n.a	n.a	n.a	n.a
Nb_2O_5	0.25	0.24	0.36	0.13	0.17	0.15	0.14	0.04	0.10	0.01	0.05	b.d.l	0.03	0.01
Ta_2O_5	b.d.l	b.d.l	b.d.l	b.d.l	b.d.l	b.d.l	b.d.l	n.a	n.a	n.a	n.a	n.a	n.a	n.a
UO_2	b.d.l	b.d.l	b.d.l	b.d.l	b.d.l	b.d.l	b.d.l	n.a	n.a	n.a	n.a	n.a	n.a	n.a
MnO	b.d.l	b.d.l	b.d.l	b.d.l	b.d.l	b.d.l	b.d.l	n.a	n.a	n.a	n.a	n.a	n.a	n.a
Cr_2O_3	b.d.l	b.d.l	b.d.l	b.d.l	b.d.l	b.d.l	b.d.l	n.a	n.a	n.a	n.a	n.a	n.a	n.a
La_2O_3	b.d.l	b.d.l	b.d.l	b.d.l	b.d.l	b.d.l	b.d.l	n.a	n.a	n.a	n.a	n.a	n.a	n.a
Ce_2O_3	b.d.l	b.d.l	b.d.l	b.d.l	b.d.l	b.d.l	b.d.l	n.a	n.a	n.a	n.a	n.a	n.a	n.a
Nd_2O_3	b.d.l	b.d.l	b.d.l	b.d.l	b.d.l	b.d.l	b.d.l	n.a	n.a	n.a	n.a	n.a	n.a	n.a
Gd_2O_3	b.d.l	b.d.l	b.d.l	0.04	0.02	0.09	0.10	0.33	0.20	0.45	0.24	0.39	0.20	0.34
Dy_2O_3	0.17	0.11	0.08	b.d.l	0.07	b.d.l	0.03	0.46	0.25	0.36	0.44	0.62	0.36	0.36
Yb_2O_3	0.11	0.07	0.09	0.02	0.20	b.d.l	b.d.l	0.40	0.52	0.61	0.45	0.68	0.55	0.73
Y_2O_3	0.28	0.14	0.16	0.47	0.33	0.61	0.28	2.90	2.72	3.90	3.79	3.92	3.89	4.34
Total	89.57	88.71	90.01	81.70	81.59	77.02	81.44	90.01	89.72	87.68	88.58	87.71	87.84	88.05
Cl	n.a	n.a	n.a	n.a	n.a	n.a	n.a	n.a	n.a	n.a	n.a	n.a	n.a	n.a
F	b.d.l	0.07	0.07	0.05	b.d.l	0.04	b.d.l	b.d.l	b.d.l	0.01	b.d.l	b.d.l	b.d.l	0.01
H_2O*	10.13	10.13	10.13	10.13	10.13	10.13	10.13	13.00	13.00	13.00	13.00	13.00	13.00	13.00
Total 2	99.70	98.91	100.21	91.87	91.71	87.18	91.56	103.01	102.72	100.69	101.58	100.71	100.84	101.06

na = não analisado

bdl = abaixo do limite de detecção

mineral	(Na,K)ZrS-I	(Na,K)ZrS-I	(Na,K)ZrS-I	(Na,K)ZrS-I	(Na,K)ZrS-I	(Na,K)ZrS-I	(Na,K)ZrS-I	(Na,K)ZrS-II	(Na,K)ZrS-II	(Na,K)ZrS-II	(Na,K)ZrS-II	(Na,K)ZrS-II	(Na,K)ZrS-II	(Na,K)ZrS-II
Sample	MR38_c1							MR26_c1						
Point ID	1	2	3	4	5	6	7	1	2	3	4	5	6	8
obs.	euhedral crystal	euhedral crystal	euhedral crystal	euhedral crystal	euhedral crystal	euhedral crystal	euhedral crystal							
								proporções catiônicas com base em 8 Si e 19 oxigênios						
Si	6.000	6.000	6.000	6.000	6.000	6.000	6.000	8.000	8.000	8.000	8.000	8.000	8.000	8.000
Ti	0.006	0.004	0.004	0.005	0.004	0.004	0.002	0.002	0.002	0.001	0.000	0.000	0.005	0.001
Zr	0.940	0.935	1.015	0.932	0.938	1.012	0.997	1.057	1.103	0.974	0.963	0.963	0.946	0.931
Hf	0.006	0.006	0.009	0.008	0.008	0.014	0.009	0.005	0.009	0.010	0.011	0.008	0.012	0.012
Th	0.002	0.000	0.000	0.000	0.000	0.000	0.001	0.002	0.002	0.001	0.002	0.001	0.001	0.002
Al	0.004	0.006	0.015	0.007	0.011	0.013	0.013	0.001	0.003	0.003	0.004	0.000	0.003	0.000
Fe	0.018	0.029	0.035	0.029	0.044	0.041	0.037	0.001	0.000	0.004	0.001	0.005	0.000	0.005
Ca	0.032	0.036	0.038	0.048	0.033	0.030	0.038	0.002	0.000	0.005	0.007	0.007	0.003	0.009
Na	0.234	0.238	0.295	0.418	0.508	0.921	0.604	1.157	1.178	1.169	1.147	0.884	1.196	1.113
K	0.023	0.022	0.032	0.196	0.151	0.078	0.080	0.461	0.528	0.181	0.414	0.354	0.368	0.351
Pb	0.000	0.000	0.000	0.000	0.000	0.000	0.000	0.000	0.000	0.000	0.000	0.000	0.000	0.000
Mg	0.000	0.000	0.000	0.000	0.000	0.000	0.000	0.000	0.000	0.000	0.000	0.000	0.000	0.000
V	0.000	0.000	0.000	0.000	0.000	0.000	0.000	0.000	0.000	0.000	0.000	0.000	0.000	0.000
P	0.000	0.000	0.000	0.000	0.000	0.000	0.000	0.000	0.000	0.000	0.000	0.000	0.000	0.000
Nb	0.010	0.010	0.015	0.006	0.008	0.008	0.007	0.002	0.006	0.000	0.003	0.000	0.002	0.001
Ta	0.000	0.000	0.000	0.000	0.000	0.000	0.000	0.000	0.000	0.000	0.000	0.000	0.000	0.000
U	0.000	0.000	0.000	0.000	0.000	0.000	0.000	0.000	0.000	0.000	0.000	0.000	0.000	0.000
Mn	0.000	0.000	0.000	0.000	0.000	0.000	0.000	0.000	0.000	0.000	0.000	0.000	0.000	0.000
Cr	0.000	0.000	0.000	0.000	0.000	0.000	0.000	0.000	0.000	0.000	0.000	0.000	0.000	0.000
La	0.000	0.000	0.000	0.000	0.000	0.000	0.000	0.000	0.000	0.000	0.000	0.000	0.000	0.000
Ce	0.000	0.000	0.000	0.000	0.000	0.000	0.000	0.000	0.000	0.000	0.000	0.000	0.000	0.000
Nd	0.000	0.000	0.000	0.000	0.000	0.000	0.000	0.000	0.000	0.000	0.000	0.000	0.000	0.000
Gd	0.000	0.000	0.000	0.002	0.001	0.004	0.004	0.015	0.009	0.021	0.011	0.018	0.009	0.016
Dy	0.005	0.003	0.003	0.000	0.003	0.000	0.001	0.020	0.011	0.016	0.019	0.027	0.016	0.016
Yb	0.003	0.002	0.003	0.001	0.007	0.000	0.000	0.017	0.022	0.026	0.019	0.029	0.023	0.031
Y	0.008	0.004	0.005	0.015	0.011	0.021	0.009	0.115	0.109	0.156	0.151	0.157	0.156	0.174

mineral	(Na,K)ZrS-II	(Na,K)ZrS-II	(Na,K)ZrS-II	(Na,K)ZrS-II	(Na,K)ZrS-II	(Na,K)ZrS-II	(Na,K)ZrS-II	(Na,K)ZrS-II	(Na,K)ZrS-II	(Na,K)ZrS-II	(Na,K)ZrS-II	(Na,K)ZrS-II	(Na,K)ZrS-II	(Na,K)ZrS-II	(Na,K)ZrS-II	(Na,K)ZrS-II
Sample														MR-21		
Point ID	9	10	11	12	13	14	15	16	17	18	19	20	21	5		
obs.														1,rim	2,rim	3,rim
SiO_2	58.79	61.10	61.04	60.94	58.88	59.56	61.24	61.14	61.36	60.45	61.05	61.31	60.56	58.51	57.64	58.95
TiO_2	0.05	0.03	0.02	0.02	b.d.l	0.01	0.02	0.04	b.d.l	0.02	b.d.l	0.03	0.05	n.a	n.a	n.a
ZrO_2	17.44	13.89	16.71	16.56	18.35	17.46	14.43	15.31	15.32	15.49	15.09	15.03	17.03	20.53	18.12	22.77
HfO_2	0.40	0.17	0.29	0.22	0.33	0.31	0.29	0.11	0.29	0.26	0.24	0.20	0.35	n.a	n.a	n.a
ThO_2	b.d.l	0.05	0.05	0.06	b.d.l	0.04	0.04	0.11	0.06	0.06	0.07	0.03	0.08	n.a	n.a	n.a
Al_2O_3	b.d.l	b.d.l	b.d.l	0.02	0.01	b.d.l	b.d.l	b.d.l	b.d.l	0.02	b.d.l	b.d.l	0.01	n.a	n.a	n.a
FeO	0.03	b.d.l	0.04	0.03	0.03	0.01	b.d.l	0.03	0.01	b.d.l	0.05	0.06	b.d.l	0.05	b.d.l	0.01
CaO	0.02	0.04	0.03	0.16	0.19	0.30	0.01	b.d.l	0.03	0.07	b.d.l	0.02	0.09	b.d.l	b.d.l	b.d.l
Na_2O	8.42	3.71	5.05	4.72	8.93	8.52	4.03	4.49	4.88	4.63	4.84	4.66	5.62	3.04	3.11	2.82
K_2O	0.21	2.05	2.55	2.48	0.19	0.23	2.14	2.15	2.04	2.11	2.03	2.03	2.56	2.43	2.21	2.43
PbO	n.a	n.a	n.a	n.a	n.a	n.a	n.a	n.a	n.a	n.a	n.a	n.a	n.a	n.a	n.a	n.a
MgO	n.a	n.a	n.a	n.a	n.a	n.a	n.a	n.a	n.a	n.a	n.a	n.a	n.a	n.a	n.a	n.a
V_2O_5	n.a	n.a	n.a	n.a	n.a	n.a	n.a	n.a	n.a	n.a	n.a	n.a	n.a	n.a	n.a	n.a
P_2O_5	n.a	n.a	n.a	n.a	n.a	n.a	n.a	n.a	n.a	n.a	n.a	n.a	n.a	n.a	n.a	n.a
Nb_2O_5	b.d.l	0.05	b.d.l	0.04	b.d.l	b.d.l	b.d.l	0.01	0.02	b.d.l	b.d.l	0.01	0.07	n.a	n.a	n.a
Ta_2O_5	n.a	n.a	n.a	n.a	n.a	n.a	n.a	n.a	n.a	n.a	n.a	n.a	n.a	n.a	n.a	n.a
UO_2	n.a	n.a	n.a	n.a	n.a	n.a	n.a	n.a	n.a	n.a	n.a	n.a	n.a	n.a	n.a	n.a
MnO	n.a	n.a	n.a	n.a	n.a	n.a	n.a	n.a	n.a	n.a	n.a	n.a	n.a	n.a	n.a	n.a
Cr_2O_3	n.a	n.a	n.a	n.a	n.a	n.a	n.a	n.a	n.a	n.a	n.a	n.a	n.a	n.a	n.a	n.a
La_2O_3	n.a	n.a	n.a	n.a	n.a	n.a	n.a	n.a	n.a	n.a	n.a	n.a	n.a	n.a	n.a	n.a
Ce_2O_3	n.a	n.a	n.a	n.a	n.a	n.a	n.a	n.a	n.a	n.a	n.a	n.a	n.a	n.a	n.a	n.a
Nd_2O_3	n.a	n.a	n.a	n.a	n.a	n.a	n.a	n.a	n.a	n.a	n.a	n.a	n.a	n.a	n.a	n.a
Gd_2O_3	0.17	0.47	0.32	0.14	b.d.l	0.24	0.31	0.43	0.32	0.28	0.47	0.28	0.48	n.a	n.a	n.a
Dy_2O_3	0.14	0.42	0.26	0.36	0.02	0.33	0.56	0.43	0.49	0.56	0.60	0.51	0.28	n.a	n.a	n.a
Yb_2O_3	0.53	0.55	0.68	0.64	0.38	0.46	0.56	0.69	0.61	0.61	0.77	0.52	0.41	n.a	n.a	n.a
Y_2O_3	2.02	4.17	2.91	2.53	1.46	1.72	4.25	3.50	3.34	3.42	3.65	3.59	2.76	n.a	n.a	n.a
Total	88.23	86.69	89.95	88.93	88.77	89.18	87.88	88.44	88.79	87.99	88.86	88.28	90.35	84.57	81.08	86.99
Cl	n.a	n.a	n.a	n.a	n.a	n.a	n.a	n.a	n.a	n.a	n.a	n.a	n.a	n.a	n.a	n.a
F	b.d.l	b.d.l	0.05	b.d.l	b.d.l	0.08	0.08	b.d.l	0.06	0.05	b.d.l	b.d.l	b.d.l	n.a	n.a	n.a
H_2O*	13.00	13.00	13.00	13.00	13.00	13.00	13.00	13.00	13.00	13.00	13.00	13.00	13.00	13.00	13.00	13.00
Total 2	101.23	99.69	103.00	101.93	101.77	102.25	100.96	101.44	101.85	101.04	101.86	101.28	103.35	97.57	94.08	99.99

na = não analisado

bdl = abaixo do limite de detecção

mineral	(Na,K)ZrS-II	(Na,K)ZrS-II	(Na,K)ZrS-II	(Na,K)ZrS-II	(Na,K)ZrS-II	(Na,K)ZrS-II	(Na,K)ZrS-II	(Na,K)ZrS-II	(Na,K)ZrS-II	(Na,K)ZrS-II	(Na,K)ZrS-II	(Na,K)ZrS-II	(Na,K)ZrS-II	(Na,K)ZrS-II	(Na,K)ZrS-II	(Na,K)ZrS-II
Sample														MR-21		
Point ID	9	10	11	12	13	14	15	16	17	18	19	20	21	5		
obs.														1,rim	2,rim	3,rim
														proporções catiônicas com base em 6 S		
Si	8.000	8.000	8.000	8.000	8.000	8.000	8.000	8.000	8.000	8.000	8.000	8.000	8.000	6.000	6.000	6.000
Ti	0.003	0.001	0.001	0.001	0.000	0.000	0.001	0.002	0.000	0.001	0.000	0.002	0.003	0.000	0.000	0.000
Zr	1.157	0.887	1.068	1.060	1.216	1.144	0.919	0.977	0.974	1.000	0.964	0.956	1.097	1.027	0.920	1.130
Hf	0.016	0.006	0.011	0.008	0.013	0.012	0.011	0.004	0.011	0.010	0.009	0.007	0.013	0.000	0.000	0.000
Th	0.000	0.001	0.001	0.002	0.000	0.001	0.001	0.003	0.002	0.002	0.002	0.001	0.002	0.000	0.000	0.000
Al	0.000	0.000	0.000	0.003	0.002	0.000	0.000	0.000	0.000	0.003	0.000	0.000	0.002	0.000	0.000	0.000
Fe	0.004	0.000	0.004	0.004	0.003	0.001	0.000	0.004	0.001	0.000	0.006	0.007	0.000	0.004	0.000	0.001
Ca	0.003	0.005	0.005	0.023	0.027	0.044	0.002	0.000	0.005	0.010	0.000	0.002	0.013	0.000	0.000	0.000
Na	2.222	0.942	1.283	1.201	2.352	2.219	1.021	1.139	1.234	1.188	1.230	1.179	1.439	0.604	0.627	0.557
K	0.037	0.342	0.426	0.415	0.033	0.039	0.357	0.359	0.339	0.356	0.339	0.338	0.431	0.318	0.293	0.316
Pb	0.000	0.000	0.000	0.000	0.000	0.000	0.000	0.000	0.000	0.000	0.000	0.000	0.000	0.000	0.000	0.000
Mg	0.000	0.000	0.000	0.000	0.000	0.000	0.000	0.000	0.000	0.000	0.000	0.000	0.000	0.000	0.000	0.000
V	0.000	0.000	0.000	0.000	0.000	0.000	0.000	0.000	0.000	0.000	0.000	0.000	0.000	0.000	0.000	0.000
P	0.000	0.000	0.000	0.000	0.000	0.000	0.000	0.000	0.000	0.000	0.000	0.000	0.000	0.000	0.000	0.000
Nb	0.000	0.003	0.000	0.003	0.000	0.000	0.000	0.001	0.001	0.000	0.000	0.001	0.004	0.000	0.000	0.000
Ta	0.000	0.000	0.000	0.000	0.000	0.000	0.000	0.000	0.000	0.000	0.000	0.000	0.000	0.000	0.000	0.000
U	0.000	0.000	0.000	0.000	0.000	0.000	0.000	0.000	0.000	0.000	0.000	0.000	0.000	0.000	0.000	0.000
Mn	0.000	0.000	0.000	0.000	0.000	0.000	0.000	0.000	0.000	0.000	0.000	0.000	0.000	0.000	0.000	0.000
Cr	0.000	0.000	0.000	0.000	0.000	0.000	0.000	0.000	0.000	0.000	0.000	0.000	0.000	0.000	0.000	0.000
La	0.000	0.000	0.000	0.000	0.000	0.000	0.000	0.000	0.000	0.000	0.000	0.000	0.000	0.000	0.000	0.000
Ce	0.000	0.000	0.000	0.000	0.000	0.000	0.000	0.000	0.000	0.000	0.000	0.000	0.000	0.000	0.000	0.000
Nd	0.000	0.000	0.000	0.000	0.000	0.000	0.000	0.000	0.000	0.000	0.000	0.000	0.000	0.000	0.000	0.000
Gd	0.008	0.022	0.015	0.007	0.000	0.011	0.014	0.020	0.015	0.013	0.022	0.013	0.022	0.000	0.000	0.000
Dy	0.006	0.018	0.011	0.016	0.001	0.015	0.024	0.018	0.021	0.025	0.026	0.022	0.012	0.000	0.000	0.000
Yb	0.023	0.023	0.029	0.027	0.017	0.020	0.024	0.029	0.026	0.026	0.032	0.022	0.017	0.000	0.000	0.000
Y	0.084	0.166	0.116	0.101	0.060	0.070	0.169	0.140	0.133	0.138	0.146	0.143	0.111	0.000	0.000	0.000

mineral	(Na,K)ZrS-II	(Na,K)ZrS-II	(Na,K)ZrS-II	(Na,K)ZrS-II	(Na,K)ZrS-II	(Na,K)ZrS-II	(Na,K)ZrS-II
Sample							
Point ID							
obs.	4,interm. Zone	5,interm. Zone	6,interm. Zone	7,rim	8,core	9,interm.zone	10,interm.zone
SiO_2	58.39	59.16	58.53	58.44	57.04	58.38	58.32
TiO_2	n.a	n.a	n.a	n.a	n.a	n.a	n.a
ZrO_2	17.31	18.89	21.25	18.64	20.92	20.01	20.49
HfO_2	n.a	n.a	n.a	n.a	n.a	n.a	n.a
ThO_2	n.a	n.a	n.a	n.a	n.a	n.a	n.a
Al_2O_3	n.a	n.a	n.a	n.a	n.a	n.a	n.a
FeO	0.05	b.d.l	0.04	0.02	b.d.l	0.02	b.d.l
CaO	b.d.l	b.d.l	b.d.l	b.d.l	b.d.l	b.d.l	b.d.l
Na_2O	3.11	3.08	2.85	2.69	2.75	3.16	3.24
K_2O	2.52	2.27	2.35	2.14	2.08	2.59	2.66
PbO	n.a	n.a	n.a	n.a	n.a	n.a	n.a
MgO	n.a	n.a	n.a	n.a	n.a	n.a	n.a
V_2O_5	n.a	n.a	n.a	n.a	n.a	n.a	n.a
P_2O_5	n.a	n.a	n.a	n.a	n.a	n.a	n.a
Nb_2O_5	n.a	n.a	n.a	n.a	n.a	n.a	n.a
Ta_2O_5	n.a	n.a	n.a	n.a	n.a	n.a	n.a
UO_2	n.a	n.a	n.a	n.a	n.a	n.a	n.a
MnO	n.a	n.a	n.a	n.a	n.a	n.a	n.a
Cr_2O_3	n.a	n.a	n.a	n.a	n.a	n.a	n.a
La_2O_3	n.a	n.a	n.a	n.a	n.a	n.a	n.a
Ce_2O_3	n.a	n.a	n.a	n.a	n.a	n.a	n.a
Nd_2O_3	n.a	n.a	n.a	n.a	n.a	n.a	n.a
Gd_2O_3	n.a	n.a	n.a	n.a	n.a	n.a	n.a
Dy_2O_3	n.a	n.a	n.a	n.a	n.a	n.a	n.a
Yb_2O_3	n.a	n.a	n.a	n.a	n.a	n.a	n.a
Y_2O_3	n.a	n.a	n.a	n.a	n.a	n.a	n.a
Total	81.38	83.40	85.03	81.93	82.79	84.16	84.71
Cl	n.a	n.a	n.a	n.a	n.a	n.a	n.a
F	n.a	n.a	n.a	n.a	n.a	n.a	n.a
H_2O*	13.00	13.00	13.00	13.00	13.00	13.00	13.00
Total 2	94.38	96.40	98.03	94.93	95.79	97.16	97.71

na = não analisado

bdl = abaixo do limite de detecção

mineral	(Na,K)ZrS-II	(Na,K)ZrS-II	(Na,K)ZrS-II	(Na,K)ZrS-II	(Na,K)ZrS-II	(Na,K)ZrS-II	(Na,K)ZrS-II
Sample							
Point ID							
obs.	4,interm. Zone	5,interm. Zone	6,interm. Zone	7,rim	8,core	9,interm.zone	10,interm.zone
i e 15 oxigênios							
Si	6.000	6.000	6.000	6.000	6.000	6.000	6.000
Ti	0.000	0.000	0.000	0.000	0.000	0.000	0.000
Zr	0.867	0.934	1.062	0.933	1.073	1.003	1.028
Hf	0.000	0.000	0.000	0.000	0.000	0.000	0.000
Th	0.000	0.000	0.000	0.000	0.000	0.000	0.000
Al	0.000	0.000	0.000	0.000	0.000	0.000	0.000
Fe	0.004	0.000	0.003	0.002	0.000	0.002	0.000
Ca	0.000	0.000	0.000	0.000	0.000	0.000	0.000
Na	0.619	0.605	0.567	0.534	0.562	0.630	0.646
K	0.330	0.294	0.308	0.281	0.279	0.340	0.349
Pb	0.000	0.000	0.000	0.000	0.000	0.000	0.000
Mg	0.000	0.000	0.000	0.000	0.000	0.000	0.000
V	0.000	0.000	0.000	0.000	0.000	0.000	0.000
P	0.000	0.000	0.000	0.000	0.000	0.000	0.000
Nb	0.000	0.000	0.000	0.000	0.000	0.000	0.000
Ta	0.000	0.000	0.000	0.000	0.000	0.000	0.000
U	0.000	0.000	0.000	0.000	0.000	0.000	0.000
Mn	0.000	0.000	0.000	0.000	0.000	0.000	0.000
Cr	0.000	0.000	0.000	0.000	0.000	0.000	0.000
La	0.000	0.000	0.000	0.000	0.000	0.000	0.000
Ce	0.000	0.000	0.000	0.000	0.000	0.000	0.000
Nd	0.000	0.000	0.000	0.000	0.000	0.000	0.000
Gd	0.000	0.000	0.000	0.000	0.000	0.000	0.000
Dy	0.000	0.000	0.000	0.000	0.000	0.000	0.000
Yb	0.000	0.000	0.000	0.000	0.000	0.000	0.000
Y	0.000	0.000	0.000	0.000	0.000	0.000	0.000

ANEXOS

ANEXO II – TABELA DE DADOS LASER ABLATION

concentrações de elementos traços (ppm) de cristais de elpidita do Plúton Papanduva, S do Brasil

Amostra	MR-43	MR-43	MR-03	MR-03	MR-03	MR-03	MR-03	MR-03	MR-21	MR-21	MR-21	MR-21	MR-21
ID análise	MR-43-2.1	MR-43-1.1	MR-03-6.1	MR-03-6.2	MR-03-4.3	MR-03-5.2	MR-03-5.3	MR-03-5.4	MR-21-4.1	MR-21-1.2	MR-21-1.3	MR-21-1.4	MR-21-1.5
P (ppm)	<44.87	<41.34	25.7	<13.22	<71.03	<48.37	<39.61	35.1	<28.16	<50.25	<61.33	<50.04	69.3
Sc	51.5	57.5	51.9	54.5	45.9	52.8	52.1	52.0	48.3	53.1	44.3	47.8	51.4
Ti	454.8	491.0	3813.4	1311.4	357.5	1024.0	230.9	483.1	938.4	832.2	355.1	457.1	822.3
Mn	80.9	31.7	82.1	17.0	59.5	26.5	74.0	31.4	80.1	18.1	45.8	23.0	17.8
Sr	10.5	8.8	29.2	4.8	27.9	11.2	39.0	13.0	10.2	4.3	8.4	5.5	2.5
Y	14812.8	3337.6	4940.5	602.0	4654.2	1061.1	5762.9	1599.7	3139.2	932.3	3348.9	1288.8	587.8
Zr	112789.4	129995.3	129018.4	141845.6	109315.4	136218.0	128757.2	135752.4	136357.1	136326.3	122197.4	122163.2	141844.1
Nb	176.9	113.1	135.8	52.7	93.0	68.7	124.5	63.0	224.0	97.2	165.6	96.0	55.4
Mo	16.2	15.3	16.4	14.2	12.7	12.6	13.2	15.2	14.9	12.7	11.7	9.7	12.9
Ba	51.0	35.5	77.4	11.7	66.3	51.3	65.6	34.9	126.6	32.0	156.5	60.3	23.0
La	83.3	36.2	83.2	4.7	8.2	3.6	9.4	4.7	22.0	15.9	27.1	16.4	19.4
Ce	188.5	215.1	152.6	13.6	28.9	11.9	29.2	16.1	47.1	53.1	110.7	66.0	218.5
Pr	25.8	12.4	28.7	2.7	5.5	2.2	5.5	2.7	6.4	5.9	10.1	6.8	8.9
Nd	150.2	64.2	135.0	19.4	34.1	17.3	34.3	16.9	30.7	26.5	48.3	25.8	39.0
Sm	50.3	10.8	23.7	42.4	16.4	57.7	44.4	28.9	132.2	110.1	102.2	216.6	9.4
Eu	18.6	9.1	7.8	6.6	3.9	5.7	5.2	3.6	4.7	5.4	3.3	3.4	6.7
Gd	453.3	234.1	225.9	48.3	223.4	70.9	258.7	87.2	61.5	32.0	93.9	42.4	33.3
Tb	165.2	74.7	79.8	13.1	80.2	22.0	98.0	29.1	36.0	12.6	41.9	18.7	12.7
Dy	1645.9	515.0	707.7	98.0	630.3	154.1	835.2	218.1	407.6	127.8	412.6	176.4	97.5
Ho	496.6	104.1	180.2	22.2	134.3	35.6	198.6	51.1	111.1	32.2	108.3	42.9	22.8
Er	1771.2	255.3	563.6	66.7	354.1	102.0	605.5	151.8	349.2	97.3	310.9	127.0	64.8
Tm	286.1	33.2	87.4	10.5	46.7	15.6	92.0	24.8	48.9	14.6	42.9	19.1	8.9
Yb	1948.9	189.9	636.8	77.6	288.8	116.2	636.9	183.8	322.3	99.3	282.2	115.3	68.6
Lu	239.4	21.3	80.7	10.5	33.1	15.0	82.3	27.0	39.4	12.9	33.2	15.0	9.9
Hf	2094.5	3556.7	3248.0	3218.3	2918.6	2760.3	2523.8	2589.6	3362.9	3758.7	2895.2	2816.5	3469.8
Ta	24.8	15.0	24.2	23.7	13.8	65.7	24.7	28.0	26.8	27.3	19.3	11.8	23.1
^{206}Pb	672.5	275.1	636.2	45.4	375.1	129.9	599.3	148.3	616.5	169.9	546.0	216.4	108.7
^{208}Pb	666.7	267.7	620.5	37.3	365.0	109.4	567.1	134.6	625.8	177.5	562.7	223.6	106.7
Th	163.2	19.3	19.7	13.5	7.3	31.6	27.7	25.8	35.6	23.5	24.9	19.6	36.9
U	346.8	82.6	180.8	93.3	116.0	331.4	370.4	183.2	98.0	52.2	76.6	40.2	81.1

erro 2σ

Amostra	MR-43	MR-43	MR-03	MR-03	MR-03	MR-03	MR-03	MR-03	MR-21	MR-21	MR-21	MR-21	MR-21
ID análise	MR-43-2.1	MR-43-1.1	MR-03-6.1	MR-03-6.2	MR-03-4.3	MR-03-5.2	MR-03-5.3	MR-03-5.4	MR-21-4.1	MR-21-1.2	MR-21-1.3	MR-21-1.4	MR-21-1.5
P	20.6	21.0	7.9	7.0	27.9	20.0	18.8	16.7	13.6	25.6	28.6	23.3	23.9
Sc	2.0	2.2	1.8	1.9	1.9	2.0	2.0	2.0	1.9	2.3	2.0	2.0	2.1
Ti	24.3	26.7	177.5	62.3	21.5	53.1	15.3	26.8	53.0	50.3	24.8	29.3	49.7
Mn	3.0	1.5	2.9	0.7	2.4	1.2	2.9	1.4	3.1	1.2	2.1	1.3	1.1
Sr	0.6	0.5	1.3	0.3	1.3	0.6	1.9	0.7	0.6	0.4	0.6	0.4	0.2
Y	663.0	149.6	227.8	28.0	224.4	52.8	288.6	80.8	169.9	51.6	186.5	72.5	33.4
Zr	4694.8	5413.8	5512.9	6089.7	4860.8	6218.4	5921.9	6287.8	6727.6	6848.7	6190.7	6238.1	7303.5
Nb	8.6	5.6	6.8	2.7	4.9	3.8	6.9	3.5	13.3	6.0	10.2	6.0	3.5
Mo	1.4	1.5	1.1	1.0	1.2	1.1	1.2	1.3	1.3	1.4	1.3	1.1	1.3
Ba	3.1	2.5	4.1	0.9	3.9	3.1	4.1	2.3	7.7	2.7	10.0	4.2	1.9
La	3.6	1.7	3.6	0.3	0.4	0.2	0.5	0.3	1.1	0.9	1.5	0.9	1.1
Ce	9.1	10.4	7.5	0.7	1.6	0.7	1.6	0.9	2.8	3.2	6.6	4.0	13.2
Pr	1.3	0.7	1.4	0.2	0.3	0.2	0.4	0.2	0.4	0.4	0.7	0.5	0.6
Nd	8.2	4.1	7.2	1.3	2.4	1.4	2.5	1.4	2.3	2.4	3.7	2.2	3.0
Sm	7.2	3.3	4.5	1.3	2.9	1.6	3.8	1.7	1.5	1.5	2.1	1.4	2.0
Eu	1.1	0.6	0.5	0.4	0.3	0.4	0.4	0.3	0.4	0.5	0.4	0.3	0.5
Gd	21.5	11.5	10.9	2.5	11.4	3.9	13.6	4.8	3.7	2.4	5.8	2.8	2.3
Tb	8.3	3.8	4.1	0.7	4.3	1.3	5.5	1.7	2.2	0.9	2.7	1.2	0.9
Dy	76.6	24.4	33.6	4.9	31.3	8.0	42.8	11.5	22.5	7.7	23.6	10.4	5.9
Ho	27.0	5.7	10.0	1.3	7.8	2.2	12.0	3.2	7.3	2.2	7.4	3.0	1.6
Er	97.8	14.3	31.8	3.9	21.0	6.3	37.2	9.5	23.2	6.8	21.4	8.9	4.7
Tm	15.5	1.9	4.8	0.6	2.7	1.0	5.6	1.5	3.2	1.0	2.9	1.3	0.7
Yb	108.9	11.2	36.4	4.6	17.5	7.4	39.7	11.8	21.8	7.3	19.9	8.4	5.2
Lu	13.1	1.3	4.5	0.6	2.0	0.9	5.0	1.7	2.6	0.9	2.3	1.1	0.7
Hf	109.8	185.9	172.1	171.4	161.3	156.8	144.6	149.4	206.9	235.7	183.2	179.6	222.9
Ta	1.4	0.9	1.3	1.3	0.8	3.8	1.5	1.7	1.7	1.8	1.3	0.8	1.5
^{206}Pb	36.1	15.1	34.3	2.6	21.2	7.7	35.0	8.9	38.6	11.2	35.2	14.3	7.4
^{208}Pb	39.3	16.1	36.9	2.4	22.8	7.2	36.7	9.0	43.6	13.0	40.5	16.4	8.0
Th	9.9	1.3	1.2	0.9	0.5	2.1	1.9	1.8	2.6	1.8	1.9	1.5	2.8
U	21.0	5.1	11.1	5.8	7.5	21.9	24.7	12.4	7.1	3.9	5.8	3.1	6.2

Concentrações normalizadas ao condrito C1 (McDonough & Sun, 1995; Chemical Geology 120: 223-253)

Amostra	MR-43	MR-43	MR-03	MR-03	MR-03	MR-03	MR-03	MR-03	MR-21	MR-21	MR-21	MR-21	MR-21
ID análise	MR-43-2.1	MR-43-1.1	MR-03-6.1	MR-03-6.2	MR-03-4.3	MR-03-5.2	MR-03-5.3	MR-03-5.4	MR-21-4.1	MR-21-1.2	MR-21-1.3	MR-21-1.4	MR-21-1.5
P	0.00	0.00	0.01	0.00	0.00	0.00	0.00	0.02	0.00	0.00	0.00	0.00	0.03
Sc	6.0	6.7	6.0	6.3	5.3	6.1	6.0	6.0	5.6	6.1	5.1	5.5	6.0
Ti	0.7	0.8	5.8	2.0	0.5	1.6	0.4	0.7	1.4	1.3	0.5	0.7	1.3
Mn	0.0	0.0	0.0	0.0	0.0	0.0	0.0	0.0	0.0	0.0	0.0	0.0	0.0
Sr	0.9	0.7	2.5	0.4	2.3	0.9	3.3	1.1	0.9	0.4	0.7	0.5	0.2
Y	6583.5	1483.4	2195.8	267.5	2068.5	471.6	2561.3	711.0	1395.2	414.4	1488.4	572.8	261.3
Zr	20359.1	23464.9	23288.5	25603.9	19732.0	24588.1	23241.4	24504.1	24613.2	24607.6	22057.3	22051.1	25603.6
Nb	471.7	301.6	362.0	140.5	248.0	183.1	332.0	168.0	597.3	259.3	441.5	256.0	147.6
Mo	11.8	11.1	11.9	10.3	9.2	9.1	9.6	11.0	10.8	9.2	8.4	7.0	9.4
Ba	14.9	10.4	22.7	3.4	19.4	15.0	19.2	10.2	37.1	9.4	45.9	17.7	6.7
La	227.1	98.5	226.7	12.8	22.4	9.9	25.5	12.8	59.9	43.3	73.7	44.8	52.9
Ce	196.9	224.7	159.5	14.2	30.2	12.4	30.5	16.8	49.2	55.4	115.7	69.0	228.3
Pr	188.3	90.8	209.4	19.4	39.8	16.3	40.2	19.6	46.7	42.8	73.9	49.9	64.8
Nd	211.2	90.3	189.8	27.3	48.0	24.3	48.2	23.7	43.2	37.3	68.0	36.3	54.9
Sm	591.2	238.8	379.3	93.5	206.3	104.8	270.2	107.0	89.0	64.4	109.8	67.2	110.8
Eu	213.5	104.9	90.0	75.3	44.9	65.2	59.9	41.8	54.3	61.6	38.0	39.0	77.3
Gd	1481.3	764.9	738.2	157.9	730.2	231.6	845.4	285.0	201.0	104.7	307.0	138.7	108.8
Tb	2848.5	1288.1	1375.4	225.9	1382.5	378.4	1689.1	501.2	620.6	217.9	722.3	322.9	218.5
Dy	4320.1	1351.7	1857.6	257.1	1654.4	404.4	2192.2	572.4	1069.9	335.4	1083.0	463.0	255.8
Ho	5835.2	1223.1	2117.3	260.6	1578.6	418.6	2334.0	600.0	1305.6	378.4	1273.1	504.5	267.9
Er	7113.3	1025.3	2263.5	267.7	1422.2	409.7	2431.6	609.5	1402.5	390.6	1248.7	510.0	260.3
Tm	8036.3	933.0	2455.1	294.0	1310.3	437.1	2583.7	697.2	1372.6	410.0	1203.5	536.1	249.8
Yb	7858.4	765.8	2567.8	313.0	1164.6	468.5	2568.2	741.2	1299.4	400.2	1138.0	464.9	276.5
Lu	6282.1	559.1	2118.0	274.8	867.9	394.2	2160.9	709.5	1032.8	337.3	870.3	394.8	260.6
Hf	11701.0	19870.0	18145.2	17979.3	16304.9	15420.5	14099.6	14467.3	18787.1	20998.1	16174.5	15734.5	19384.5
Ta	954.5	576.5	929.3	910.1	530.6	2527.6	948.1	1078.1	1029.3	1048.4	741.3	452.5	886.7
^{206}Pb	184.3	75.4	174.3	12.4	102.8	35.6	164.2	40.6	168.9	46.5	149.6	59.3	29.8
^{208}Pb	182.7	73.4	170.0	10.2	100.0	30.0	155.4	36.9	171.5	48.6	154.2	61.3	29.2
Th	3839.3	454.2	463.0	317.5	172.7	744.1	651.6	606.2	837.3	552.2	585.2	460.0	868.4
U	28422.7	6771.8	14815.7	7648.1	9504.6	27160.4	30362.5	15017.0	8029.4	4280.7	6276.4	3296.0	6648.3

concentrações de elementos traços (ppm) de cristais de elpidita do Plúton Papanduva, S do Brasil

Amostra	MR-21	MR-21	MR-21	MR-21	MR-21	MR-21	MR-21	MR-21
ID análise	MR-21-1.6	MR-21-3.1	MR-21-3.3	MR-21-3.5	MR-21-3.6	MR-21-2.1	MR-21-2.2	MR-21-2.3
P (ppm)	<54.45	<15.76	16.9	27.4	<19.33	13.1	11.0	18.3
Sc	48.3	50.6	53.9	49.7	49.8	51.1	50.4	52.0
Ti	2236.7	915.7	665.6	790.7	720.4	924.3	715.4	415.1
Mn	14.6	10.9	18.2	13.5	36.9	31.4	37.2	21.2
Sr	2.8	3.6	7.2	3.2	8.0	9.6	10.9	6.7
Y	438.4	917.0	1009.8	903.7	1747.1	751.4	2159.5	1616.5
Zr	126781.1	138228.6	142297.5	135811.7	138310.0	137991.0	138374.0	140367.9
Nb	63.2	201.2	159.7	82.8	211.4	202.4	195.8	104.0
Mo	17.3	12.8	11.7	12.1	11.3	11.9	11.5	11.9
Ba	17.6	36.4	53.3	31.6	103.5	65.5	72.6	57.2
La	89.6	12.8	7.5	6.4	17.4	31.6	82.2	132.2
Ce	1059.2	36.9	26.7	18.5	44.4	94.0	163.8	253.1
Pr	31.7	3.7	3.6	2.6	5.5	14.9	30.0	30.9
Nd	140.3	15.0	19.7	15.0	25.7	71.9	204.2	145.4
Sm	27.3	10.0	12.0	85.8	79.3	61.1	218.5	62.4
Eu	6.8	4.1	5.2	6.1	4.8	23.3	17.2	8.6
Gd	52.6	27.3	39.1	32.5	40.0	58.9	237.0	130.2
Tb	13.9	12.3	16.1	13.9	21.2	16.2	56.0	34.3
Dy	113.3	121.8	145.9	131.7	228.3	122.7	386.5	252.2
Ho	25.5	32.9	36.7	32.3	61.4	27.4	75.9	54.4
Er	72.6	103.4	108.1	97.0	186.8	75.7	185.2	144.0
Tm	10.8	15.3	16.3	14.1	27.4	9.9	21.3	18.1
Yb	71.1	105.1	104.5	90.8	182.8	60.7	114.5	95.9
Lu	8.6	13.7	14.8	11.5	22.8	7.0	11.6	9.9
Hf	3324.7	3623.0	3385.1	3113.1	3145.1	2282.7	2394.0	2506.9
Ta	24.0	31.6	41.6	35.5	34.8	48.6	41.0	19.0
^{206}Pb	205.5	135.8	231.7	169.4	373.5	280.6	550.2	177.2
^{208}Pb	204.6	139.0	233.2	172.5	384.0	269.8	552.3	167.1
Th	132.4	60.2	35.9	19.9	23.5	43.8	32.1	11.4
U	76.9	89.8	129.5	79.4	78.0	273.6	337.0	194.5

erro 2σ

Amostra	MR-21	MR-21	MR-21	MR-21	MR-21	MR-21	MR-21	MR-21
ID análise	MR-21-1.6	MR-21-3.1	MR-21-3.3	MR-21-3.5	MR-21-3.6	MR-21-2.1	MR-21-2.2	MR-21-2.3
P	23.6	6.9	7.4	8.7	8.5	4.8	4.9	5.3
Sc	2.0	1.8	2.0	1.9	1.9	1.9	1.9	1.9
Ti	131.0	53.9	40.1	48.9	45.2	57.9	45.4	26.9
Mn	1.0	0.5	0.8	0.6	1.5	1.3	1.5	0.9
Sr	0.2	0.2	0.4	0.2	0.5	0.6	0.6	0.4
Y	25.1	52.9	59.3	54.6	106.5	46.2	134.1	101.3
Zr	6583.1	7230.7	7572.7	7416.7	7618.7	7665.3	7753.0	7932.6
Nb	4.0	12.8	10.4	5.5	14.3	13.8	13.5	7.2
Mo	1.5	1.0	0.9	1.0	0.9	0.9	0.9	1.0
Ba	1.5	2.4	3.4	2.2	6.8	4.3	4.8	3.9
La	4.7	0.7	0.4	0.4	1.0	1.8	4.6	7.4
Ce	64.3	2.3	1.7	1.2	2.9	6.1	10.8	16.8
Pr	1.9	0.2	0.2	0.2	0.4	1.0	1.9	2.0
Nd	9.4	1.1	1.4	1.2	1.9	5.0	14.3	10.3
Sm	3.0	0.9	1.2	1.2	1.1	2.4	9.6	4.9
Eu	0.5	0.3	0.4	0.4	0.4	1.5	1.2	0.6
Gd	3.4	1.7	2.4	2.1	2.6	3.7	14.8	8.3
Tb	0.9	0.8	1.1	0.9	1.4	1.1	3.8	2.4
Dy	6.8	7.1	8.7	8.0	14.0	7.6	23.9	15.8
Ho	1.8	2.3	2.6	2.4	4.5	2.0	5.7	4.1
Er	5.2	7.3	7.8	7.2	14.0	5.7	14.1	11.0
Tm	0.8	1.1	1.2	1.0	2.0	0.7	1.6	1.4
Yb	5.3	7.6	7.7	6.9	13.9	4.7	8.8	7.5
Lu	0.6	1.0	1.1	0.9	1.7	0.5	0.9	0.8
Hf	215.3	236.1	224.4	211.6	215.5	157.7	166.7	176.0
Ta	1.6	2.1	2.8	2.4	2.4	3.4	2.9	1.4
^{206}Pb	13.7	9.0	15.6	11.7	25.9	19.6	38.7	12.6
^{208}Pb	15.2	10.3	17.5	13.3	29.8	21.1	43.6	13.3
Th	10.1	4.6	2.8	1.6	1.9	3.6	2.6	1.0
U	5.9	6.9	10.1	6.4	6.3	22.3	27.7	16.1

Concentrações normalizadas ao condrito C1 (McDonough & Sun, 1995; Chemical Geology 120: 223-253)

Amostra	MR-21	MR-21	MR-21	MR-21	MR-21	MR-21	MR-21	MR-21
ID análise	MR-21-1.6	MR-21-3.1	MR-21-3.3	MR-21-3.5	MR-21-3.6	MR-21-2.1	MR-21-2.2	MR-21-2.3
P	0.00	0.00	0.01	0.01	0.00	0.01	0.00	0.01
Sc	5.6	5.9	6.2	5.8	5.8	5.9	5.8	6.0
Ti	3.4	1.4	1.0	1.2	1.1	1.4	1.1	0.6
Mn	0.0	0.0	0.0	0.0	0.0	0.0	0.0	0.0
Sr	0.2	0.3	0.6	0.3	0.7	0.8	0.9	0.6
Y	194.8	407.5	448.8	401.6	776.5	333.9	959.8	718.4
Zr	22884.7	24951.0	25685.5	24514.7	24965.7	24908.1	24977.3	25337.2
Nb	168.7	536.5	425.9	220.7	563.8	539.8	522.2	277.4
Mo	12.6	9.3	8.5	8.8	8.2	8.6	8.3	8.7
Ba	5.2	10.7	15.6	9.3	30.4	19.2	21.3	16.8
La	244.1	34.8	20.3	17.4	47.5	86.2	223.9	360.3
Ce	1106.8	38.6	27.9	19.4	46.4	98.3	171.1	264.5
Pr	231.3	26.9	25.9	18.8	40.1	108.8	219.0	225.6
Nd	197.4	21.1	27.7	21.1	36.2	101.1	287.2	204.5
Sm	189.2	52.1	77.8	73.7	63.9	151.5	623.5	312.7
Eu	78.4	47.0	59.4	70.3	55.0	267.4	197.7	99.3
Gd	171.9	89.1	127.8	106.3	130.9	192.6	774.4	425.3
Tb	238.7	211.8	276.9	240.3	366.0	279.0	965.1	591.9
Dy	297.3	319.6	382.9	345.6	599.2	322.0	1014.5	661.8
Ho	299.5	386.1	431.8	379.8	721.6	322.2	892.3	639.7
Er	291.4	415.1	434.1	389.5	750.2	304.1	744.0	578.2
Tm	302.1	428.7	456.6	395.8	768.8	278.2	599.3	509.6
Yb	286.8	423.9	421.2	366.0	736.9	244.8	461.6	386.8
Lu	224.9	360.6	387.3	302.8	599.0	182.8	303.3	261.0
Hf	18573.7	20240.2	18911.1	17391.4	17570.2	12752.7	13374.3	14005.0
Ta	922.4	1213.3	1599.2	1365.4	1337.5	1868.0	1577.7	731.2
^{206}Pb	56.3	37.2	63.5	46.4	102.3	76.9	150.7	48.5
^{208}Pb	56.1	38.1	63.9	47.3	105.2	73.9	151.3	45.8
Th	3115.0	1416.8	845.2	468.0	552.0	1029.8	754.7	269.2
U	6305.7	7356.8	10613.9	6507.6	6395.7	22425.4	27622.7	15942.4